BORON NITRIDE AND ITS COMBINATIONS AS PROCESSING AIDS IN THE EXTRUSION OF ZIEGLER-NATTA POLYETHYLENES

by

EDWARD BUDI MULIAWAN

B.A.Sc., The University of British Columbia, 2001

A THESIS SUBMITTED IN PARTIAL FULFILLMENT OF THE REQUIREMENTS FOR THE DEGREE OF MASTER OF APPLIED SCIENCE

in

THE FACULTY OF GRADUATE STUDIES
Department of Chemical Engineering

We accept this thesis as conforming to the required standard

THE UNIVERSITY OF BRITISH COLUMBIA

August 2004

Library Authorization

In presenting this thesis in partial fulfillment of the requirements for an advanced degree at the University of British Columbia, I agree that the Library shall make it freely available for reference and study. I further agree that permission for extensive copying of this thesis for scholarly purposes may be granted by the head of my department or by his or her representatives. It is understood that copying or publication of this thesis for financial gain shall not be allowed without my written permission.

EDWARD BUDI MULIAWAN — Name of Author *(please print)*

Sept 1, 2004 — Date (dd/mm/yyyy)

Title of Thesis: Boron Nitride And Its Combinations As Processing Aids in the Extrusion of Ziegler - Natta polyethylenes

Degree: Master of Applied Science Year: 2004

Department of Chemical and Biological Engineering
The University of British Columbia
Vancouver, BC Canada

ABSTRACT

It is widely known that the rate of production in many commercial polymer processing operations is limited by the appearance of flow instabilities. Flow instabilities may manifest themselves as regular distortions on the extrudate surface (sharkskin or surface melt fracture) or in the form of irregular helix distortions (gross melt fracture) at higher shear rates. Usually, polymer processing aids are used to postpone/eliminate these melt fractures. Fluoropolymer has been found to be effective in eliminating sharkskin melt fracture, but its effect in the gross melt fracture region is rather poor. Boron nitride, on the other hand, has been found not only to be effective in eliminating sharskskin melt fracture but also postpone the onset of gross melt fracture. In addition, it has also been found that the combination of fluoropolymer and boron nitride seems to enhance their performance even further.

The main objective of this work is to investigate the performance of boron nitride and its combinations as polymer processing aids in the processing of Ziegler-Natta polyethylenes. A number of different polyethylene resins were tested including a variety of processing aids at various combinations and concentrations. It was found that mixing fluoropolymer in a dry form into boron nitride-compounded resin allows the synergistic effect of fluoropolymer and boron nitride to be shown. This is because separately mixing fluoropolymer and boron nitride prevents the adsorption of fluoropolymer onto the boron nitride particles. Lastly, it was observed that a relatively new processing aid, CarboGlide™, which is a proprietary mixture of boron nitride and other processing aids, is able to perform equally well as the combination of boron nitride and fluoropolymer.

TABLE OF CONTENTS

Page

Page

LIST OF FIGURES

Page

Page

Page

LIST OF TABLES

Page

ACKNOWLEDGEMENTS

I would like to express my sincere gratitude to my supervisor Dr. Savvas G. Hatzikiriakos for his guidance throughout the course of this work, and to NOVA Chemicals for the sponsorship of this thesis project.

I also wish to thank Dr. Martin Sentmanat of Xpansion Instruments for all of his help with regards to the extensional experiments. My gratitude also goes to the members of the Rheology team of the University of British Columbia (Rheolab) for their help and support.

Finally, I would like to extend a special note of thanks to Natural Sciences and Engineering Research Council of Canada for its financial support, and to others who have in one way or other helped me with the completion of this project.

1 INTRODUCTION

Advances in polymer technology over the past decades have allowed polymeric materials to replace many other conventional engineering materials. Unfortunately, polymer covers a wide spectrum and it is impossible to understand its technology fully. Currently, studies on polymers are usually aimed towards either increasing the production rate of the polymer or developing polymers as a more economic or superior substitute for other materials.

One of the most widely manufactured polymers is the polyolefin class. It includes all types of polyethylene (high-density, low-density and linear low density) and polypropylene. These polymers are used for various applications such as food packaging, garbage bags, containers and many other household items. As the world's population grows, so does the demand for these polymers. The current demand for polyethylene is estimated to be about 66 million tonnes and projected to increase significantly (*World Polyethylene Market Report, 1999*). In order to meet this demand, it is important that polyethylene can be efficiently processed. This is one of the main reasons of continued research on polymer processing.

The molecular structure of high-density polyethylene (HDPE) is shown in Figure 1.1.

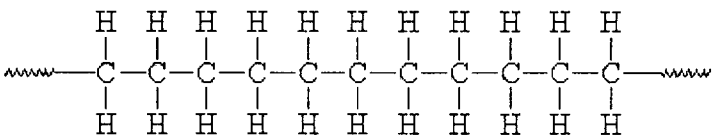

Figure 1.1 Molecular structure of linear polyethylene (HDPE).

Commercial production of polyethylene was first carried out in 1939 based on the ICI technology. This process used free radical polymerization at very high pressure and temperature of the order of 1400 bar and 200 ^{0}C. Polyethylene produced was strong and virtually unbreakable. This polyethylene had side branches, which made it flexible and translucent. It is known as low density polyethylene (LDPE).

In 1950s, Karl Ziegler and Giulio Natta succeeded in developing a catalyst for the polymerization of ethylene. The Ziegler-Natta catalytic polymerization could be carried out at much lower pressure and temperature and it also improved the linearity of the polymer chain. The absence of side branching resulted in more closely packed structure leading to higher density, greater strength and rigidity and opaque appearance. This type of polyethylene is known as high density polyethylene (HDPE). With the help of Ziegler-Natta catalyst, branched polyethylene chains could still be developed by copolymerizing ethylene with an alkyl branched comonomer. Copolymerization usually reduces the density of the produced polyethylene and with the linearity of the polymer chains achieved by using the Ziegler-Natta catalyst, the resulting polymer is linear-low density polyethylene (LLDPE). It has the advantages of LDPE's flexibility and transparency and at the same time greater strength due to controlled branching and narrow molecular weight distribution.

The most recent finding in polymer synthesis was the development of the single-site metallocene catalysts. The single-site catalyst allows the structure and the tacticity of a specific polymer to be controlled during its synthesis. With this catalyst, a HDPE with

extremely linear structure and very high molecular weight, known as Ultra High Molecular Weight Polyethylene (UHMWPE) can be produced. Due to its extremely high molecular weight, it has a uniquely high strength. This polymer can even be used for bullet proof jackets because of its strength. Similarly, LLDPE made using metallocene catalysts (m-LLDPE) has relatively narrow molecular weight distribution. Thus m-LLDPE has greater mechanical strength in particular puncture toughness, lower melt elasticity and die swelling and it permits higher level of pre-stretching for films as compared to Ziegler-Natta LLDPE *(Rohse et al, 1997)*.

As may be expected, density is usually used to classify the different types of polyethylene which is essentially a function of the molecular structure of the polymer. HDPE, for example, has a density range between 0.941 to 0.965 g/cm^3 at 25°C. Polyethylenes that have densities below that range are considered as low density polyethylene and maybe either LLDPE or LDPE as described above. In LDPE, usually there is significant long chain branching on the main backbone chains of the polymer. The primary differences between polyethylenes of different densities are in rigidity, heat resistance, chemical resistance, and ability to sustain load. Generally, as density increases, hardness, heat resistance, stiffness, and resistance to permeability increases. Figure 1.2 schematically shows the molecular structures of the different types of polyethylene. Low density polyethylene is characterized by the large amount of side branches, which may also be relatively long. Linear low density polyethylene has less branching, while high density polyethylene has very little amount of side branches.

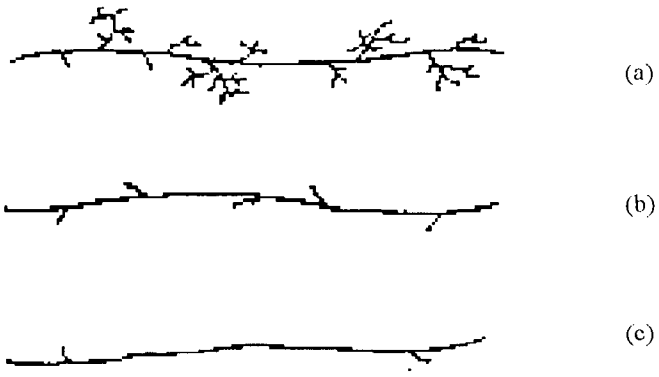

Figure 1.2 Schematics of (a) Low Density Polyethylene (LDPE), (b) Linear Low Density Polyethylene (LLDPE), and (c) High Density Polyethylene (HDPE).

Various processes are used to transform polyethylene into useful products. Some of these processes are profile extrusion, film casting, film blowing and blow moulding. For any of these processes to be economically feasible, the rate of production should be high enough. However, it is well known that in many commercial polymer processing operations, including extrusion, wire coating, blow molding, film blowing, flow instabilities occur *(Petrie and Denn, 1976; Ramamurthy, 1986).* In these processes, a polymeric melt emerging from the die often shows surface distortions at throughput rates above a critical value. As a result of these instabilities, the final product becomes unattractive and commercially unacceptable. This effect can range from loss of gloss of extrudate surface to the appearance of gross distortions. Some of the parameters affecting the degree of extrudate distortion include the process temperature, the flow rate, concentration and type of additive, geometrical dimensions of the die, the chemical nature of the polymer, the entrance geometry to the die and many others. These flow instabilities, collectively known as *melt fracture,* can manifest themselves in the form of

either small amplitude periodic distortions appearing on the surface of extrudates (surface melt fracture or sharkskin) or severe irregular distortions at higher throughput rates (gross melt fracture). Figure 1.3 shows typical extrudates exhibiting surface and gross melt fractures, obtained from the capillary extrusion of m–LLDPE resin. A relevant and practical way to evaluate the processability of polymers, particularly in extrusion applications, is to determine their melt fracture performance, i.e. to determine the critical shear stress and/or shear rate for the onset of the appearance of extrudate irregularities.

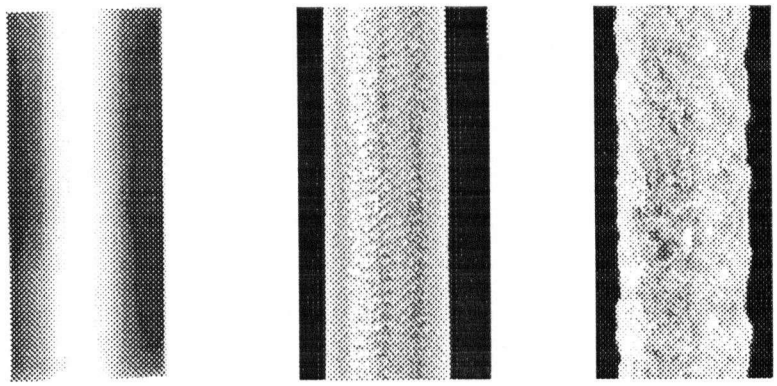

(a) (b) (c)

Figure 1.3 Typical pictures of m-LLDPE extrudates at different shear rates, (a) Smooth extrudate ($\dot{\gamma}_A$ < 70 s^{-1}), (b) Surface or Sharkskin melt fracture ($\dot{\gamma}_A$ = 70-350 s^{-1}), (c) Gross melt fracture ($\dot{\gamma}_A$ > 350 s^{-1}) *(Rathod, 2003).*

In order to increase the rate of production by overcoming melt fracture, processing additives/aids are used. These are mainly fluoropolymers that are widely used in the processing of polyolefins and other commodity polymers. Fluoropolymers are added to the base polymer at low levels (approximately 0.1 weight %) *(Hatzikiriakos, 2004a)*. They essentially act as die lubricants, modifying the properties of the polymer-wall interface essentially increasing the slip of polymer melt on die wall *(Anastasiadis and Hatzikiriakos, 1998; Denn, 2001; Migler et al, 2001a; Achilleos et al, 2002)*. As a result

of this lubrication effect along the die wall, surface melt fracture is completely eliminated. However, these fluoropolymers are not effective for overcoming gross melt fracture *(Yip et al, 2000; Achilleos et al, 2002; Seth et al, 2002).*

It has recently been demonstrated that certain grades of Boron Nitride (BN) act as effective processing aids in the extrusion of polyolefins *(Kazatchkov et al, 2000; Yip et al, 2000; Achilleos et al, 2002; Seth et al, 2002).* BN is a solid lubricant, with a structure resembling that of graphite. BN can successfully be used as a processing aid not only to eliminate surface melt fracture but also to postpone gross melt fracture to significantly higher shear rates. Figure 1.4 illustrates the effectiveness of BN in overcoming the GMF.

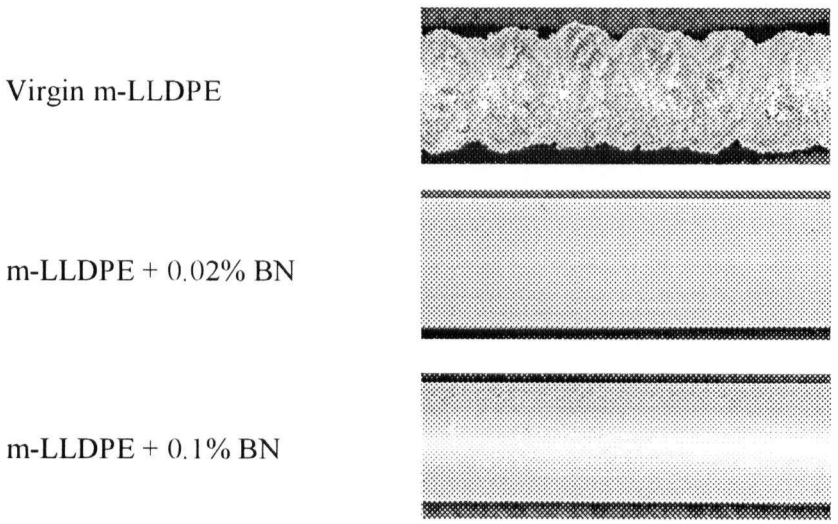

Figure 1.4 Effect of BN on extrudate appearance at $\dot{\gamma} = 617\ s^{-1}$, 163 ^{0}C *(Kazatchkov et al, 2000).*

It has also been observed that a combination of BN and fluoropolymer enhances the performance of the extrusion even further, where fluoropolymer essentially eliminates the

sharkskin and BN delays the appearance of gross melt fracture *(Rosenbaum, 2000; Achilleos et al, 2002)*. Most of the studies utilizing boron nitride as a processing aid were done on metallocene linear-low density polyethylenes.

The main objective of the present work is to assess the effectiveness of the different processing aids; BN-based, fluoropolymer-based and the combination of both of these two types, on the processing of Ziegler-Natta polyethylenes. It is also desired to investigate the effect of adding both BN and fluoropolymer together and separately. This study may prove to be useful in understanding the mechanism by which these two processing aids eliminate melt fracture. In addition, this study may also help in understanding the interaction between BN and fluoropolymer and polyethylene and its effects on the performance of the processing aids. Finally, an attempt is made to justify the need of a masterbatch step in preparing the polymer samples when a twin screw extruder is used.

2 LITERATURE REVIEW

This chapter presents an overview of important concepts and terminologies, useful for better understanding the experimental results and analysis presented in the later chapters. The topics covered in this section include rheological measurements, melt fracture, and polymer processing aids.

2.1 RHEOLOGICAL MEASUREMENTS

Rheology is defined as the science of material behavior under deformation, due to the presence of external forces *(Dealy and Wissbrun, 1995)*. It attempts to understand why a material behaves in a certain way when a force is applied. As discussed in previous section, in polymer processing, a polymer is usually subjected to various external forces, and thus a study on the rheology of polymer is necessary.

2.1.1 Rotational Concentric Rheometer

An important aspect of polymer rheology is the study of the viscoelastic behaviour of the molten polymer. Most polymeric materials are said to be rheologically viscoelastic, i.e. possess a combination of viscous (representing liquid – loss of energy) and elastic (representing solid – storage of energy) components. Concentric plate rheometers are commonly used to study the viscoelastic properties of polymers *(Dealy and Wissbrun, 1995)*. Typically, these rheometers are also used in industry for quality control purposes because experimental data from these rheometers is relatively fast to collect and able to reveal structural information *(Dealy and Wissbrun, 1995)*.

The parallel plate rheometer shown in Figure 2.1 is one of the most versatile rheometers available for rheological analysis. In this rheometer, two plates are mounted on a common axis of symmetry, and the sample is inserted in the space between them. The upper plate is rotated at a specified angular velocity $\omega(t)$ and as a result the sample is subjected to shear. The motion of the upper plate is programmed, and the resulting torque, M, is measured (so called constant strain rheometers). Another mode of operation is fixing the torque and measuring the displacement (constant-stress rheometers).

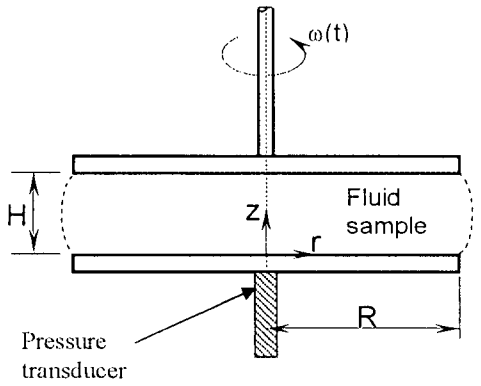

Figure 2.1 Schematic of a parallel plate rheometer.

Since most polymeric materials are said to be rheologically viscoelastic, if sufficiently large strain is applied, it is possible to break the structure or elastic component of the material, resulting in purely viscous flow. This is the simplest type of test possible on this rheometer, leading to determination of bulk viscosity of the sample or its characterization in terms of one of the several non-Newtonian flow models.

The real power of this instrument lies in its ability to apply very small amount of deformations in dynamic or oscillatory fashion, without breaking the elastic structure of the sample. This is known as linear viscoelastic characterization of the material and provides very useful information about the morphology of the material.

In addition, the rheometer can also carry out creep analysis (slow deformation of material, measured under constant stress) and stress relaxation (stress response of the material under constant strain). Creep analysis is useful for predicting effects such as sedimentation, sagging and leveling. The stress relaxation is mainly used as a quality control tool.

Since the oscillatory linear viscoelastic characterization is the most important and useful test, a brief overview of it is presented here. In this test, a very small shear strain is applied to the sample sinusoidally – this is similar to vibrating the sample within its linear elastic range, and the stress response of the sample is observed. Since viscoelastic sample is composed of viscous and elastic component, the elastic or solid component is expected to follow Hook's law, where stress is directly proportional to strain – leading to stress responses 'in phase' with the applied sinusoidal strain. The viscous or liquid component on the other hand, tends to follow Newton's law, where stress is directly proportional to shear rate and not strain – leading to stress responses completely 'out of phase' to the applied strain. This is explained schematically in Figure 2.2.

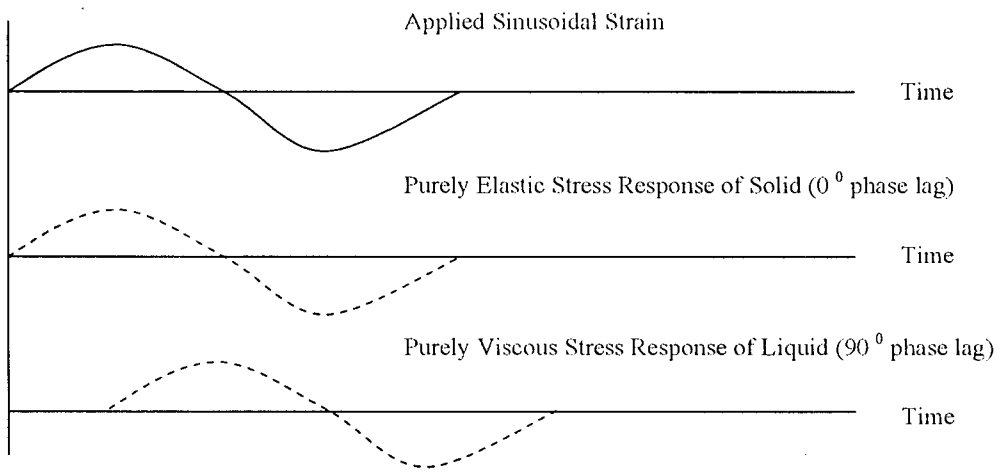

Figure 2.2 Oscillatory linear viscoelastic characterization.

In practice, most materials are a combination of viscous and elastic components and so the measured phase angle (δ) will be somewhere between 0^0 and 90^0. Since in this test, stress and strain are constantly changing, the viscoelastic properties are described in terms of Elastic (storage) Modulus (G') and Viscous (Loss) Modulus (G'') defined below. Applied sinusoidal strain can be represented as:

$$\gamma(t) = \gamma_0 \sin(\omega t) \tag{2.1}$$

where γ_0 is the strain amplitude and ω is the frequency. The stress response can be shown as:

$$\sigma(t) = \sigma_0 \sin(\omega t + \delta) \tag{2.2}$$

where σ_0 is the stress amplitude and δ is a phase angle shift in the response. Using a trigonometric identity, one can rewrite equation 2.2 in the following form:

$$\sigma(t) = \gamma_0\left[\frac{\sigma_0}{\gamma_0}\cos(\delta)\sin(\omega t) + \frac{\sigma_0}{\gamma_0}\sin(\delta)\cos(\omega t)\right] \tag{2.3}$$

From equation 2.3, we can define the dynamic moduli as $G' = \left[\frac{\sigma_0}{\gamma_0}\cos(\delta)\right]$ and $G'' = \left[\frac{\sigma_0}{\gamma_0}\sin(\delta)\right]$.

There are two other parameters that are frequently used to present the test results. These are complex modulus (G^*) and complex viscosity (η^*), defined as

$$G^* = G' + iG'' \tag{2.4}$$

$$\eta^* = \eta' - i\eta'' \tag{2.5}$$

where, $\eta' = \frac{G'}{\omega}$ and $\eta'' = \frac{G''}{\omega}$.

As mentioned earlier, the oscillatory tests are very sensitive to the molecular structure of the polymer sample. Figure 2.3 *(Dealy and Wissbrun, 1995)* shows the indicative plot of storage modulus for three samples of a linear polymer. It may be observed that at high frequencies, glassy behaviour is exhibited. At smaller frequencies, molecular rearrangement becomes possible and there is a transition zone. For the low molecular weight materials (A) such transition zone does not exist and we move to the terminal

zone directly. For the higher MW sample (B), we have a plateau zone. The plateaue zone is not clear for polydisperse material (C).

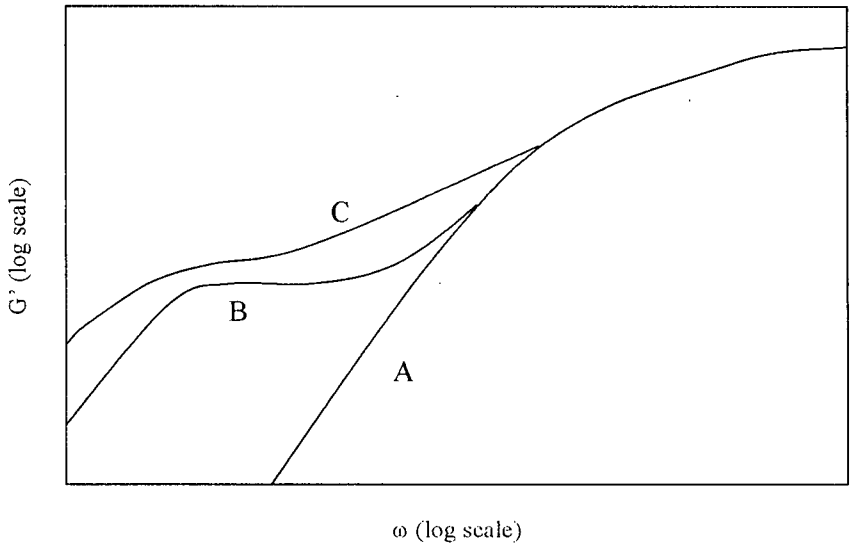

Figure 2.3 Indicative plot of G'(ω) for three samples of a linear polymer. (A) is monodisperse with low MW, (B) is monodisperse with high MW, and (c) is polydisperse with high MW *(Dealy and Wissbrun, 1995)*.

There are a few interesting features of typical linear viscoelastic plot for polyethylene such as the one shown in Figure 2.4. It may be observed that at small frequencies (terminal zone) G' tends to become proportional to ω^2 (slope of ~ 2) whereas G" is proportional to ω (slope of ~ 1). It may also be noted that at low frequency, G" > G', implying a liquid like behaviour. At higher frequency, a crossover takes place indicating the start of the rubber like behaviour.

Several empirical relationships between molecular structure and linear viscoelastic properties have been proposed for linear polymers. No such relationships have been proposed for branched polymers because of the difficulty of seperating the effects of the

degree and the type of branching from that of molecular weight distribution *(Dealy and Wissbrun, 1995; Münstedt, 1980).*

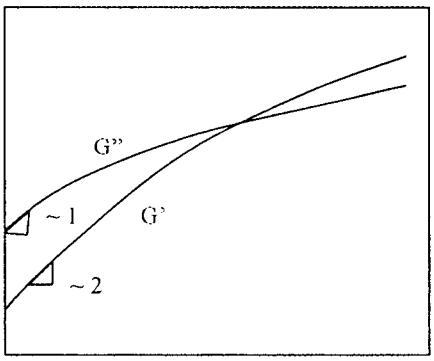

Figure 2.4 Indicative plot of G'(ω) and G" (ω) for polyethylene.

2.1.2 Extensional Rheometer

Another important method in characterizing polymeric material is to study its behaviour under extensional deformation. In this kind of experiment, the ends of a polymer sample are stretched apart at relatively high extensional rates. This high extensional rate subjects the polymer under non-linear deformation, which helps us to understand and reveal structural information that is otherwise impossible to obtain from linear viscoelastic data. For example, molecular distribution and degree of long branching may have the same effect on the linear viscoelastic properties of a polymer. However, these effects may be separated by studying the sample's behaviour under extensional flow *(Münstedt, 1980).*

A schematic of the extensional rheometer used in this study is shown in Figure 2.5.

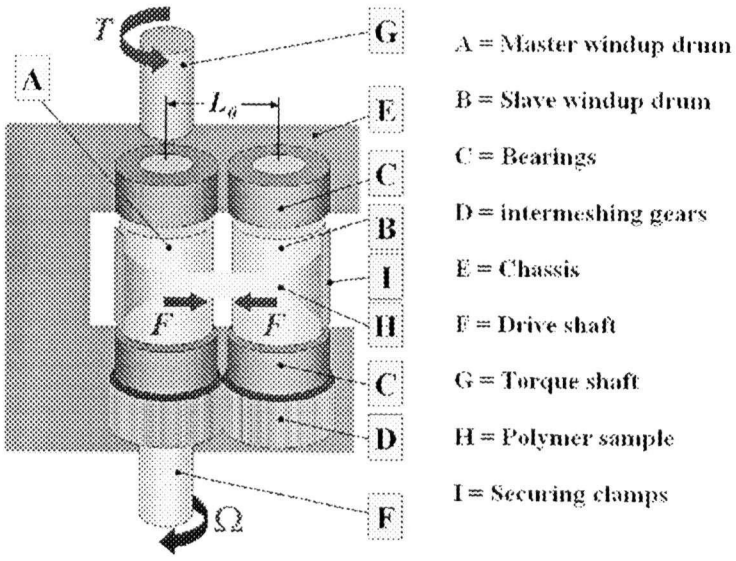

Figure 2.5 Schematic of Sentmanat Extensional Rheometer *(Sentmanat, 2003a).*

This extensional rheometer is designed for use as a detachable fixture on commercially available rotational rheometer host systems, whose main function is described in previous section. As such, this rheometer is able to fit within the host oven chamber, and thus allows temperature-controlled testing.

The extensional rheometer consists of master and slave windup drums. Rotation of the master drum by an angular speed, Ω, results in an equal but opposite rotation of the slave drum. This causes the ends of the affixed sample to be wound up onto the drums resulting in the sample being stretched over an unsupported length, L_o. For a constant drive shaft rotation rate, Ω, the Hencky strain rate applied to the sample specimen can be expressed as *(Sentmanat, 2003b)*

$$\dot{\varepsilon}_H = \frac{2\Omega R}{L_o} \tag{2.6}$$

where R is the radius of the windup drums, and L_o is the fixed, unsupported length of the specimen sample being stretched which is equal to the centerline distance between the master and slave drums.

The material's resistance to stretch is observed as a tangential force, F, acting on the drums which is then translated as a torque upon the chassis housing the assembly. The resultant torque transmitted through the chassis to the torque shaft is determined from the summation of moments about the axis of the torque shaft. This yields *(Sentmanat, 2003b)*

$$T = 2(F + F_F)R \tag{2.7}$$

where T is the resultant torque measured by the torque transducer, and F_F is the frictional contribution from the bearings and intermeshing gears. With precision bearings and gears, the frictional term is typically quite small (< 2% of the measured torque signal) and can be neglected such that equation 2.7 may be simplified to *(Sentmanat, 2003b)*

$$T = 2FR \tag{2.8}.$$

For polymer melts, if there is no deviation between the nominal and actual strain rates, the instantaneous cross-sectional area, A(t), on the stretched material changes exponentially with time for a constant Hencky strain rate experiment and can be expressed as *(Sentmanat, 2003b)*

$$A(t) = A_o \exp[-\dot{\varepsilon}_H t] \tag{2.9}$$

where A_o is the initial cross-sectional area of the unstretched specimen. For a constant Hencky strain rate, the tensile stress growth coefficient, $\eta_E^+(t)$, of the stretched sample can then be expressed as *(Sentmanat, 2003b)*

$$\eta_E^+(t) = \frac{F(t)}{\dot{\varepsilon}_H A(t)} \tag{2.10}$$

where F(t) is the instantaneous extensional force at time t exerted by the sample as it resists stretch.

2.1.3 Capilary Rheometer – Capillary Die

Flow of molten polymer through a tube or a channel under pressure is commonly encountered in polymer processing, for example in an extrusion die or in the runner feeding of an injection mold. A capillary rheometer simulates this type of flow behaviour. Capillary rheometers are also used widely to determine the viscosities in the shear rate range of 5 to 5000 s^{-1} *(Dealy and Wissbrun, 1995)*. Reproducibility of capillary rheometer experiments is typically ± 5%. In the present research work, capillary rheometer is primarily used to extrude pure polyethylenes and blends of polyethylene mixed with different polymer processing aids to study the effect of these polymer processing aids in eliminating / postponing the appearance of melt fracture at a given shear rate.

The capillary rheometer consists of a melt reservoir or barrel in which the polymer is melted and a plunger or piston that forces the melt to flow through a die of known

measurements (e.g diameter, D,or length, L). The quantities normally measured are the volumetric flow rate, Q and the driving pressure, P_d. A schematic diagram of the rheometer and the capillary die is shown in Figure 2.6.

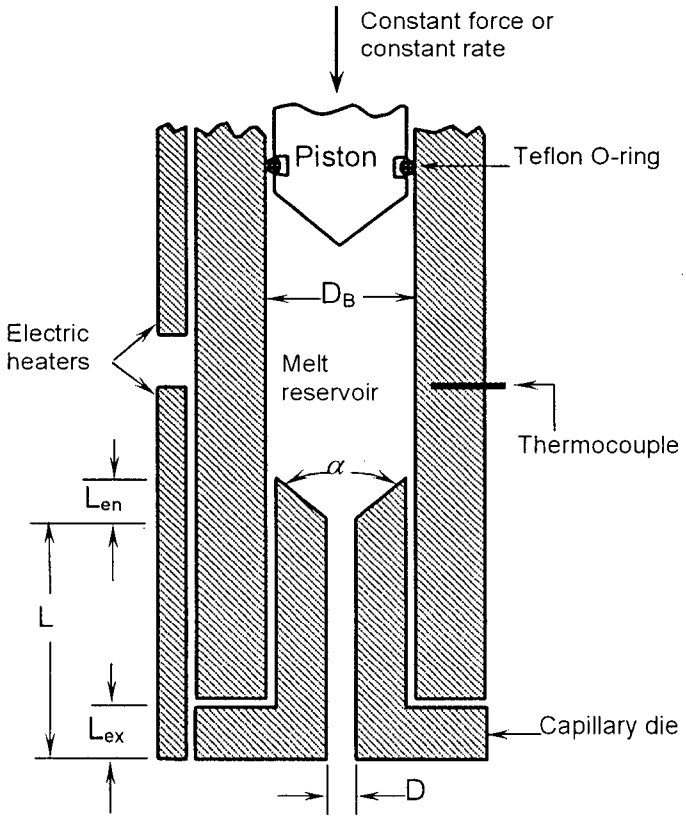

Figure 2.6 A schematic diagram of ROSAND Capillary Rheometer fitted with a capillary die.

For this particular flow, simple equations can be derived to determine shear viscosity as far as Newtonian and power law fluid is concerned. For other types of fluid, where no specific constitutive equation is known to be valid, special computational techniques are required to calculate the shear stress, shear rate and viscosity.

For a steady and fully developed flow of an incompressible fluid in a tube of radius R, a force balance can be performed to yield the absolute value of shear stress at the tube wall, σ_w:

$$\sigma_w \equiv -\sigma_{rz}\Big|_{r=R} = -\frac{\Delta P_w . R}{2L} \tag{2.11}$$

where ΔP is the pressure drop over the length of the tube, L. For a Newtonian fluid, shear stress is related to deformation by:

$$\sigma = \eta \dot{\gamma} \tag{2.12}$$

where the viscosity η, is constant at a given temperature. Combining Equations 2.11 and 2.12, the fully developed parabolic velocity profile of Newtonian fluid can be obtained.

Knowing the velocity profile, the shear rate at the tube wall can be calculated by differentiating the velocity profile with respect to the radius of the tube to yield:

$$\dot{\gamma}(Newtonian) = \frac{dV}{dr}\Big|_{r=R} = \frac{4Q}{\pi R^3} \tag{2.13}$$

where Q is the volumetric flow rate.

For non-Newtonian fluids, the same velocity profile cannot be used to derive the equation for shear rate. A different constitutive equation is also needed to determine the viscosity of the fluid, which is no longer a constant.

If a power law model is assumed, the constitutive equation is given by:

$$\sigma = K\dot{\gamma}^{n} \tag{2.14}$$

where K and n are the consistency index and the power law exponent, respectively. Note that the special case of Newtonian flow behavior is recovered for $n=1$. It can be shown that the wall shear rate for a power law fluid is given by *(Dealy and Wissbrun, 1995)*:

$$\dot{\gamma} = \frac{3n+1}{4n}\left(\frac{4Q}{\pi R^3}\right) \tag{2.15}.$$

It is noted that the term in parentheses in the above equation is the wall shear rate for a Newtonian fluid (Equation 2.8). This term in itself has no significance in the non-Newtonian case. It is, however, referred to as the 'apparent shear rate', $\dot{\gamma}_A$.

Using Equation 2.14 and 2.15, it can be shown that

$$\sigma_w = K\left(\frac{3n+1}{4n}\right)^{n} \cdot \left(\dot{\gamma}_A\right)^{n} \tag{2.16}.$$

The constants K and n can be determined from the intercept and the slope of the straight-line plot of the above equation in a double log scale.

If no specific constitutive equation is assumed, it is then not possible to calculate the true shear rate at the wall directly, knowing only $\dot{\gamma}_A$. A special technique which requires pressure drop data for a number of flow rates is needed. This technique makes use of the fact a plot of $log(\sigma_w)$ versus $log(\dot{\gamma}_A)$ yield a single curve. The true wall shear rate is then given by

$$\dot{\gamma}_w = \left(\frac{3+b}{4}\right) \cdot \dot{\gamma}_A \tag{2.17}$$

where b is the Rabinowitsch correction given by

$$b = \frac{d\left(\log \dot{\gamma}_A\right)}{d\left(\log \sigma_w\right)} \tag{2.18}.$$

This correction term measures the fluid deviation from Newtonian behaviour. It equals unity for a Newtonian fluid and $1/n$ for a power-law fluid. A large number of data is needed for this technique since differentiation is required to determine b.

In a capillary rheometer, the shear stress is determined by monitoring the driving pressure, P_d, in the barrel and assuming that the pressure at the outlet of the capillary is equal to the ambient pressure, P_a. P_d can be related to the force that is driving the piston (plunger), F_d, as:

$$P_d = \frac{F_d}{\pi R_b^2} \tag{2.19}$$

where R_b is the radius of the barrel. The pressure drop ($-\Delta P_w$) in Equation 2.11 is then given by (P_d-P_a) or, since for melts P_d is nearly always much larger than P_a, the pressure drop can simply be replaced by P_d. However, this is not the actual pressure drop that is observed for a fully developed flow in a capillary of length L. End correction is needed to take into account the large pressure drop at the entrance of the capillary and the small residual pressure at the exit. Figure 2.7 shows the pressure profile for a flow in a capillary.

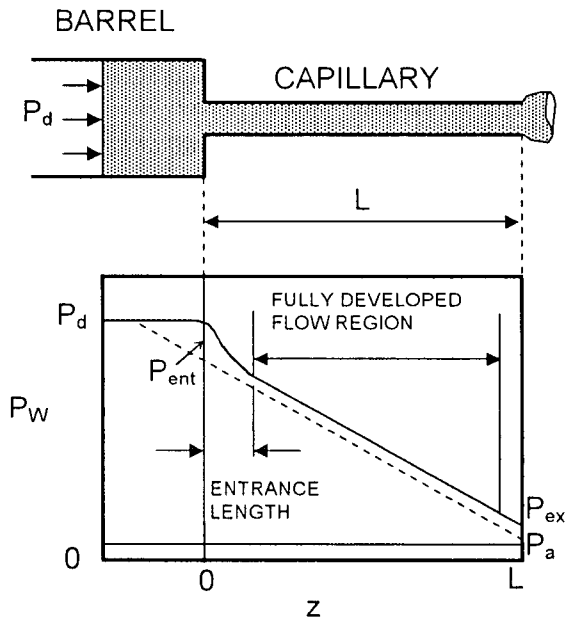

Figure 2.7 Pressure profile for a flow in a capillary.

The pressure end correction can be determined as outlined by *Bagley (1931)* in which the driving pressure, P_d is plotted versus the length to diameter (L/D) ratio of capillaries of

fixed diameter for each value of wall shear rate. This plot is also referred to as the 'Bagley plot'. A typical Bagley plot is shown in Figure 2.8. The end correction is obtained by extrapolating the plot to $L/D=0$ (another way of determining P_{end} is by making use of an orifice die with $L=0$). Using the corrected pressure drop, the wall shear stress can then be calculated as

$$\sigma_w = \frac{(P_d - P_{end})}{4(L/D)} \qquad (2.20).$$

In general, the Bagley plot may include some curvature at high L/D ratio. This is due to the dependence of viscosity on pressure, slip at the die wall or viscous heating *(Hatzikiriakos and Dealy, 1992)*.

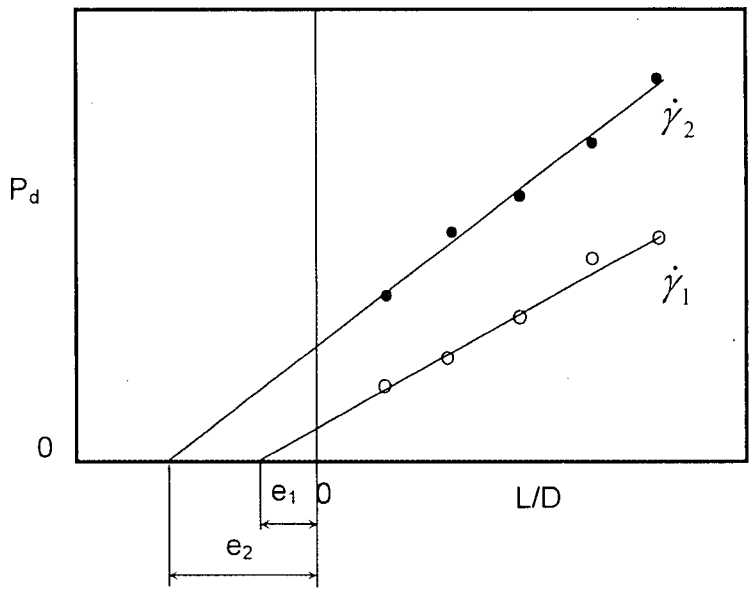

Figure 2.8 A typical Bagley plot.

2.1.4 Capilary Rheometer – Crosshead Die

In addition to capillary die, a crosshead die can also be used to assess the processability of the various polyethylenes and their blends with the polymer processing aids. The schematic of the crosshead is shown in Figure 2.9.

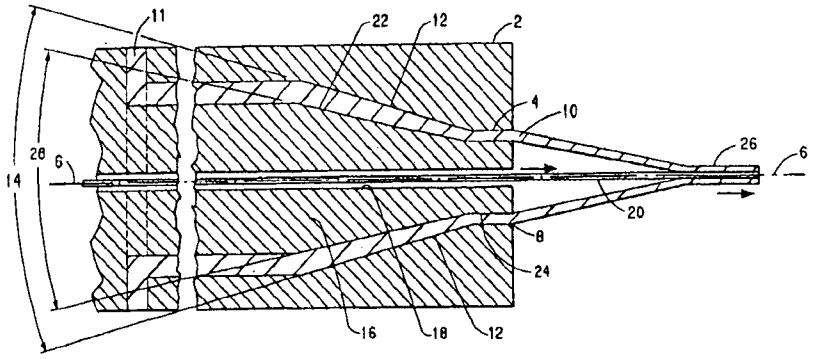

Figure 2.9 Crosshead die for wire coating *(Buckmaster et al, 1997)*.

The molten polymer enters the port 11 of the die 2. Then the polymer is guided through to orifice 8 by the wire guide 16. The interior and the exterior surface of the wire tubular shape are formed by the passage 24 and 4 respectively. The wire guide provides a channel as a mandrel to produce the tubular shape extrudate (10). Polymer reaches orifice 8 and draws down to a thinner cross-section, making a thin coating 26 on the wire. Wire was not used in our study. Therefore, a hollow shape extrudate was obtained during the experiment.

The apparent shear rate for this crosshead die can be calculated by using the formula applied for slit dies having a large aspect ratio *(Bird et al, 1987)*:

$$\dot{\gamma}_A = \frac{6Q}{0.25(D-d)^2 0.5\pi(D+d)} \tag{2.21}$$

where Q is the volumetric flow rate, d and D are the tip and die diameters respectively. The apparent wall shear stress is estimated as the average of the shear stress at the inner and outer walls by using the following formula which is based on the assumption of a power-law fluid *(Bird et al, 1987)*. The general formula for the shear stress distribution is:

$$\tau_{rz} = \frac{\Delta P D}{4L}\left(\frac{2r}{D} - \beta^2 \frac{D}{2r}\right) \tag{2.22}$$

where τ_{rz} is the shear stress at radius r, ΔP is the pressure drop, L is the length of the die land, and β is the parameter depending on the geometry and the power law index.

2.2 TIME TEMPERATURE SUPERPOSITION

Rheological properties of molten polymers such as those obtained from parallel plate or capillary rheometer usually depend on temperature. This means that to obtain a complete picture of the behaviour of the polymer, experiments must be carried out at several temperatures. It is often found that rheological data measured at several temperatures can be brought together on a single master curve by means of "time-temperature superposition" *(Dealy and Wissbrun, 1995)*. This greatly simplifies the description of the effect of temperature. Furthermore, it makes possible the display on a single curve of material behaviour covering a much broader range of time or frequency than can ever be measured at a single temperature. Materials whose behaviour can be displayed in this way are said to be "thermorheologically simple" *(Dealy and Wissbrun, 1995)*.

It is found that data for different temperatures can often be superposed by introducing a shift factor, a_T, determined empirically. Thus, if one makes a plot of a rheological property versus a quantity with a time unit, a_T is obtained from the horizontal shift necessary to bring the data corresponding to a specific temperature T onto the same curve as data corresponding to another temperature T_0. For example, to superpose flow curves (shear stress versus shear rate) obtained from different temperatures, the curves have to be plotted on a shear stress versus shear rate·a_T scale. Note that no shift factor is required for quantities containing no units of time. This implies that a plot of such a quantity versus another, both containing no units of time, will be temperature independent.

The shift factor is a function of temperature, and the WLF equation has been found to be a useful correlation for a_T *(Ferry, 1980)*:

$$\log(a_T) = \frac{-C_1^0(T - T_0)}{C_2^0 + (T - T_0)} \tag{2.23}$$

where C_1^0 and C_2^0 are constants determined at T_0 for each material. This equation holds at temperatures very close to glass transition temperature, T_g. At temperatures at least 100 K above T_g, an empirical relationship, the Arrhenius equation, has been found to be valid *(Dealy and Wissbrun, 1995)*:

$$\log(a_T) = \frac{E_a}{R}\left(\frac{1}{T} - \frac{1}{T_{ref}}\right) \tag{2.24}$$

where E_a is the flow activation energy, R is the gas constant, and T_{ref} is the reference temperature. Since polyethylenes are processed at temperatures much higher than T_g, equation 2.24 is often used by rheologists.

2.3 MELT FRACTURE

Melt fracture is a term, used collectively for appearance of instability, which occurs beyond a critical shear rate in capillary, slit or annular dies during extrusion of polymers. The term melt fracture was introduced by *Tordella (1956)* because of the audible tearing noises which accompanied the distortion of the extrudate. Melt fracture is a major problem in the extrusion of polyolefins and many other commercial polymeric materials. In addition to shear rate or processing speed, it depends on various operational and geometric factors which mainly include the polymer structure and its molecular characteristics, die geometry and the process temperature.

There are various types of flow instabilities observed in the flow of polymeric liquids through capillary, slit and annular dies. These are also reflected in the apparent flow curve, determined by means of a capillary rheometer. An apparent flow curve is basically a log-log plot of the wall shear stress as a function of the apparent shear rate. Depending on the geometries of the dies and the types of polymer tested, the flow curve may exhibit different flow regions.

A typical apparent flow curve for a linear polymer such as high-density polyethylene and linear low-density polyethylene is shown in Figure 2.10. One can easily identify the five

different flow regions in the flow curve. Initially, there is a *stable* region where the extrudate appears smooth and glossy (region 1). In this region, the behavior of the melt resembles that of a Newtonian fluid and no slip boundary condition can be assumed to be valid.

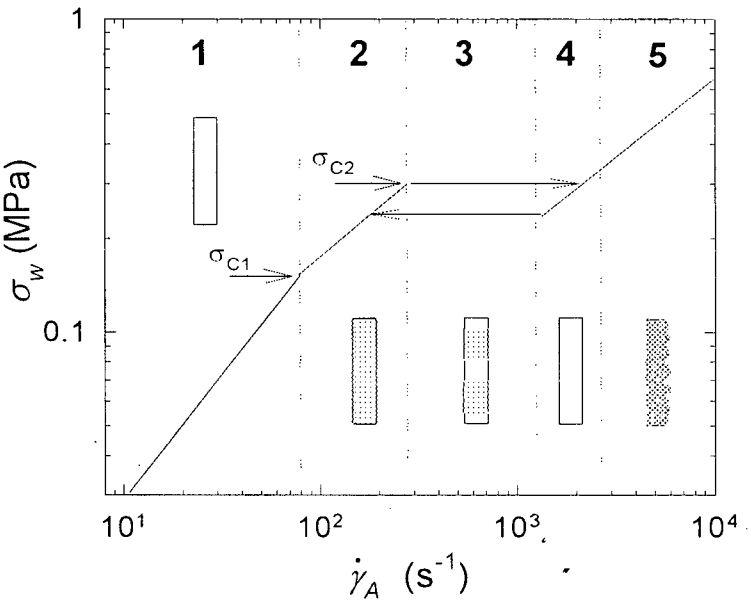

Figure 2.10 A typical apparent flow curve of a linear polymer.

Beyond some critical wall shear stress, σ_{c1}, the first visual manifestation of flow instability appears. The extrudate beyond this critical value exhibits high-frequency, small-amplitude distortion on its surface, a phenomena known as *sharkskin* (region 2). As the name implies, sharkskin is a roughness that usually modulates the extrudate diameter by no more than 1% and consists of semiregular cracks or grooves that run mainly perpendicular to the flow *(Benbow and Lamb, 1963; Piau, 1990)*. The onset of

sharkskin appears to coincide with a change in the slope of the apparent flow curve *(Achilleos et al, 2002; Hatzikiriakos et al, 1995; Kalika and Denn, 1987).*

At a second critical wall shear stress value, σ_{c2} and within a certain range of apparent shear rates, the flow ceases to be stable (region 3). This is the region of *oscillating* or *stick-slip* melt fracture where the extrudate exhibits alternating smooth and distorted portions. In this region, the extrusion pressure oscillates between two extreme values. The periodic variations of the pressure define a hysteresis loop that connects the two branches of the apparent flow curve. Despite the scatter in the reported values of the second critical shear stress, it is generally accepted that gross melt fracture is a basic characteristic of polymer systems. The greater the molecular weight and the narrower its distribution is, the greater the amplitude of the hystersis loop (*Lin, 1985; Myerholtz, 1967).*

At higher throughputs, there is sometimes a transition to a second stable flow regime in which the extrudate again becomes smooth. This is called the *superextrusion* region (region 4).

Finally, at still higher shear rates, melt fracture takes the form of a wavy chaotic distortion, commonly called *gross melt fracture.* Gross melt fracture gradually becomes more severe with an increase in apparent shear rate $\dot{\gamma}_A$ (region 5).

This typical behavior has been observed in the capillary die extrusion of many linear polymers such as high density and linear low-density polyethylene *(Kalika and Denn, 1987)*, polytetrafluoroethylene *(Tordella, 1969)*, polybutadiene *(Vinogradov et al, 1972)*, and others. Different behaviour is observed for highly branched polymers, for example LDPE, or if extrusion is carried out through a die of different geometry, for example through a crosshead die.

2.4 MECHANISMS TO EXPLAIN MELT FRACTURE

As a result of the large number of research work and the use of sophisticated flow visualization techniques, there is a general agreement among the researchers about the causes of two types of melt fracture – Sharkskin Melt Fracture (SMF) and Gross Melt Fracture (GMF).

2.4.1 Die exit effects: Sharkskin / Surface Melt Fracture (SMF)

There is a general agreement about the site of initiation of sharkskin which is located at the die exit. The first theory about surface melt fracture (sharkskin) was proposed by *Howells and Benbow (1962)* and later by *Cogswell (1977)*. They hypothesized that the polymer fractures due to high stretching rates and to high stresses as a result of the abrupt change (shear to free surface flow) in the boundary condition at the exit of the die. The melt leaving the die in the neighborhood of the wall experiences a large, rapid, tensile deformation as the velocity field adjusts from the no-slip boundary condition to the free-surface condition. Polymer chains are stretched during the tensile deformation, which

causes the highly entangled polymer to respond like a rubber. The large stresses on the free surface cause the cracks to open up giving them the appearance of sharkskin.

There are several other views available on the origin of sharkskin. However, this original proposition of fracture at the die exit as the cause of sharkskin has been substantiated by the microscopic flow visualization observations made by *Migler et al (2001a)*. Figure 2.11 presents a schematic view of the surface melt fracture taking place at the die exit. If the dynamics of polymer melt movement near the die exit were analyzedd, as shown in Figure 2.11, it is realized that inside the die, there is a typical boundary layer velocity distribution having zero or a small sliding velocity close to the wall and maximum at the centre. Outside the die, the velocity distribution is uniform throughout the cross-section as there is no resistance to flow. Therefore, as the melt is extruded out of the die, it experiences a sudden jump in velocity near the die exit leading to large extensional stresses on the polymer surface which result in the surface distortion or sharkskin. In short, the absence of lubrication at the die exit is considered as the main cause of sharkskin.

The original findings by *Howells and Benbow (1962)* and *Cogswell (1977)* on the theory of sharkskin initiation are also supported by other researchers. *Bergem (1976)* carried out capillary experiments for different polymers, using a tracer technique. He found that sharkskin arose from a tearing of the melt at the exit of the capillary. *Piau et al (1988)* showed that cracks on the surface of extrudate always originate at the exit of the die. It should be noted that the existence of localized stresses at the die exit is also confirmed by

birefringence photographs *(Vinogradov and Malkin, 1980)*. *Tremblay (1991)* simulated the flow of a linear polydimethylsiloxane melt and showed that high stresses at the die exit produce negative hydrostatic pressure. He suggested that cavitation should occur very close to the die lip, thus leading to surface effects.

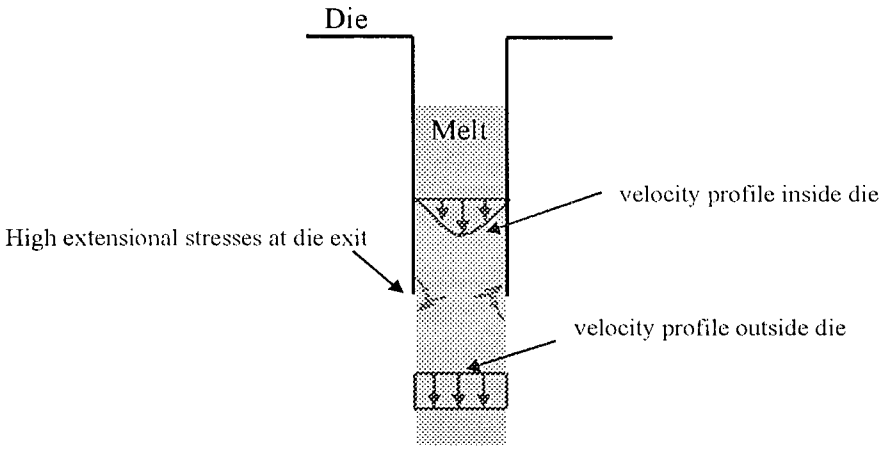

Figure 2.11 Schematic view of surface melt fracture occurring at the die exit.

Kurtz (1992) suggested that two critical conditions are required for sharkskin. First, a critical value of the wall shear stress must be exceeded and, second, the extrudate must be stretched for a sufficient period of time as it leaves the die. *Moynihan et al (1990)* added to this conclusion that the melt should be first "pre-stressed" critically at the entry region of the die.

Ramamurthy (1986) suggested that the onset of sharkskin was accompanied by the occurrence of wall slip in the capillary. This suggestion is supported by a noticeable slope change in the flow curve at the onset of sharkskin *(Kurtz, 1984)* which can be

interpreted as slip. However, *Piau and El Kissi (1992)* argued that slip in the die cannot explain the origin of the sharkskin. *Hatzikiriakos (1994)* carried out numerical simulations of the flow of high density and linear low density polyethylenes under slip conditions and showed that slip is not a necessary condition for the occurrence of the sharkskin phenomenon, although it may affect it. Instead, a critical extension rate at the capillary exit and a critical pre-stress of the polymer at the land region of the die provide the necessary conditions for its occurrence.

Wang et al (1996) speculated that the slope change in the flow curve arises from a combination of interfacial slip and cohesive failure due to chain disentanglement initiated on the die wall in the exit region. Since the disentanglement state is unstable for the adsorbed chains, it is followed by a consequent re-entanglement, thus producing entanglement-disentanglement fluctuations that cause the sharkskin phenomenon. However, perhaps the most significant finding made by *Wang et al (1996)* was that the sharkskin dynamics is in good correlation with chain relaxation process. They used capillaries of different diameter and measured the period of surface distortions. Regardless of the capillary geometry, the period of surface distortions was found to be directly proportional to a polymer characteristic relaxation time, which was determined as an inverse of the crossover frequency of the storage and loss moduli.

Sharkskin does not occur for all polymers *(Denn, 1990)*, and for those for which it does occur, the onset condition has been found to depend on various operational and geometric factors which include die design and geometry, the structure of the polymer and its

molecular characteristics and the process temperature. Melt fracture is most easily observed during extrusion at high throughputs through a long die *(Moynihan et al, 1990)*. In some cases, the material of construction of the die may also affect the melt fracture behaviour of the polyethylene *(Ramamurthy, 1986; Hatzikiriakos and Dealy, 1991)*. Usually, the critical shear rate or shear stress decreases with an increase in process temperature *(Kurtz 1992)*.

2.4.2 Wall Slip Effects: Stick-slip

There is a second critical stress at which periodic pressure pulsations are frequently observed. The extrudate surface alternately shows relatively smooth and sharkskin regions. This is known as *stick-slip*, or *spurt* flow. In this region, the average stress remains approximately constant in the stick-slip region. Although this phenomenon has been reported by several authors *(Tordella, 1963; Myerholtz, 1967)*, the mechanism of the initiation of this oscillation has not been explained thoroughly.

Both *Lin (1985)* and *Myerholtz (1967)* who performed studies on the oscillating flow in different polyethylene samples, reported that oscillating melt fracture occurs more prominently in polymers that have narrower molecular weight distribution or higher molecular weight, or if the experiments were done at lower operating temperature or using longer dies. *Tordella, (1963)* suggested that this oscillating phenomenon is precipitated by slippage of the melt at the capillary wall. This explanation was further justified by experiments done by *Lupton and Regester (1965)*.

Probably the best explanation for stickslip melt fracture was given by *Leonov (1984)*. He explained that as polymer is extruded through a die, the shear stress increases up to a certain level (upper extreme value of shear stress) above which the polymer starts to slip. This slippage instantaneously reduces the stress level to a lower value (lower extreme value of shear stress) that causes the shear stress to increase again. This process repeats itself, thus resulting in an oscillating flow where the stress level varies between two extreme values. This oscillating flow occurs until the shear rate is increased to a value that is large enough to promote total wall slip. This explanation also helps in understanding the occurrence of stick-slip only in linear polymers. In non-linear polymer, such as LDPE, there is significant branching that allows the polymer to stick to the die wall, thus preventing wall slip.

In an interesting observation, *Pudjijanto and Denn (1994)* as well as *Waddon and Keller (1990, 1992)* found a stable "island" in the stick-slip region of polyethylene, where pressure oscillations stopped, extrusion pressure significantly dropped, and the extrudate became reasonably smooth. This island exists only in a narrow temperature window and a small variation of temperature, e.g. of the order of 1°C, can interchange oscillations with a stable response.

2.4.3 Die Entry Effects: Gross Melt Fracture (GMF)

Most authors agree in claiming that above a certain extrusion rate, the flow upstream of the die contraction becomes unstable. These instabilities occur in the form of sudden pulsations or cavitation which were confirmed by visualization *(Piau et al, 1990;*

Kazatchkov et al, 2000; Son and Migler, 2002) and birefringence measurements *(Tordella, 1969)*. They showed that such instabilities started along the upstream flow axis owing to the high elongation stresses that develop in this area. These instabilities trigger the phenomenon of gross melt fracture, which is often seen in the form of a regular helix oscillating at the same frequency as that of the pulsations of the upstream elongational flow *(Piau et al, 1990)*. It is then generally accepted that gross melt fracture is a die entrance phenomenon.

Figure 2.12a shows the flow visualization of virgin PP at various shear rates in the die entrance region, carried out by *Kazatchkov et al (2000)*. It can be observed that as the melt flow rate increases, flow streamlines are no longer smooth ($\dot{\gamma}_A$= 650 s^{-1}). By observing the above visualization in a movie format, it can be readily seen that at higher rates, the flow is discontinuous with breaks in the motion, causing the zigzag streamlines. A schematic in Figure 2.12b explains this flow pattern at higher rate. The flow in the die entry region appears to be broken into several layers, and each layer moves with its own velocity. At regular time intervals, different in each layer, the motion stops for a brief period. The frequency of flow and stops are higher in the layers close to the centre of the stream. This instability observed in the form of discontinuous streamlines is believed to be caused by the absence of lubrication in the bulk of the polymer melt resulting in the form of severe distortions or gross melt fracture.

Further evidence that gross melt fracture is initiated at the die entrance is presented by *Kalika and Denn (1987)* and Piau *et al (1990)*. Their studies show that gross melt

fracture occurs when the wall shear stress reaches a critical condition that seems to depend only on the polymeric fluid and little or not at all on the characteristics of the die (diameter, length, and the material of construction).

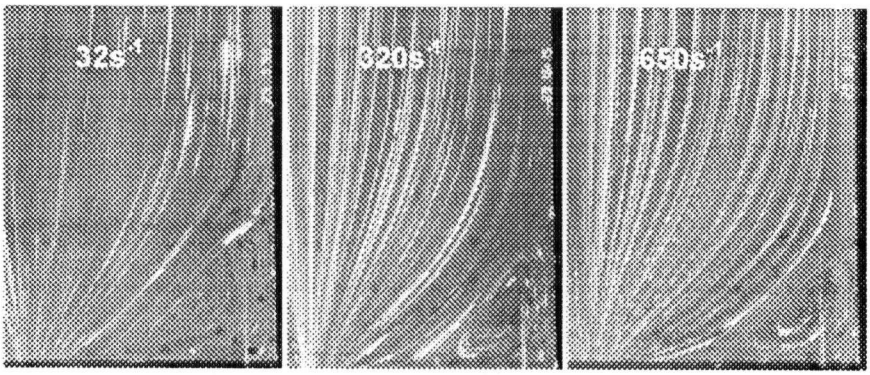

(a)

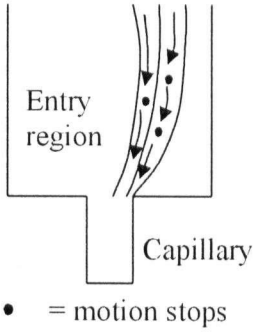

(b)

Figure 2.12 a) Pictures of the flow of polypropylene at various apparent shear rates of 32 s^{-1}, 320 s^{-1} and 650 s^{-1} at 200°C *(Kazatchkov et al, 2000)*. b) A schematic diagram illustrating the unstable flow development in the die entrance region.

2.5 POLYMER PROCESSING AIDS (PPAs)

As discussed earlier, melt fracture poses an undesirable constraint on the rate of production. It is necessary to eliminate melt fracture or postpone it to higher rates in order to increase the rate of production. Typically, polymer processing aids are used to improve the processability of polymers. PPAs are usually used in small quantities of the

order of about 1000 ppm *(Hatzikiriakos, 2004a)*. Typical polymer processing aids are fluoropolymers, stearates and certain waxes which have been used traditionally for surface melt fracture elimination *(Hatzikiriakos, 2004a)*.

2.5.1 Fluoropolymer – Based Processing Aids

Fluoropolymer-based PPAs have a good affinity with the die wall and thus a tendency to create a fine coating on the die wall during extrusion. The extruding polymer then slips along the smooth coating on the die, thus eliminating the surface melt fracture *(Rudin et a,l 1985; Anastasiadis and Hatzikiriakos, 1998; Denn, 2001; Migler et al, 2001a; Achilleos et al, 2002)*. This in turn also reduces the extrusion pressure.

Priester and Stewart (1992) suggested that the factors that may affect the performance of the processing aid include the level of additive, dispersion quality and the interaction with other ingredients (antioxidants and stabilizers) in the resin. They also mentioned that a large number of small particles of the additive can result into a better dispersion quality than a small number of large particles. It was also reported that a masterbatching step was required in order to provide a good quality of dispersion of additives into the resin.

This view, however, has recently changed through the work of *Oriani and Chapman (2003)*. It was demonstrated that large fluoropolymer particles dispersed into the polymer, coat the die easier and faster. This allows melt fracture to be eliminated faster. *Rudin et al (1985)* performed experiments to study the effect of Dynamar^{TM}, a fluoropolymer-based processing aid, on the processability of LLDPE. He found that the

presence of Dynamar™ at the die surface causes the polymer to slip and that the slip velocity increases with increasing concentration of fluoropolymer in the resin. An examination on the surface of the extrudates was also done by using an X-ray photoelectron spectroscopy (ESCA) to detect the levels of fluorine. In addition, the extrudates were fractured in liquid nitrogen and the cross section was analyzed to measure the fluorine concentration. The data indicated that a measurable concentration of fluorine at the surface exists, while the average concentration through the cross section of the extrudate was too low for the ESCA reading. From these data, one may suggest that processing aid such as Dynamar™ adheres at the die/metal interface. Dynamar™ then acts as a lubricant and as a result reduces the driving pressure of extrusion. This observation was also supported by the work of *Migler et al (2001a, 2001b)* who used stroboscopic optical microscopy to image the coating process of fluoropolymer additive onto the capillary wall. From the experimental images, the authors also demonstrated that the slip occurred at the interface between the polyethylene and the fluoropolymer, indicating that the two polymers were fully disentangled.

In an interesting study done by *Kharchenko et al (2003)*, it was found that initial fluoropolymer coating of the die actually took place at the entrance region. Shear induced migration then results in the processing aid to gradually and slowly propagate along the die wall towards the die exit with a certain migration speed. This migration speed depends on the flow rate and the initial thickness of the processing aid coating *(Kharchenko et al, 2003)*.

In the extrusion of a polyolefin with the aid of fluoropolymer, proper die conditioning was found to be a necessity to observe the full effect of the processing aid *(Kazatchkov et al, 1995)*. Transient capillary experiments done by *Kazatchkov et al (1995)* showed that the first few initial extrusions of polypropylene through TEFLON®-coated capillary die resulted in a gradual decrease of the wall shear stress. After a long induction time (about six extrusions), it was noticed that the wall shear stress leveled off, indicating that equilibrium condition was reached.

In general, fluoropolymer based processing aid reduces the pressure required to extrude the resin at a particular flow rate and eliminate or postpone surface melt fracture to higher extrusion rates. Note that these additives can eliminate only sharkskin and the so-called stick-slip (oscillating or cyclic) melt fracture. They do not appear to have an effect on the extrudate appearance in the gross melt fracture region *(Rosenbaum et al, 1998a)*.

2.5.2 Boron Nitride – Based Processing Aids

It has been reported that certain Boron Nitride (BN) based compositions may act as effective processing aids in the extrusion of a number of fluoropolymers and polyolefins *(Buckmaster et al, 1997; Rosenbaum et al, 2000; Yip et al, 1999; Lee et al, 2000; Hatzikiriakos, 2004b)*. It has been reported that BN can successfully be used as a processing aid to eliminate not only sharkskin melt fracture but also substantially postpone gross melt fracture to significantly higher shear rates well within the gross melt fracture region.

Yip et al (1999) reported that BN is an effective processing aid when it possesses the following characteristics (i) average particle size of up to about 10μm, (ii) no agglomerations (iii) absence of boron oxides in its structure and (iv) good dispersion into the resin under process. Also, BN must be used at its optimal concentration depending on the type of polymer and the extrusion temperature. It is observed that the presence of BN does not alter the linear viscoelastic behaviour (for BN loadings < 0.5 wt. %) as well as the flow curve during extrusion of m-LLDPE. However, it was found to have a significant effect on extrudate appearance *(Rosenbaum et al, 1998a; Yip et al, 1999; Kazatchkov et al, 2000)*.

It had also been reported that the BN additive had little additional effect on the extrudate appearance in the capillary geometry (both capillary and orifice dies with different entrance angle) compared to the effect seen in the case of fluoropolymer *(Rosenbaum et al, 1998b)*. The greatest influence of the additive occurred in crosshead dies and tips where the additive particles seemed to enhance melt slippage and relieve internal stresses *(Rosenbaum et al, 1998b; Yip et al, 2000)*.

Lee et al (2000) reported that the critical apparent shear rate for onset of melt fracture and the shape of extrudate are highly dependent on processing temperature, length of die and content of the BN. They found that the addition of 0.5 wt. % of BN in m-LLDPE eliminate or delay sharkskin, stick-slip melt fracture and gross melt fracture to much higher rates, even though there is no difference in the linear viscoelastic and mechanical properties between the virgin polymer and the one containing BN.

In addition, effects of BN on the processibility of polyethylene in other processes such as blow molding *(Yip et al, 2000; Seth et al, 2000)*, film blowing *(Pruss et al, 2002)*, and fiber spinning *(Vogel et al, 2003)* has been tested. In general, the presence of BN is beneficial in these operations.

2.5.3 Fluoropolymer - Boron Nitride Based

Combining a BN powder with fluoropolymer has been reported to have an enhanced effect on melt fracture elimination. Fluoropolymers mainly act as a slip promoter, eliminating sharkskin and reducing the extrusion pressure whereas BN primarily influences the melt flow in die entrance region, delaying the gross melt fracture. The fact that these two additives act by different mechanisms for suppressing the instabilities, explains why their combination results in a synergistic effect for melt fracture elimination *(Rosenbaum, 2000; Achilleos et al, 2002)*. The study, however, pertains to metallocene polyethylenes. The interactions between fluoropolymer molecules and BN particles might be very important for the effectiveness of this combined processing aid. Since each of the constituents is desired to act differently, adsorptions of fluoropolymer on boron nitride is not desired. A thorough discussion on the subject of adsorption follows below.

2.6 ADSORPTION

2.6.1 Introduction

Adsorption exploits the ability of certain solids to preferentially concentrate specific substances from a solution onto their surfaces. The solid surface is termed as adsorbent and the component preferentially separated by the adsorbent is known as adsorbate.

There are two types of adsorption phenomenon; physical adsorption and chemisorption. Chemisorption is the result of chemical interaction and formation of chemical bond between the solid and the adsorbed substance. It is particularly important in catalytic processes and not pertinent to the present topic.

Physical adsorption is a result of intermolecular forces of attraction between molecules of the adsorbent and adsorbate. In this case, the adsorbed substance does not penetrate within the crystal lattice of the adsorbent and does not get dissolved in it but stays on the surface. Thus, this process is readily reversible. However, the adsorbate can get inside the capillaries of a porous adsorbent *(Rathod, 2003)*.

Two important physiochemical aspects of the adsorption process are the equilibria of the adsorption and the kinetics *(Rathod, 2003)*. The equilibrium studies give the capacity of the adsorbent to selectively adsorb the adsorbate. The equilibrium relations between adsorbent and adsorbate are normally described by the adsorption isotherm, representing the relationship between the quantity adsorbed and that remaining in the solutions. There are two types of adsorption isotherms: Langmuir adsorption isotherms and Frendlich adsorption isotherms.

Langmuir adsorption isotherm represents a theoretical adsorption isotherm in the ideal case. It is often used for adsorption of a solute from a liquid solution. The Langmuir adsorption isotherm can be expressed as *(Rathod, 2003)*:

$$Q_e = \frac{X_m K_L C_e}{1 + K_L C_e} \qquad (2.25)$$

where Q_e is the adsorption density at equilibrium solute concentration (mg of adsorbate per g of adsorbent), C_e is the concentration of adsorbate in solution at equilibrium (mg/l), X_m is the maximum adsorption capacity corresponding to a complete monolayer coverage (mg of solute adsorbed per g of adsorbate), and K_L is the Langmuir constant related to energy of adsorption (l of adsorbent per mg of adsorbate).

The above equation can be rearranged to the following linear form.

$$\frac{C_e}{Q_e} = \frac{1}{X_m K_L} + \frac{C_e}{X_m} \tag{2.26}$$

The Langmuir constants X_m and K_L can be evaluated from the slope and intercept of a straight line, obtained by plotting C_e/Q_e against C_e.

Freundlich presented an empirical adsorption isotherm for non-ideal systems. The Freundlich isotherm can be expressed as *(Rathod, 2003)*:

$$Q_e = K_F C_e^n \tag{2.27}$$

where K_F and n are the empirical constants dependent on several environmental factors.

The equation can be conveniently linearized by taking logarithmic on both sides as:

$$\ln Q_e = \ln K_F + n \ln C_e \tag{2.28}$$

A plot of ln Q_e vs. ln C_e yielding a straight line indicates the confirmation of the Freundlich isotherm for adsorption. The constants can be determined from the slope and intercept.

2.6.2 Adsorption of Polyethylene and Fluoropolymer onto Boron Nitride

In an attempt to study the interaction between fluoropolymer and polyethylene on Boron Nitride, *Rathod (2003)* performed an adsorption study. In the study, a solution of mLLDPE was prepared into which a specific grade of BN was mixed (diphenyl ether (DPE) was chosen as the solvent). After allowing the mixture to reach its adsorption equilibrium, BN particles and adsorbed mLLDPE were separated from the solution by filtration. The adsorbed PE was then estimated from the change in weight of the BN. A similar experiment was done to determine the adsorption of fluoropolymer on BN. Acetone was used to make the fluropolymer solutions.

The Freundlich isotherm plot was used to summarize the adsorption of polyethylene on BN and it is depicted in Figure 2.13. From this plot, *Rathod (2003)* deduced that in general, the extent of adsorption of polyethylene onto BN surface is high. This observation was found to apply to all of the different grades of BN that were tested. This also validates his earlier inference regarding the high affinity of BN for polyethylene melt based on the surface energy study *(Rathod, 2003)*. It also suggests that during extrusion, polyethylene molecules which are adsorbed on the surface of the BN particles, incorporate BN into the bulk of the polymer system forming a possible network. This

network of polyethylene and BN disrupts the entanglement density of polyethylene and helps in eliminating gross melt fracture to a certain extent *(Rathod, 2003)*.

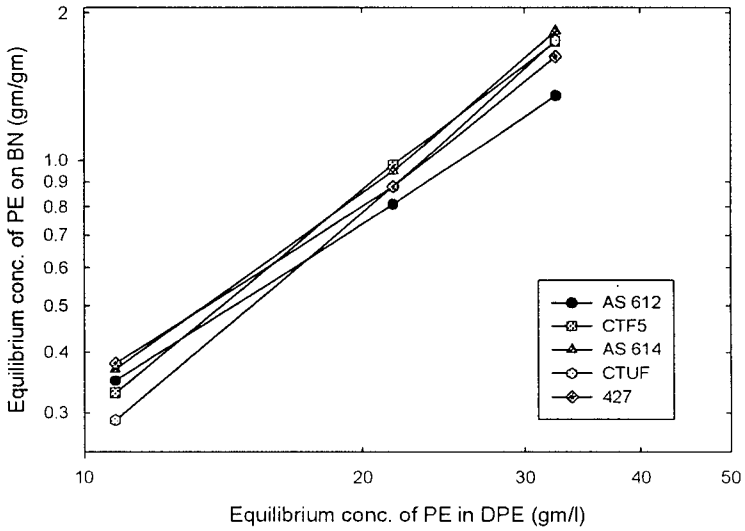

Figure 2.13 Freundlich adsorption isotherm for BN-polyethylene *(Rathod, 2003)*.

A similar experiment was done by *Rathod (2003)* to understand the interaction of fluoropolymer with BN. Figure 2.14 illustrates the results from this study.

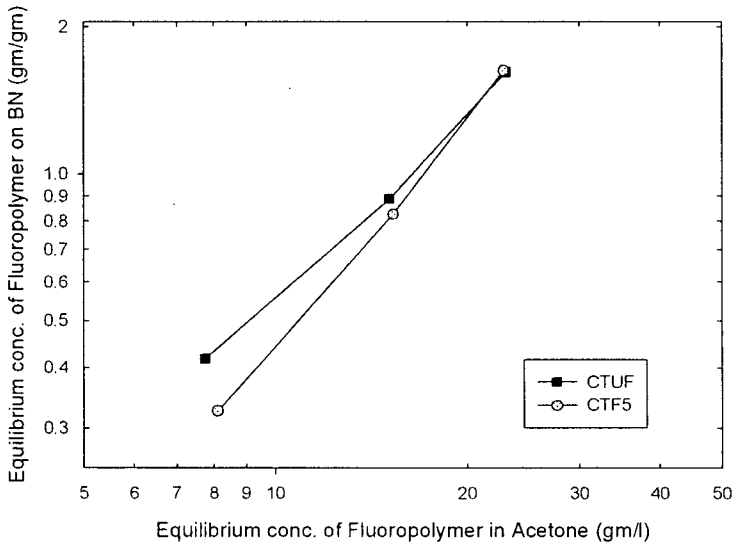

Figure 2.14 Freundlich adsorption isotherm for BN-fluoropolymer *(Rathod, 2003)*.

Again from this study, it was observed that the adsorption capacity of BN for fluoropolymer (Dynamar – FX 9613) is significant, comparable to that for polyethylene *(Rathod, 2003)*.

3 THESIS OBJECTIVES

The main objective of the present work is to study the performance of Boron Nitride-based and fluoropolymer-based polymer processing aids in the extrusion of Ziegler-Natta polyethylenes. In addition, experiments will also be done to assess the need of a masterbatch process in preparing the final polymer blends. The specific answers sought are as follows.

- How does the performance of Boron Nitride and fluoropolymer as a processing aid improve if they are used together? Will the synergistic effect shown in the extrusion of m-LLDPE be shown also in Ziegler-Natta Polyethylenes?
- How does the interaction between Boron Nitride and fluoropolymer and polyethylene affect the performance of these polymer processing aids when used together?
- Does diluting concentrates to achieve a specific level of polymer processing aid concentration result in a better performance of the polymer processing aid?

4 MATERIALS AND METHODOLOGY

This chapter describes the various types of polyethylene samples and the polymer processing aids (PPAs) used in this study. In addition, the procedures used in the determination of the rheological properties and the processability of the polyethylene resins will also be presented.

4.1 POLYMERS AND BLENDS PREPARATIONS

Six different polyethylenes were used as the base resins. Five were film grade and one was blow molding grade. The technologies used to produce the resins include gas phase and solution technology using either Ziegler-Natta catalyst or a proprietary single site catalyst developed by NOVA Chemicals Corp. The molecular characteristics of these resins are summarized in Table 4.1.

In addition to the pure resins, samples compounded with different processing aids were also supplied. Compounding was done by using a twin-screw extruder. All of the polyethylene samples were in pellets form and supplied by NOVA Chemicals Corp. A summary of the various blends prepared to examine their processing behaviour is given in Table 4.2.

All of the blends indicated in Table 4.2 were prepared by means of direct dilution, i.e. processing aids were compounded into the host polymer to achieve the desired concentration in one step. In addition to these samples, blends with base resin A were also prepared by means of masterbatch. In a masterbatch process, concentrate blends

containing 5 wt.% of processing aids were prepared. These concentrates were then diluted to the desired concentration of 0.1 wt. % (1000 ppm). The blends prepared by means of masterbatch are summarized in Table 4.3.

Table 4.1 A summary of the molecular characteristics of the polyethylene resins that were studied in this work.

Resin	Commercial Nomenclature	Melt Index (g/10 min) (I_2)	Density (g/cm^3)	Co-monomer	Catalyst Type	Additive	Process Technology	Application
A	*PF-Y821-BP*	0.80	0.9230	Butene	Z-N	1° + 2° AO, Slip, AB	Unipol Gas Phase	Film
B	*TD-9022-D*	0.80	0.9195	Hexene	Z-N	1° + 2° AO, Slip, AB	Unipol Gas Phase	Film
C	*FP-120-F*	1.00	0.9218	Octene	Z-N	1° + 2° AO, AB	AST Solution	Film
D	*FPs-117-A*	1.00	0.9170	Octene	Single site	1° + 2° AO	AST Solution	Film
E	*FP-015-A*	0.55	0.9175	Octene	Z-N	1° + 2° AO, Slip, AB	AST Solution	Film
F	*58G*	0.95 (I_6)	0.9575	-	Z-N	1° AO	SCLAIR Solution	Blow Molding

Notes: 1° = Primary Anti-Oxidant, 2° = Secondary Anti-Oxidant, AB = Antiblock Agent, Slip = Slip Additive

Table 4.2 A summary of the polyethylene blends that were studied in this work. Blends prepared by direct dilution

Base Resin	1000 ppm BN	1000 ppm Dynamar	500 ppm BN + 500 ppm Dynamar	1000 ppm CarboGlide
A	✓ A-BN	✓ A-FP	✓ A-BN-F	-
B	✓ B-BN	✓ B-FP	-	✓ B-CG
C	✓ C-BN	✓ C-FP	-	✓ C-CG
D	✓ D-BN	✓ D-FP	-	✓ D-CG
E	✓ E-BN	✓ E-FP	-	✓ E-CG
F	✓ F-BN	✓ F-FP	✓ F-BN-FP	-

Table 4.3 A summary of the polyethylene blends prepared by masterbatch process that were studied in this work.

Base Resin	1000 ppm BN	1000 ppm Dynamar	500 ppm BN + 500 ppm Dynamar	1000 ppm CarboGlide
A	✓ A-BN-M	-	-	✓ A-CG-M

All of the blends indicated in Tables 4.2 and 4.3 were compounded blends. In order to determine the effect of the different methods of fluoropolymer-based PPA introduction, blends where fluoropolymer was dry-mixed into the host polymer were prepared. Generally, the fluoropolymer was dry-mixed into the blends containing only BN or both BN and fluoropolymer.

In dry-mixing, fluoropolymer was added to the polymer sample in a 500 mL plastic container. Before experiments, the mixture was thoroughly mixed for at least 15 minutes by means of thoroughly rotating the container.

4.2 POLYMER PROCESSING AIDS (PPAs)

Three types of polymer processing aids were used in this study. These are fluoropolymer-based, BN-based and fluoropolymer-BN-based. The fluoropolymer-based processing aid is a Dynamar™ fluorocarbon elastomer processing aid. This processing aid is a copolymer of vinylidene fluoride and hexafluoropropylene, with 10% of inorganic partitioning agent, primarily microtalc *(Dyneon, 2001)*. The physical form of the elastomer was a free-flowing powder ground to a 25 mesh particle size. The commercial name of this processing aid is Dynamar™ Brand Polymer Processing Additive FX-9613 from Dyneon, a 3M Company.

The second type of processing aid used was Boron Nitride (BN) based. Boron nitride is a white solid lubricant. It has a high thermal conductivity, low dielectric loss modulus, low thermal expansion and high lubricity over a wide temperature range. BN has one of the highest thermal conductivity of any commercial electrical insulator in the polymer system. Boron nitride powder has been shown to be an excellent additive for coatings and release agents, as well as for oils, potting compounds, friction plates, etc. Figure 4.1 shows a typical structure for BN. Each boron atom is connected to four nitrogen atoms, and each nitrogen atom is connected to four boron atoms. The structure of BN is similar to that of graphite. The BN used in this study has an average particle size of approximately 10 μm and it was not agglomerated. It has a commercial name of Carbotherm™ CTF5 supplied by Saint-Gobain Advanced Ceramics Corporation.

The third processing aid used was a proprietary mixture Boron Nitride and other

fluoropolymer-based processing aids. The commercial name of this processing aid is CarboGlide™ Boron Nitride, supplied by Saint-Gobain Advanced Ceramics Corp.

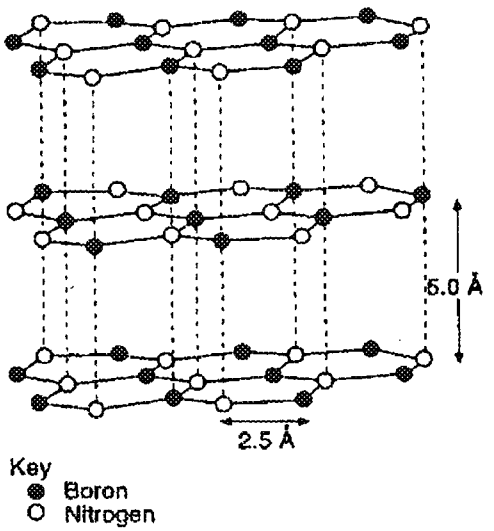

Figure 4.1 Molecular structure of boron nitride *(Rosenbaum et al, 2000).*

4.3 EXPERIMENTAL METHODOLOGY

In this study, a rotational concentric rheometer, an extensional rheometer, as well as a capillary rheometer were used to assess the performance and effect of the various processing aid on the processing and rheological behaviour of polyethylenes. This section provides an overview of the experimental procedure employed in this study.

4.3.1 Rotational Concentric Rheometery

In this work, a Rheometrics System IV Rheometer was used to study the linear viscoelasticity of the various polyethylene samples and their blends with PPAs. The concentric plates used were both flat plates with a diameter of 25 mm. The rheometer comes with a software that allows data to be logged and processed automatically.

Before the rotational concentric test is carried out, round polymer sample of 25 mm in diameter and 1.5 mm in thickness need to be prepared. This can be done by heating the polymer pellets to about 170°C and compressing it using a Carver laboratory press to achieve the desired thickness. The sample was left compressed for about 10 minutes before it was cooled. Sample preparation is critical in this procedure since it is important to ensure that the samples contain no air voids. Circular samples were then cut from the film.

Linear viscoelastic tests began by heating the concentric plates to the desired temperature. After zeroing the gap between the two plates at the desired temperature, the polymer sample was inserted into the gap, after which the gap was reduced to about 1.2 mm. Excess polymer on the sides was trimmed before the gap was reduced further to 1 mm. Settings for the experiment (e.g. stain % and frequency range) were input into the software and the experiment was then started. Data was logged and processed automatically by the software. The file created by the software contains all of the necessary viscoelastic properties such as G', G" and η^* as functions of frequency. After the experiment, the plates were separated and the sample was scraped off the plates before it solidified.

4.3.2 Extensional Rheometry

The Sentmanat Extensional Rheometer (SER) from Xpansion Instruments was used in this study to examine the extensional behaviour of polymers. The SER can be hosted by any rotational rheometer. In this work, a RDA II Rheometrics was used. All extensional

experiments were done by Dr. Martin Sentmanat of Xpansion Instruments.

Extensional melt rheology specimens were prepared by compression molding polymer sample between polyester films to a gage of 0.5-1 mm using a hydraulic press. Long polymer strips approximately 15-17 mm in width were then cut from the molded polymer sheets. From these long strips, individual polymer specimens were then cut to a width of 6.4-12.7 mm using a dual blade cutter with an adjustable gap spacing. Typical SER extensional melt rheology specimens range from 40-150 mg in mass.

Extensional rheology tests began by loading the polymer sample onto the drums and heating the SER unit to the desired temperature. Settings for the experiment (e.g. strain rate and frequency of data collection) were input into the software that comes with the rotational rheometer. Raw torque data was logged and processed manually as explained in Chapter 2 to obtain extensional properties of the polymer sample. After the experiment, the sample was scraped off the drums before it solidified.

4.3.3 Capillary Rheometry

To examine the behaviour of polymers in capillary die flow, the ROSAND RH-2000 capillary rheometer was used. The barrel is equipped with a three zone electric heater and an adaptive PID temperature controller with an accuracy of 0.1°C. The barrel is 190 mm in length and 15 mm in diameter. A stepper motor is used to drive the piston from a speed of 0.1 mm per minute to a maximum speed of 600 mm per minute. A pressure transducer installed on top of the piston driver measures the extrusion pressure. The

rheometer also comes with data analysis software.

Only one type of capillary die was used in this study. The capillary die is made of tungsten carbide, with a diameter of 1 mm, length to diameter ratio of 16 and entrance angle of 180°. In this study, no Bagley correction was applied on the extrusion pressure because the length of the die is considered to be long enough that the end pressure corrections would be insignificant.

To examine the processability of polymers and their blends in crosshead die flow, an Instron piston driven constant speed capillary rheometer was used. The barrel is equipped with a four zone electric heater and an adaptive PID temperature controller with an accuracy of 0.1°C. The temperatures in the die adapter and the crosshead die itself were also controlled with an adaptive PID temperature controller, similar to those used to control the temperature of the barrel. The barrel is 431.8 mm in length and 25.4 mm in diameter. A stepper motor is used to drive the piston from a speed of 0.0254 mm per minute to a maximum speed of 508 mm per minute. Force is measured by means of a load cell standard installed on top of the piston driver. The rheometer also comes with data analysis.

The crosshead die used in this work is a Nokia Maillefer 4/6 that includes a die and a tip ("tip" is the wire guide) with equal entry cone angles of 60° and die land length of 7.62 mm. The tip and the die have diameters of 1.52 mm and 3 mm respectively. Both the tip and the die are made of tungsten carbide (see chapter 2, section 2.1.4 for more details).

Each experimental run began with the loading of resin in pellet form into the heated barrel (at a temperature of 170°C). After the barrel was filled and compacted manually, the piston was put in place. This is followed by pre-heat and pre-compression which ran for a total of approximately 300 seconds. During pre-heating and pre-compression, the piston was set to travel down at a speed of about 5"/min until a force of about 10 lb_f was measured, after which the piston was stopped. After about 150 seconds, the piston was set to travel down again at about the same speed until a force of about 25 lb_f was indicated. Again, it was left for about 150 seconds, after which the extrusion process would proceed. Pre-heating and pre-compressing would allow air bubbles to escape. This process would allow extrudates free of air bubble to be collected, which makes the presence of surface melt fracture easier to detect. The presence of air bubbles also affects the steady extrusion pressure.

During the extrusion process, the piston was allowed to travel down the barrel at a preset speed corresponding to a desired shear rate. The speed was maintained until an obvious steady extrusion pressure was recorded. Polymer samples extruded under steady extrusion pressure are collected. The extruded samples were then inspected visually to detect the presence of melt fracture. Sometimes, optical microscope was used to aid in detecting the presence of melt fracture. Performance of the PPA is measured in terms of critical shear rate (CSR), which is the maximum possible shear rate at which the polymer blend can be extruded without any melt fracture appearance.

After each polymer sample which contains processing aids was tested, the barrel, the

piston and the die were cleaned thoroughly to prevent any contamination. This was done by heating the barrel to about 250°C and the die and piston on a hot plate for about 2 hours. In addition, the rheometer was purged several times prior to experimental runs involving a different resin.

No Bagley and Rabinowitch corrections were applied to any of the data obtained for all the resins. Hence, these experiments would yield the apparent flow curves of the resins that is the relationship between the apparent shear stress – apparent shear rate.

5 RESULTS AND DISCUSSION

5.1 INTRODUCTION

This chapter is divided into four main parts. In the first part, the linear viscoelastic properties of all polymers are presented. This is followed by the presentation of the results obtained from the extensional rheometer. The third part of the chapter focuses on the results obtained from capillary rheometry. This part of the chapter is subdivided into two subsections; one for the capillary die extrusion experiments and the other for the crosshead die extrusion experiments. In addition, the effect of dry-mixing fluoropolymer into BN-compounded blends is also discussed. The last part of this chapter examines the effect of using a masterbatch process to prepare the blends on the performance of the processing aids.

5.2 LINEAR VISCOELASTIC STUDIES

Characterization of all virgin polyethylene samples was done using a Rheometrics System IV rheometer equipped with 25 mm parallel plates. Possible effects of processing aids on the rheology of the host polymer were also examined through linear viscoelasticity. The characterization was done by performing frequency sweep experiments in the frequency range of 0.01 rad/s to about 600 rad/s. All of the tests were done at temperatures of 170°C, 190°C, and 210°C.

Time temperature superposition with a reference temperature of 170°C was performed for all virgin resins to obtain their master curves and these are shown in Figures 5.1 to 5.6.

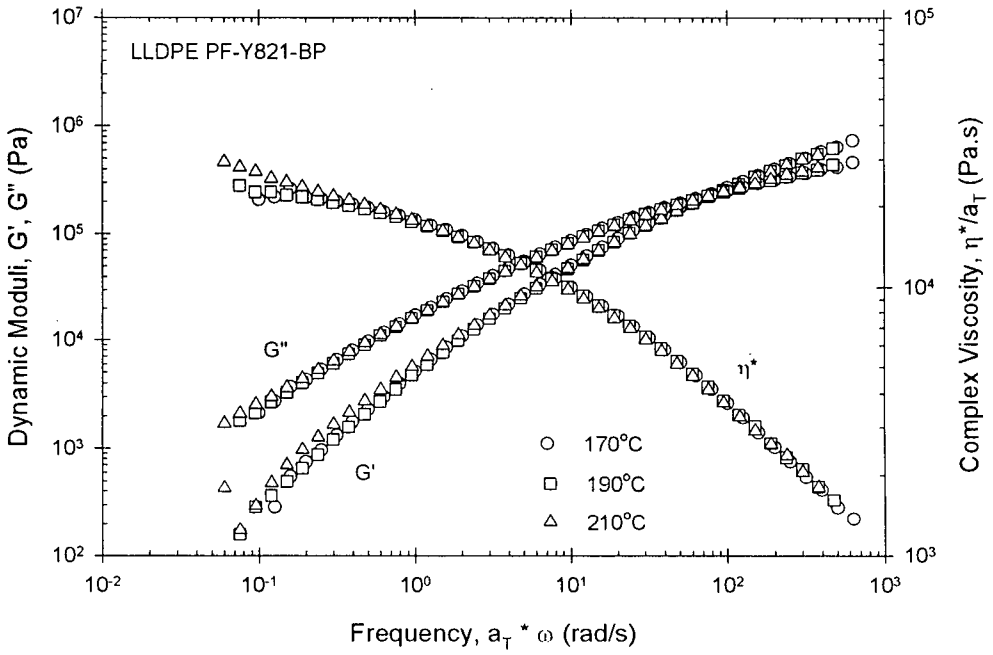

Figure 5.1 Master curve of linear viscoelastic properties for LLDPE PF-Y821-BP (Resin A) at a reference temperature of 170°C.

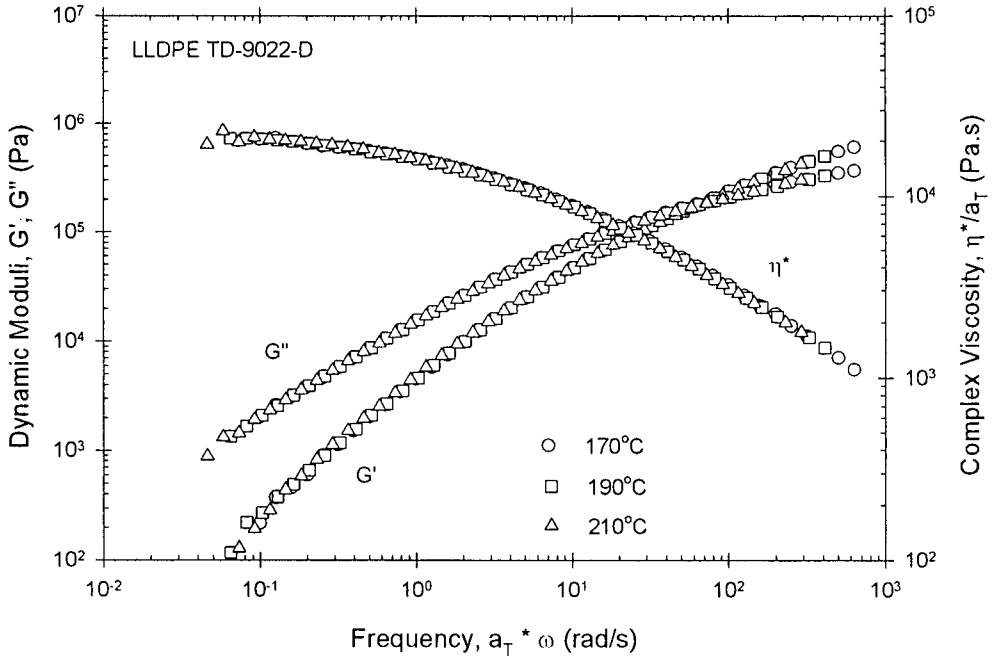

Figure 5.2 Master curve of linear viscoelastic properties for LLDPE TD-9022-D (Resin B) at a reference temperature of 170°C.

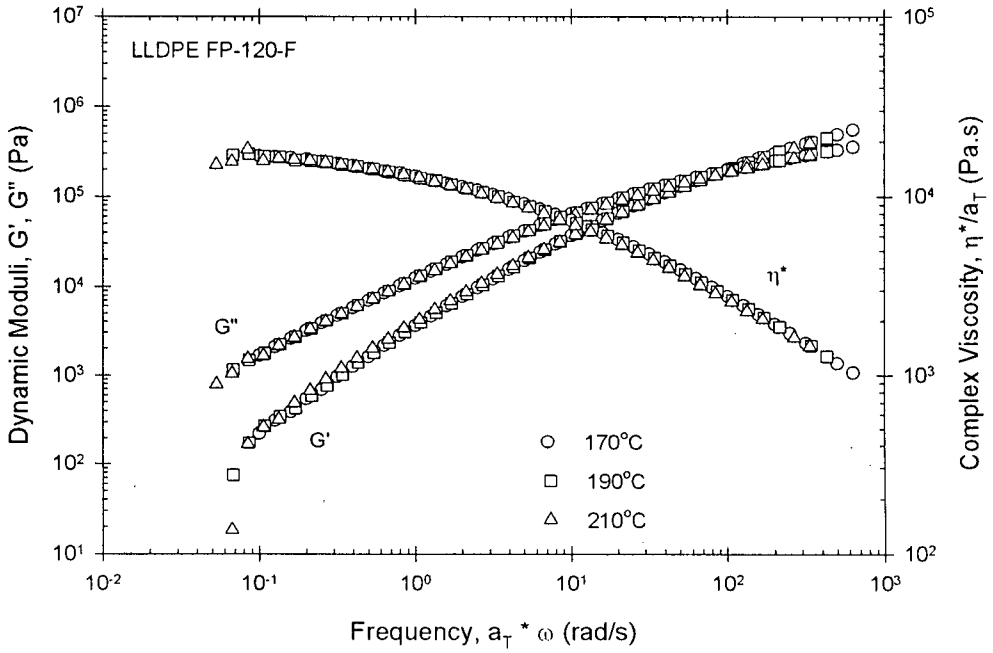

Figure 5.3 Master curve of linear viscoelastic properties for LLDPE FP-120-F (Resin C) at a reference temperature of 170°C.

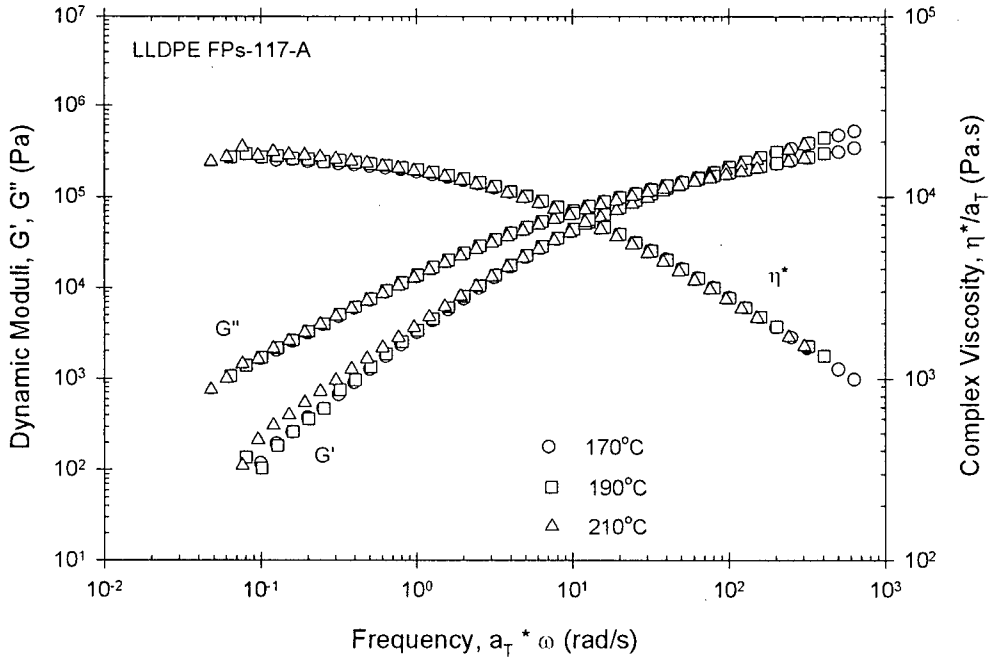

Figure 5.4 Master curve of linear viscoelastic properties for LLDPE FPs-117-A (Resin D) at a reference temperature of 170°C.

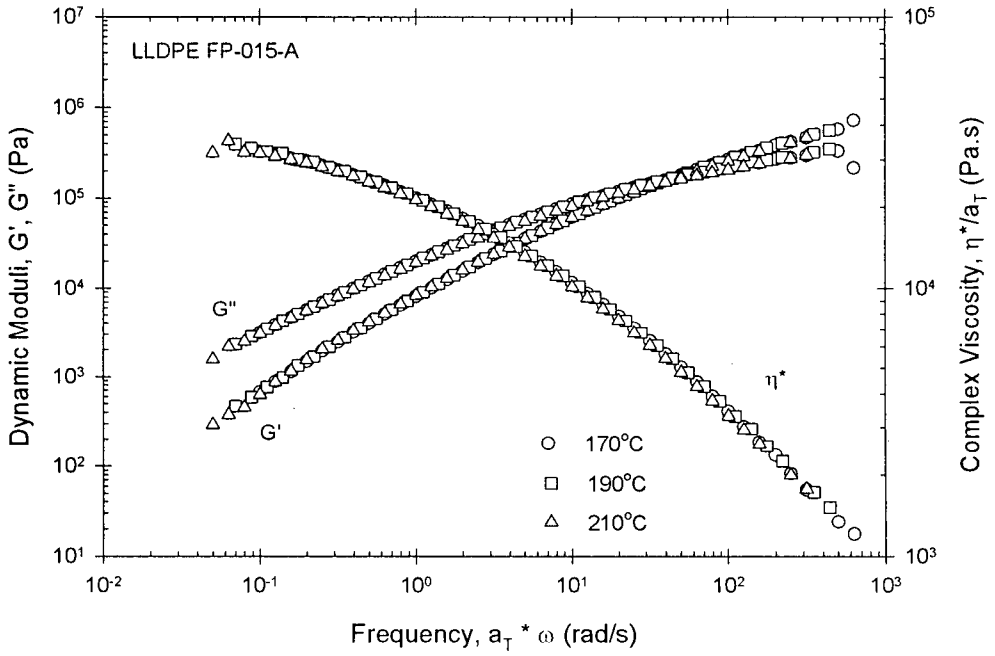

Figure 5.5 Master curve of linear viscoelastic properties for LLDPE FP-015-A (Resin E) at a reference temperature of 170°C.

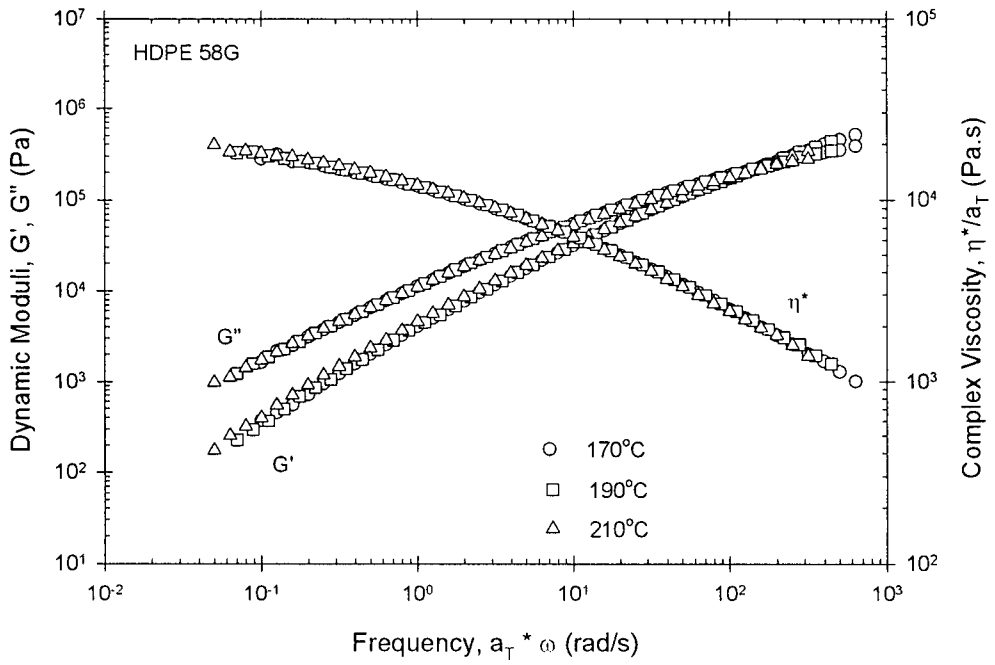

Figure 5.6 Master curve of linear viscoelastic properties for HDPE 58G (Resin F) at a reference temperature of 170°C.

From Figures 5.1 to 5.6, it can be seen in general, that the time temperature superposition applies well for all virgin resins.

The dynamic moduli and complex viscosity of the virgin resins at 170°C are compared in Figures 5.7, 5.8 and 5.9.

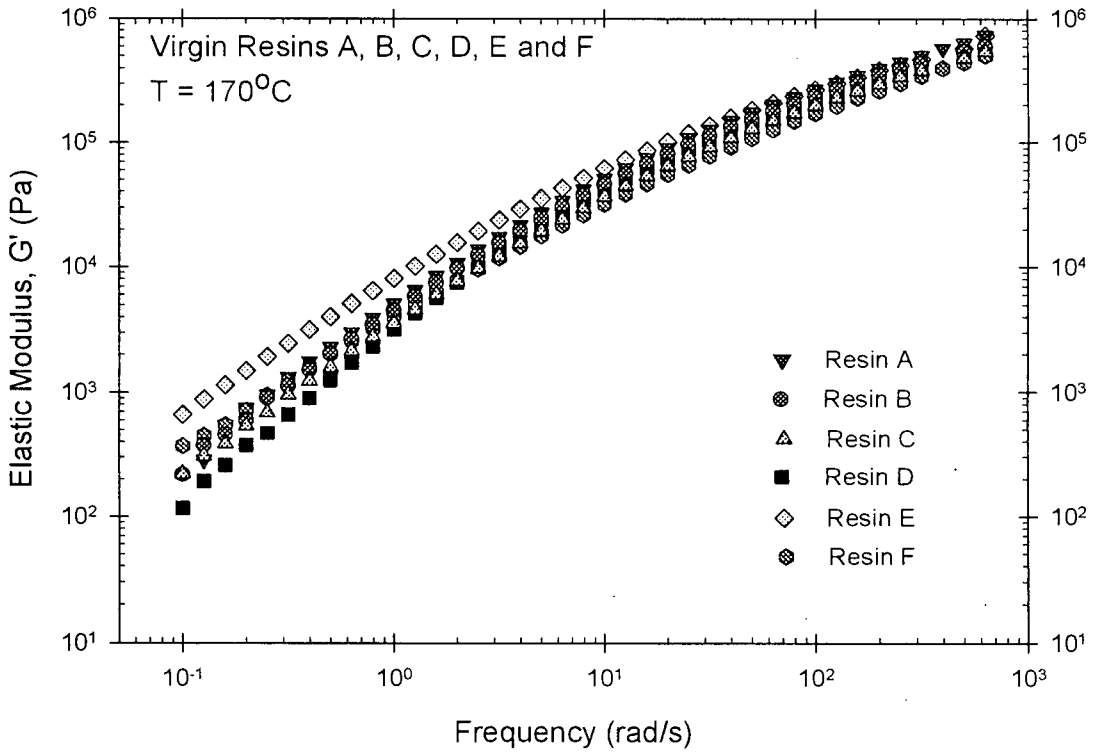

Figure 5.7 Elastic moduli of virgin resins A, B, C, D, E and F at 170°C.

Figure 5.9 shows that the trend of the complex viscosities of the virgin resins are consistent with the melt index data shown in Table 4.1 (chapter 4). It can be seen from Table 4.1 that the melt index for resin E is the lowest which translates to a higher viscosity. On the other hand, resins C, D and F have relatively higher melt indexes which means that they possess relatively lower viscosities

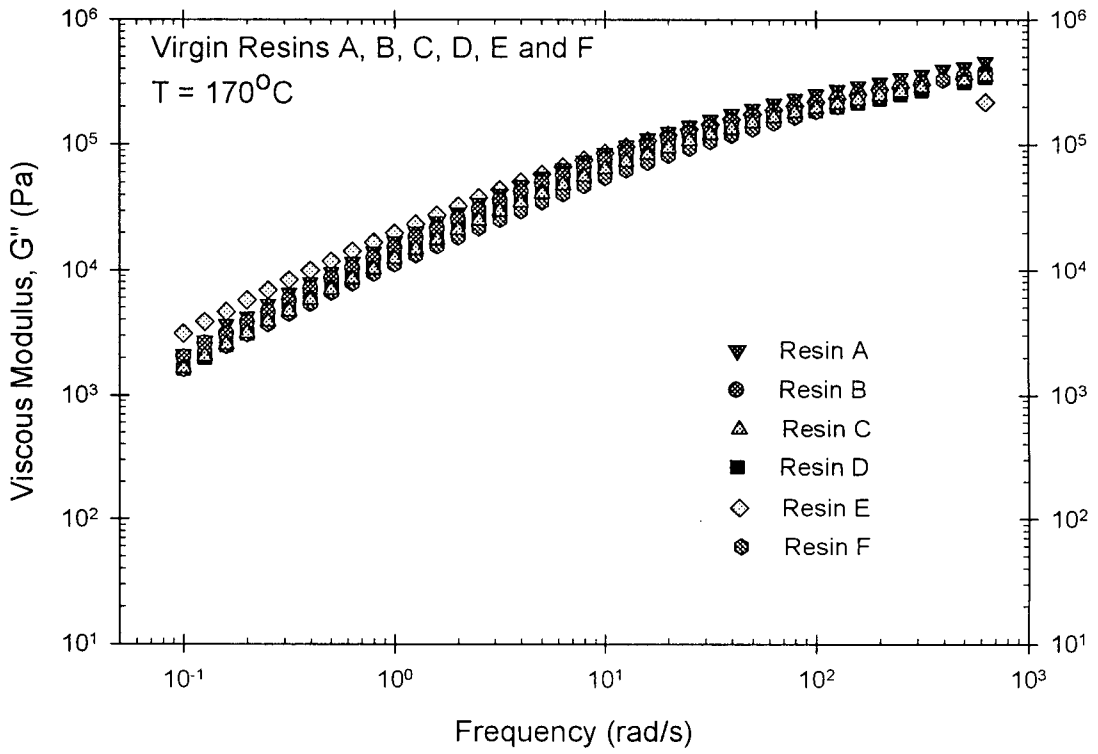

Figure 5.8 Viscous moduli of virgin resins A, B, C, D, E and F at 170°C.

Figure 5.10 shows the comparison of complex viscosity, η* and dynamic moduli, G' and G", of resin A with and without processing aids. It can be seen that there is practically no effect in the linear viscoelastic properties of the polymer with the addition of BN, fluoropolymer or both BN and fluoropolymer. This observation is in agreement with studies done by *Rosenbaum et al (1998b)* who performed a detailed study on the effect of BN on the rheological characteristics of several resins.

This observation is further justified by the rheological characterization of resin F as shown in Figure 5.11. It can be seen that this resin, even though it has a different molecular structure than resin A, the presence of BN, fluoropolymer and the combination

of both BN and fluoropolymer does not alter the linear viscoelastic properties of the host polymer. The blends whose rheological properties are shown in Figures 5.10 and 5.11 were prepared by direct dilution.

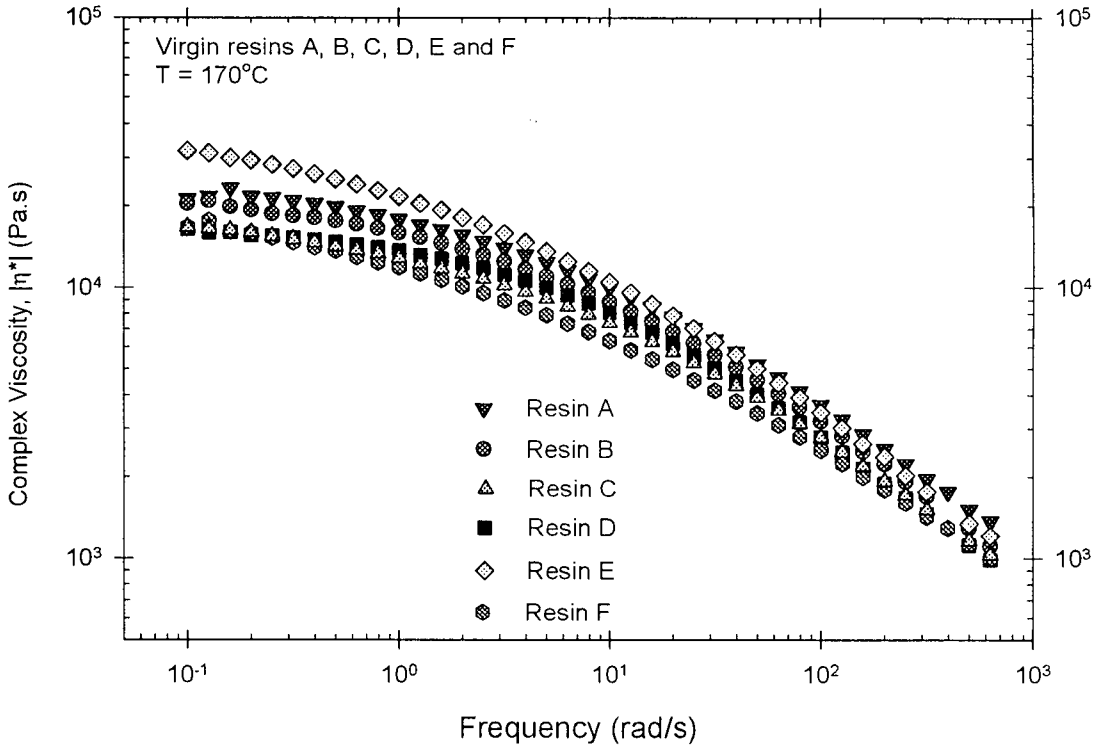

Figure 5.9 Complex viscosities of virgin resins A, B, C, D, E and F at 170°C.

Frequency sweep tests done on the blends prepared by materbatch were also performed. Figure 5.12 summarizes the linear viscoelastic properties of resin A and its combinations with processing aids prepared by means of masterbatch process. Again, it is clear that the presence of processing aids does not alter the rheological properties of the polymer. From this Figure, it can also be seen that there is no effect in the linear viscoelastic properties with the addition of CarboGlide™.

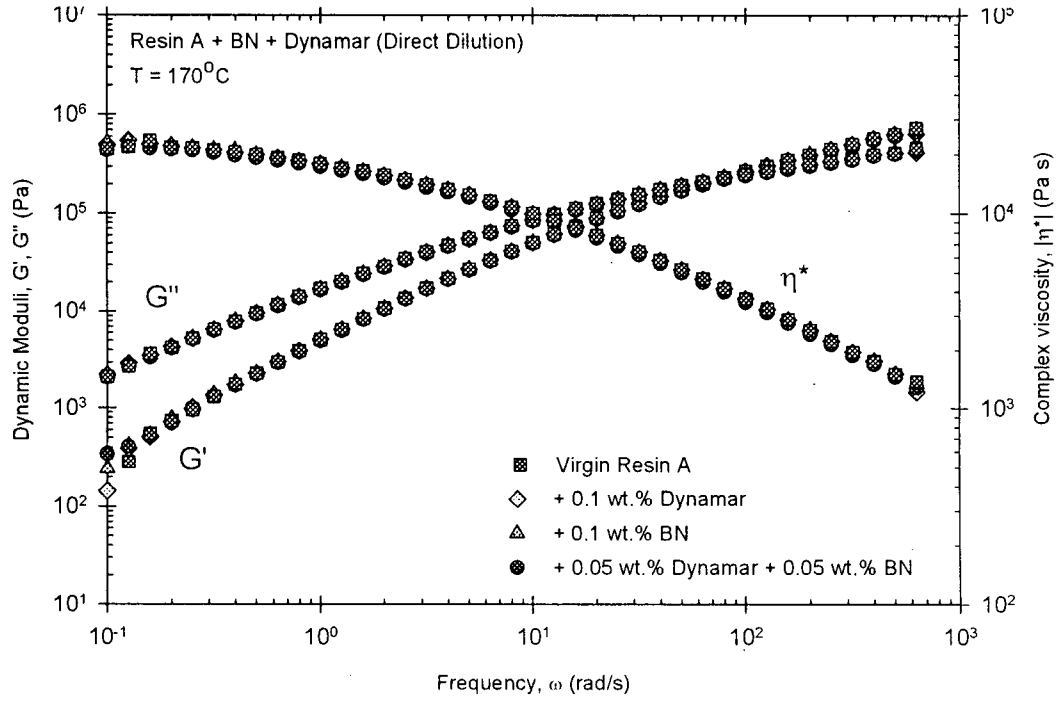

Figure 5.10 Viscoelastic properties of resin A (LLDPE PF-Y821-BP) with and without PPAs (direct dilution).

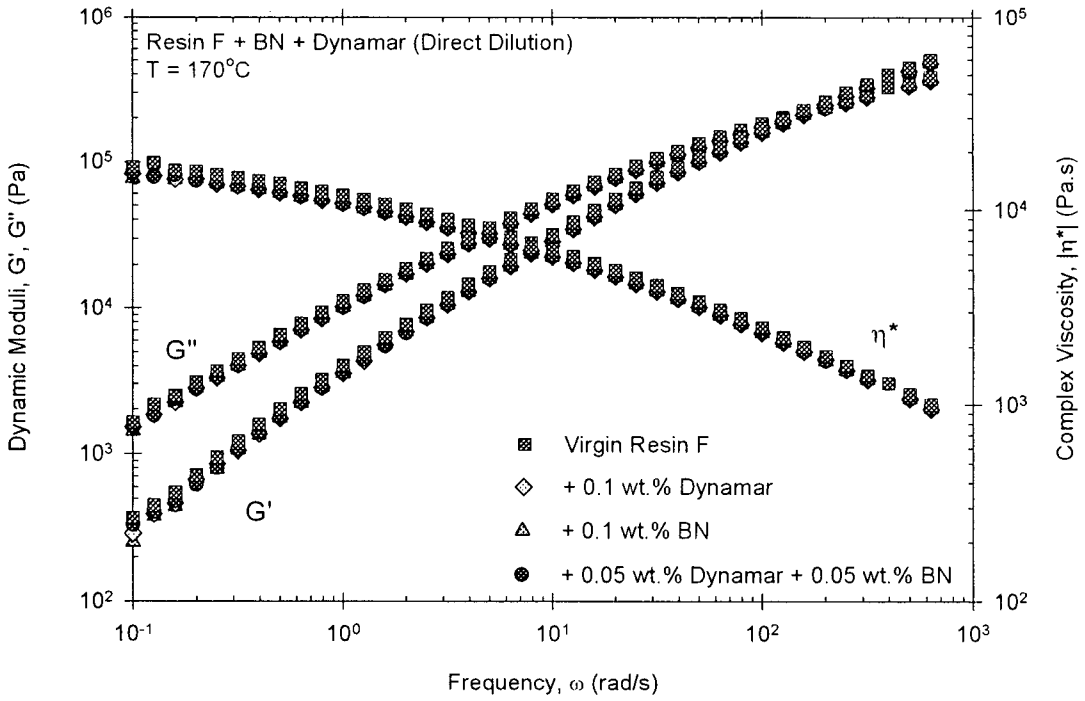

Figure 5.11 Viscoelastic properties of resin F (HDPE 58G) with and without PPAs (direct dilution).

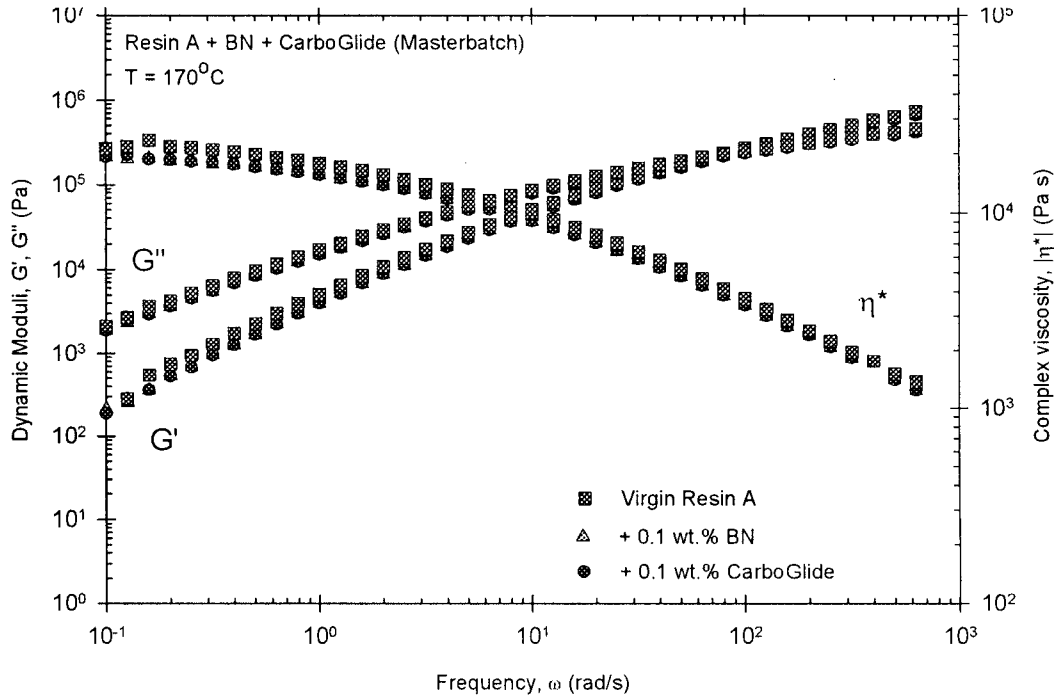

Figure 5.12 Viscoelastic properties of resin A (LLDPE PF-Y821-BP) with and without PPAs (masterbatch).

From this study, it can then be concluded that the presence of PPAs (up to 0.1 wt.%), introduced by direct compounding or masterbatch process, does not alter the linear rheological properties of the polymer. Finally, it must be noted that the accuracy of the linear viscoelasticity result is typically within $\pm$ 2%.

5.3 EXTENSIONAL RHEOMETRY STUDIES

Extensional rheological characterization of the virgin polyethylene samples was also performed using the Sentmanat Extensional Rheometer SER-HV-A01, hosted in a RDS II Rheometrics rotational rheometer. The characterization was done by performing extensional experiments with Hencky strain rates from 0.1 s^{-1} to 20 s^{-1}. All of the tests were performed at a constant temperature of 170°C.

The tensile stress growth plots that provide the characterization of the extensional melt flow behaviour of the virgin resins are shown in Figures 5.13 to 5.18.

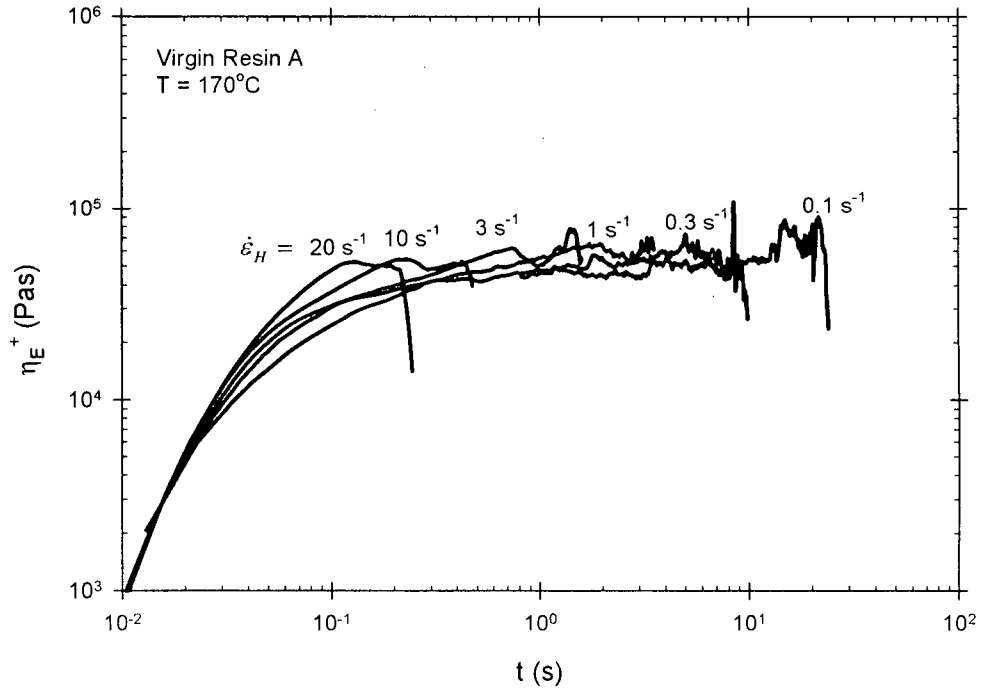

Figure 5.13 Tensile stress growth curves over a range of Hencky strain rates from 0.1 s^{-1} to 20 s^{-1} at 170°C for virgin resin A.

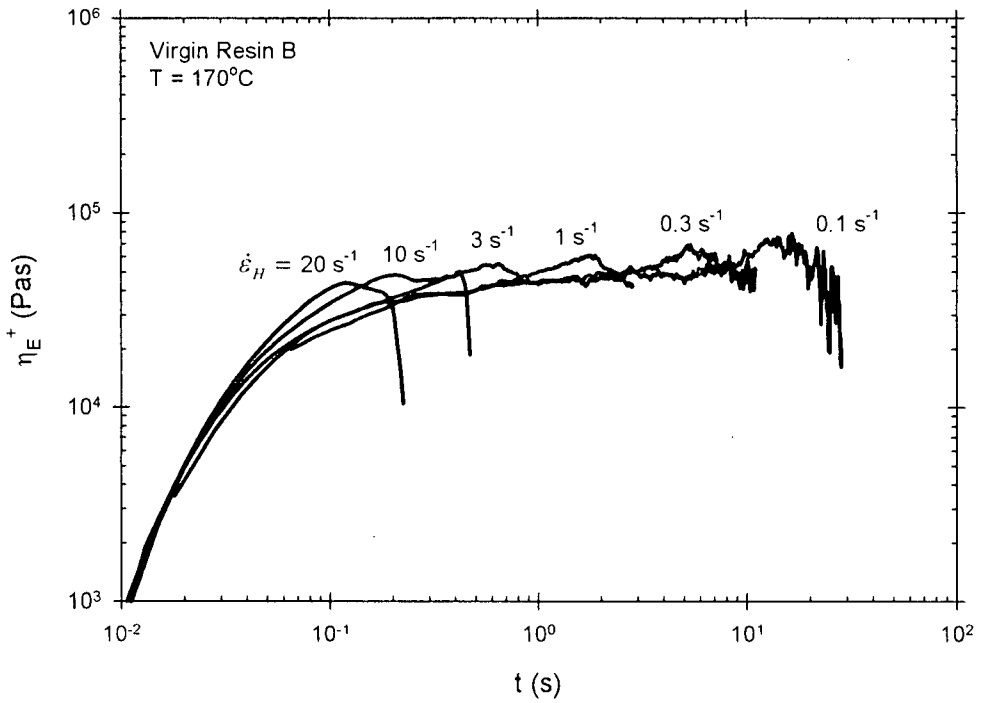

Figure 5.14 Tensile stress growth curves over a range of Hencky strain rates from 0.1 s^{-1} to 20 s^{-1} at 170°C for virgin resin B.

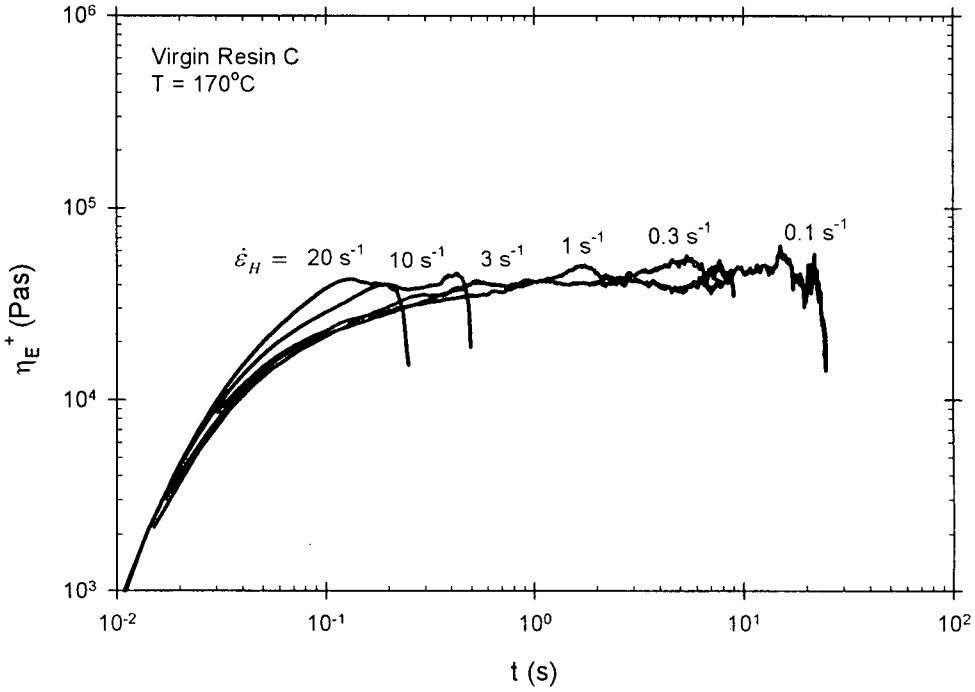

Figure 5.15 Tensile stress growth curves over a range of Hencky strain rates from 0.1 s^{-1} to 20 s^{-1} at 170°C for virgin resin C.

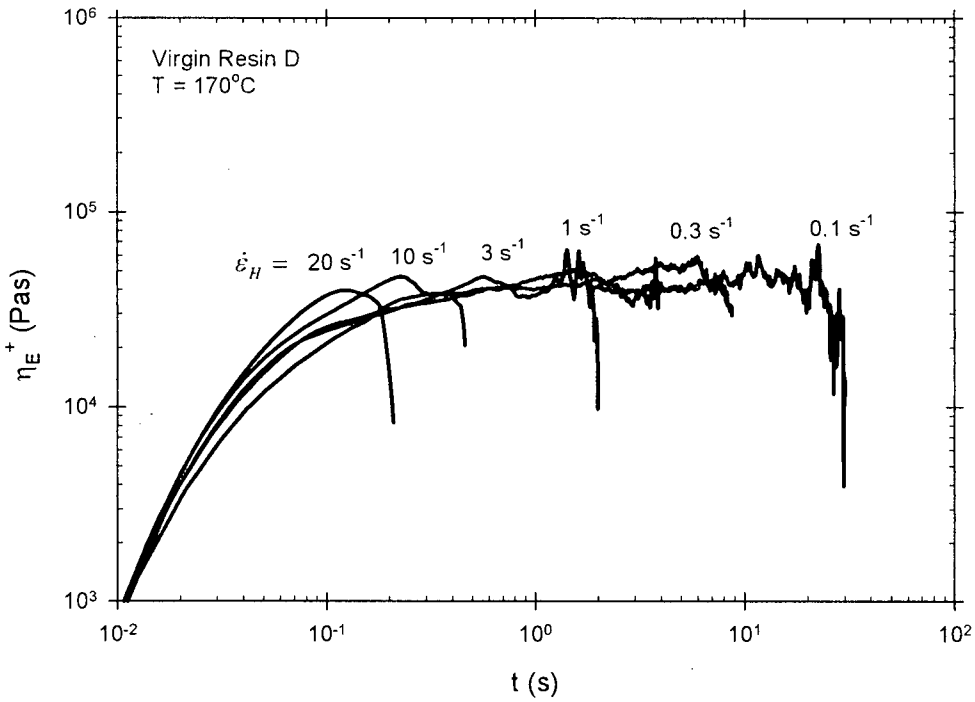

Figure 5.16 Tensile stress growth curves over a range of Hencky strain rates from 0.1 s^{-1} to 20 s^{-1} at 170°C for virgin resin D.

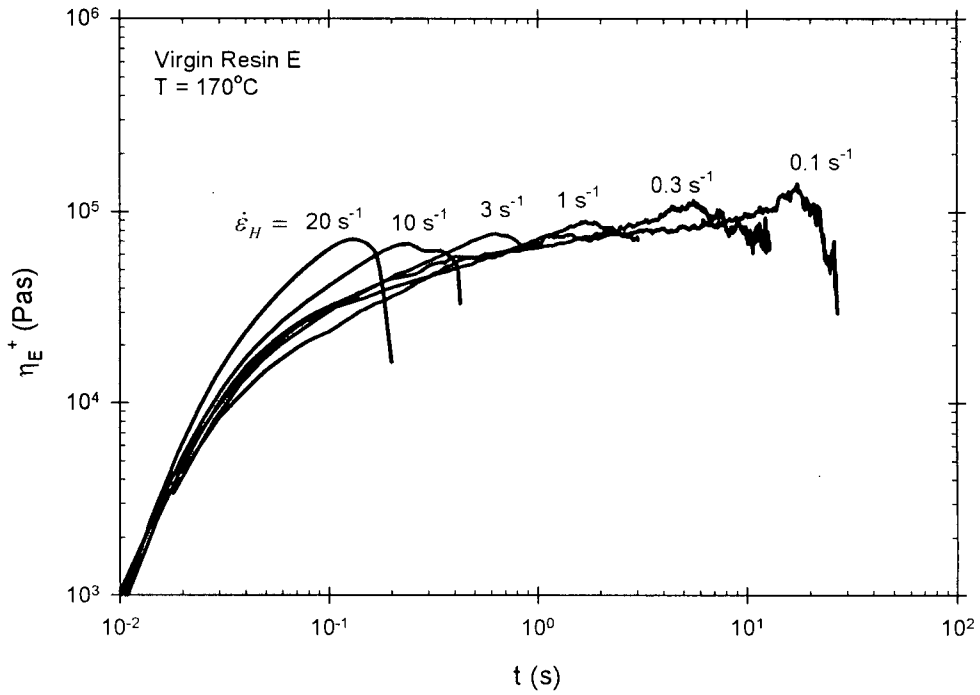

Figure 5.17 Tensile stress growth curves over a range of Hencky strain rates from 0.1 s^{-1} to 20 s^{-1} at 170°C for virgin resin E.

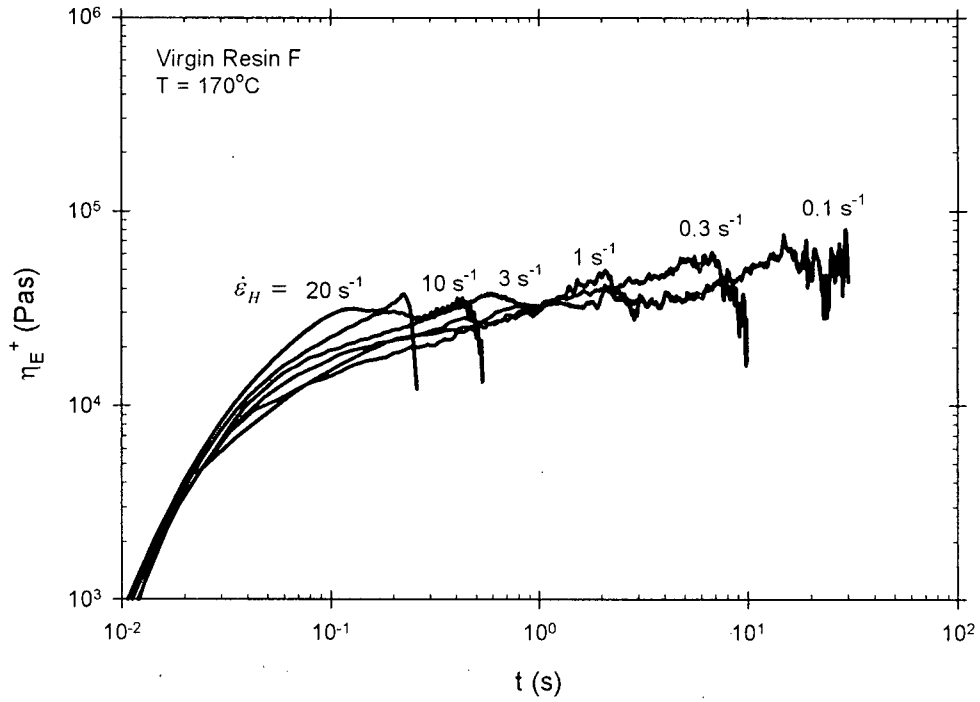

Figure 5.18 Tensile stress growth curves over a range of Hencky strain rates from 0.1 s^{-1} to 20 s^{-1} at 170°C for virgin resin F.

From Figures 5.13 to 5.18, it can be seen that each of these plots exhibits behaviours typical for linear polymers. One common characteristic in all of these plots is that there is no strain hardening effect. In each of these cases, the tensile stress tends to plateau to a certain level before it suddenly decreases which translates to the rupture of the polymer specimen. Strain hardening is usually associated with polymers with high molecular weight components and high degree of long branching *(Münstedt, 1980)*. For highly branched polymer, for example LDPE, extensional stress is dissipated by the associative flow and deformation behaviour of long chain branches along the backbone before it is sustained by the main polymer chain backbone. This leads to significant strain hardening before it finally ruptures when the backbone eventually fails. Higher strain hardening is usually noticed at higher extensional rates in the case of highly branched polymers. However, all of the virgin polymers tested were either LLDPE or HDPE, which have mainly short side branches. In linear polymers, tensile stress that is generated by the extension of the polymer is almost immediately borne by the main polymer chain backbone and this leads to faster melt rupture of the polymer chain.

5.4 CAPPILARY RHEOMETRY STUDIES

The performance of the various PPAs was assessed by determining the critical shear rate for the onset of sharkskin and gross melt fractures, as described in Chapter 4. All extrusion experiments (both for capillary and crosshead die) were carried out at 170°C over a shear rate range from about 10 s^{-1} to 2000 s^{-1} or 3000 s^{-1} depending on how easily the polymer examination exhibited fracture.

5.4.1 Capillary Die Results

The critical shear rates for the onset of sharkskin, stick-slip and gross melt fracture for resins A and F and their combinations with the processing aids at 170°C are summarized in Table 5.1. It can be seen that pure resin A exhibits sharkskin melt fracture at a critical shear rate of 75 s^{-1}. This is followed by oscillating flow at 300 s^{-1} and gross melt fracture that occurs at a shear rate of 850 s^{-1}.

Addition of 0.1 wt% BN (A-BN) does not improve the processability of the resin as sharkskin still starts at a relatively small shear rate value of 75 s^{-1}. However, the presence of BN postpones the onset of gross melt fracture significantly to about 1500 s^{-1}. This is consistent with findings reported by *Rosenbaum et al (2000)* who performed a similar study on m-LLDPE.

Table 5.1 Critical shear rates for resins A and F and their combinations with PPAs in capillary die extrusion at 170°C.

	Critical Shear Rate For The Onset of (S^{-1})		
Sample ID	Sharkskin	Stick Slip	Gross Melt Fracture
A	75	300	850
A-BN	75	250	1500
A-FP		700	800
A-BN-FP	85	250	1000
F	175	300	1500
F-BN	200	350	1500
F-FP		1000	1500
F-BN-FP		800	1750

As expected, the addition of 0.1 wt% Fluoropolymer (A-FP) improves the extrudate appearance significantly. The blend containing 0.1 wt% fluoropolymer does not exhibit

any sharkskin; rather stick slip is the first manifestation of melt fracture for this blend. However, the usage of both fluoropolymer and BN simultaneously (sample A-BN-FP) does not improve the processability of the resin in the sharkskin region, with sharkskin starting at 85 s^{-1}. Gross melt fracture for this blend appears at a slightly higher shear rate (1000 s^{-1}) compared to the pure resin. The synergistic effect of BN and fluoropolymer as found by *Rosenbaum et al (2000)* and discussed into detail by *Achilleos et al (2002)* is not obvious in this case; rather this blend (A-BN-FP) shows similar behaviour as the blends containing no fluoropolymer (sample A or A-BN). This surprising result can be explained in terms of the strong interaction between BN-polyethylene and BN-fluoropolymer.

As presented in Chapter 2, BN has a high adsorption capacity for polyethylenes as well as for fluoropolymer *(Rathod, 2003)*. Plots to summarize an adsorption study done by *Rathod (2003)* are shown in Figures 2.13 and 2.14. These adsorption results mean that when compounding BN and fluoropolymer together at the same time (sample A-BN-FP), most of the fluoropolymer molecules tend to be absorbed onto the surface of BN particles. Thus, during extrusion, fluoropolymer molecules stay together with the BN particles, within the polymer melt. This prevents the fluoropolymer to perform its main aim; that is to create a layer of lubrication between the polymer and die wall. At the same time, the presence of fluoropolymer within the polymer melt may reduce the lubrication effect of BN. On the other hand, when BN is first compounded into the polymer, the strong interaction between BN and polyethylene allows most of the adsorption sites on the BN particles to be occupied by the polyethylene molecules.

Consequently, post-compounding addition of fluoropolymer in a dry form would allow the fluoropolymer molecules to be "free" and able to migrate towards the die wall to provide lubrication. As discussed earlier, during gross melt fracture, the polymer flow is segmented into different layers and the absence of fluoropolymer within these polymer layers will also allow the effect of BN to be more effective. Figure 5.19 illustrates this phenomenon schematically.

To avoid the interaction of fluoropolymer with BN, a blend (sample A-BN-FP-FP DM) is prepared where a small amount of fluoropolymer (0.05 wt. %) was added to the blend containing 0.1 wt% BN (sample A-BN) at the time of processing. As expected, this blend generally shows improved performance, showing no sharkskin, stick slip behaviour at a shear rate of 650 s^{-1} and gross melt fracture at 1100 s^{-1}. Table 5.2 summarizes the effect of this dry-mixing case.

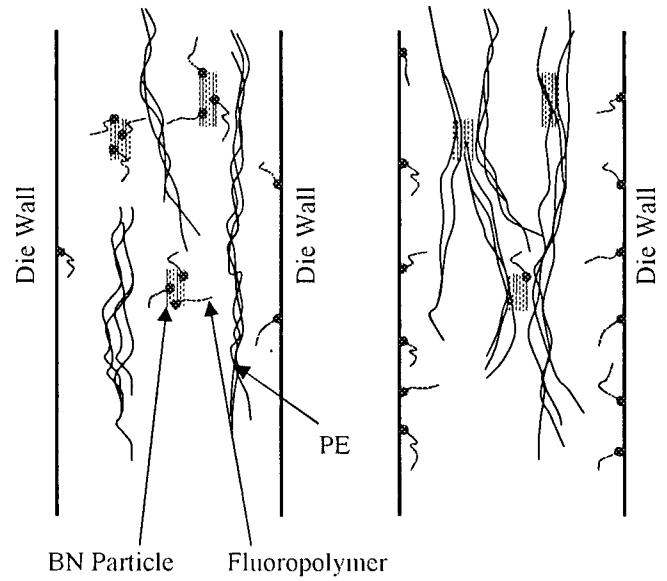

Figure 5.19 a) Adsorption of fluoropolymer on BN particles when fluoropolymer and BN are compounded at the same time. b) Adsorption of PE on BN particles and migration of fluoropolymer towards the die wall when fluoropolymer is added to BN-compounded resin just prior to extrusion.

Table 5.2 Critical shear rates for resin A with the addition of BN and fluoropolymer (compounded and dry-mixed) in capillary die extrusion at 170°C.

	Critical Shear Rate For The Onset of (S^{-1})		
Sample ID	Sharkskin	Stick Slip	Gross Melt Fracture
A	75	300	850
A-BN-FP	85	250	1000
A-BN-FP-FP DM		650	1100

The phenomenon where the separate addition of fluoropolymer and BN improves the processability of the polymer is also shown with the HDPE samples (resin F). From Table 5.1, it can be seen that virgin resin F exhibits sharkskin at a critical shear rate of 175 s^{-1}, followed by stick slip at 300 s^{-1} and gross melt fracture at 1500 s^{-1}. For this sample it can be seen that the addition of BN does not affect its processability, showing practically no effect in both sharkskin and gross melt fracture regions. The addition of fluoropolymer, however, shows significant improvement in the sharkskin region. This blend (F-FP) shows no sharkskin and stick slip at about 1000 s^{-1}. The use of both BN and fluoropolymer (compounded at the same time) for this resin results in a smaller critical shear rate (stick slip at 800 s^{-1}) compared to the critical shear rate corresponding to the blend in which only fluoropolymer (F-FP) is present. In this case, as can be seen from Table 5.3, dry-mixing 0.05 wt.% fluoropolymer into a BN-compounded resin (F-BN) shows the best performance (sharkskin fracture at 1000 s^{-1} and gross melt fracture at 1500 s^{-1}). This again demonstrates the interaction effect between BN and fluoropolymer.

The critical shear rates for the onset of sharkskin, stick-slip and gross melt fracture for resins B, C, D and E are summarized in Table 5.4. It can be seen from the Table that the

addition of BN slightly improves the processability of resin D in terms of sharkskin but appears to have no effect on the other resins. However, there is some degree of improvements in the gross melt fracture region, with resin C and E showing the most and least improvement respectively. The reason behind this varying effect of BN is difficult to justify. These resins possess different properties, such as density and melt index and are synthesized differently. In addition, these resins contain different additive packages. Thus, it is difficult to qualitatively compare the performance of BN on these resins, as there may be interaction effects between the different additives in these resins. These interactions effects may cause unpredictable response during processing of these resins in combination with BN.

Table 5.3 Critical shear rates for resin F with the addition of BN and fluoropolymer (compounded and dry-mixed) in capillary die extrusion at 170°C.

	Critical Shear Rate For The Onset of (S^{-1})		
Sample ID	Sharkskin	Stick Slip	Gross Melt Fracture
F	175	300	1500
F-BN-FP		800	1750
F-BN-FP-FP DM	1200		1500

The addition of fluoropolymer on these resins, as expected, shows significant improvement in the sharkskin melt fracture region. In resin B, however, the addition of fluoropolymer seems to have an effect in the gross melt fracture region. In fact, the fluoropolymer is as effective as BN in the gross melt fracture region, postponing the onset for gross melt fracture to about 1200 s^{-1} for resin B. Again this phenomenon of

varying effect of fluoropolymer in the gross melt fracture region may be due to the nature of the polymer and the interaction between the additives that it may contain.

Table 5.4 Critical shear rates for resins B, C, D and E and their combinations with PPAs in capillary die extrusion at 170°C.

	Critical Shear Rate For The Onset of (S^{-1})		
Sample ID	Sharkskin	Stick Slip	Gross Melt Fracture
B	100	225	900
B-BN	100	250	1200
B-FP	800		1200
B-CG	800		1200
C	100	325	1100
C-BN	125	325	1750
C-FP	1100		1200
C-CG	1000		1500
C-CG-FP DM	1000		1500
D	50	600	700
D-BN	200		800
D-FP	700		800
D-CG	700		800
E	40	200	700
E-BN	40	200	800
E-FP	650		700
E-CG			700
E-BN-FP DM			700

The addition of the commercial processing additive of CarboGlide shows surprisingly similar performance as fluoropolymer for all of these resins. Compared to the pure resins, the blends that contain CarboGlide (B-CG, C-CG and D-CG) all show improvements in the sharkskin as well as in the gross melt fracture region. Blend E-CG, however, shows improvement only in the sharkskin melt fracture region. A blend where fluoropolymer was dry-mixed into the blend that contains only BN (E-BN) was prepared to investigate if the processability of this blend can be further improved. This blend (E-

BN-FP DM) shows the exact performance as CarboGlide, similar to the performance of fluoropolymer. This result may mean that the possible maximum critical shear rate for resin E may have been reached at around 800 s^{-1}.

Based on the results from these resins (B, C, D and E), it can be said that the commercial processing aid CarboGlide, generally performs well even without the dry-mixing addition of fluoropolymer. In fact, the presence of extra fluoropolymer in the dry form does not help in the extrusion of the blend that already contains CarboGlide. As can be seen from Table 5.4, the blend in which fluoropolymer was dry-mixed (C-CG-FP DM) shows exact performance as the blend that contains only CG (C-CG) in terms of both sharkskin and gross melt fracture. In addition, if the results obtained from the dry-mixing cases of resins A and F and from resin E are considered, it can then be said that CarboGlide performs equally well with the case when fluoropolymer is dry-mixed into BN-compounded resin.

Figure 5.20 shows the apparent flow curve obtained from the capillary die extrusion of resin A at 170°C. It can be seen that the addition of BN does not result in reduction of the extrusion pressure. This is consistent with the trend observed by *Rosenbaum et al (1998b)*. The presence of fluoropolymer, on the other hand, results in significant extrusion pressure reduction. This is as expected since fluoropolymer coats the die during extrusion and thus promotes wall slip and reduces extrusion pressure. However, the blend that contains both BN and fluoropolymer (compounded at the same time) does not show any pressure reduction. This observation further confirms the interaction effect

of BN and fluoropolymer that was discussed previously. Since most of the fluoropolymer particles are absorbed onto BN particles, the free-moving fluoropolymer particles that are able to migrate towards the die wall are not able to provide sufficient die wall coating. This is further justified by the apparent flow curve of the blend where fluoropolymer is added by dry-mixing. This dry-mixed blend (A-BN-FP DM) shows significant extrusion pressure reduction; similar to the behaviour observed for the sample containing only fluoropolymer. In other words, the trend from these flow curves also suggests that dry-mixing of fluoropolymer allows its particles to be "free-moving" and thus able to provide adequate coating on the die wall to promote wall slip.

This trend is also observed in the flow curves obtained for resin F. Figure 5.21 shows the apparent flow curves of resin F and its blends with the different PPAs obtained from capillary die extrusion. It can be seen from Figure 5.21 that again the addition of BN does not reduce the extrusion pressure. On the other hand, the addition of fluoropolymer reduces the extrusion pressure significantly. If BN and fluoropolymer are both compounded at the same time, it was observed that there is a slight reduction in the extrusion pressure. This is also reflected in the extrudate appearance. It is noticed, for this resin that the blend in which both BN and fluoropolymer are compounded at the same time (blend F-BN-FP) shows an improvement in the critical shear rate compared to when only BN (F-BN) or fluoropolymer (F-FP) is used independently. However, the performance of the processing aids is further improved if fluoropolymer is dry-mixed into the BN-compounded blend (F-BN-FP DM). This observation is also consistent with the

apparent flow curve of the dry-mixed blend. The extrusion pressure for this dry-mixed blend is observed to be the lowest in shear rate range of 600 to 1000 s^{-1}.

The flow curves of resin B and its blends with various processing aids show similar trends as the ones obtained for resins C, D and E and their blends. A typical plot is shown in Figure 5.22. The flow curves of these resins show that the addition of BN does not decrease the extrusion pressure; a trend also observed earlier for resins A and F. As expected, the addition of fluoropolymer reduces the extrusion pressure significantly which also agrees with the results obtained in resins A and F. The addition of CarboGlide in these resins also results into significant decrease of the extrusion pressure similar to that shown by blends containing only fluoropolymer. This behaviour scales with the critical shear rates for the onset of surface melt fracture of these blends. Furthermore, it can be seen from Figure 5.23 that even when fluoropolymer is added in a dry form to the blend that contains only CarboGlide, no further pressure reduction is observed. This is again consistent with the critical shear rates of these blends (C-CG and C-CG-FP DM) which show that dry mixing fluoropolymer onto the blend that contains only CarboGlide does not change the critical shear rate any further. It must be noted that in capillary die extrusion, the accuracy of the generated flow curve is typically within $\pm$ 5% and therefore these results have a significant statistical meaning.

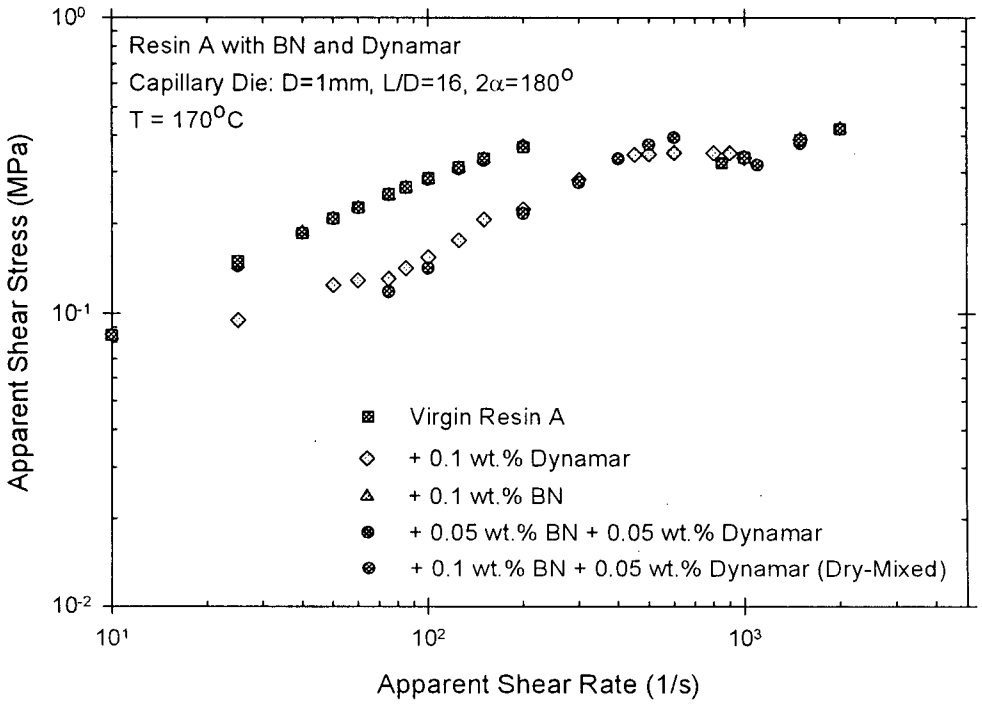

Figure 5.20 Flow curves of Resin A (LLDPE PF-Y821-BP) with and without PPAs in capillary die extrusion at 170°C.

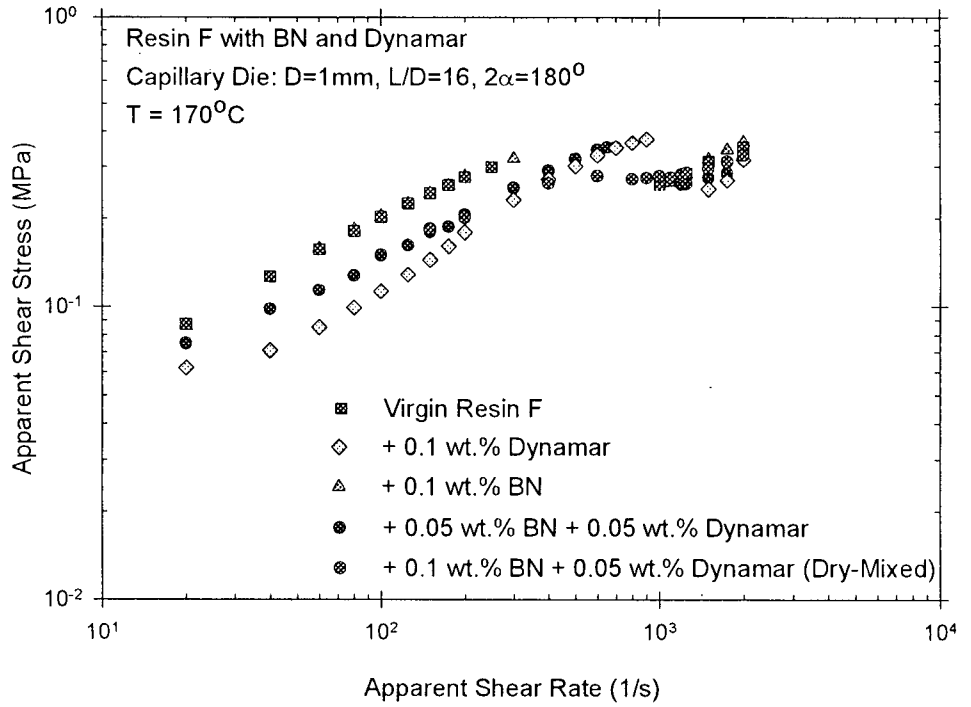

Figure 5.21 Flow curves of Resin F (HDPE 58G) with and without PPAs in capillary die extrusion at 170°C.

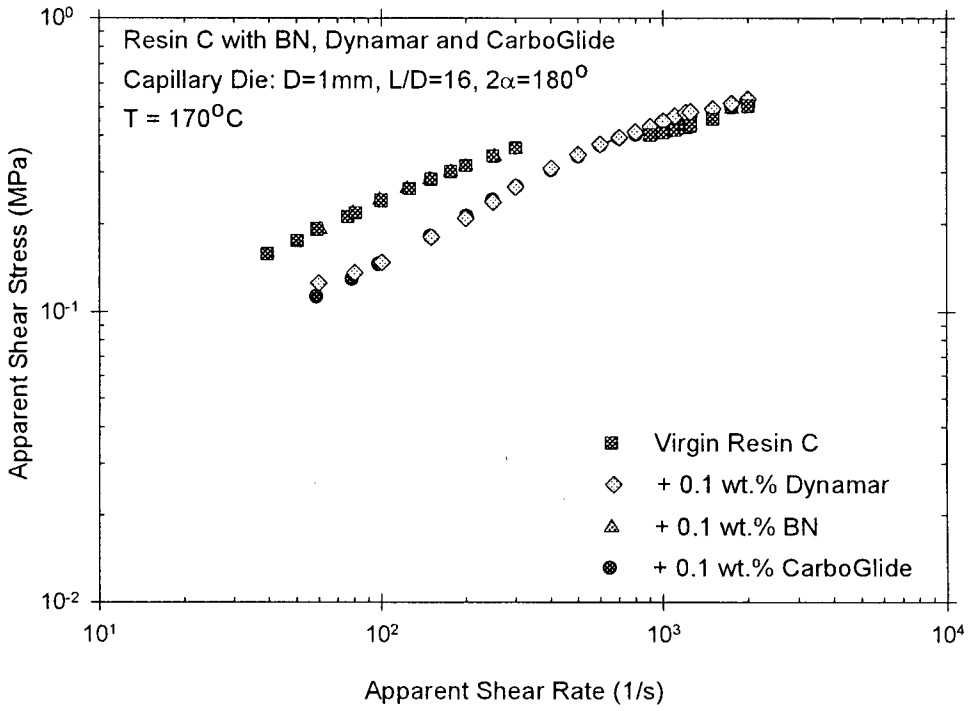

Figure 5.22 Flow curves of Resin C (LLDPE FP-120-F) with and without PPAs in capillary die extrusion at 170°C.

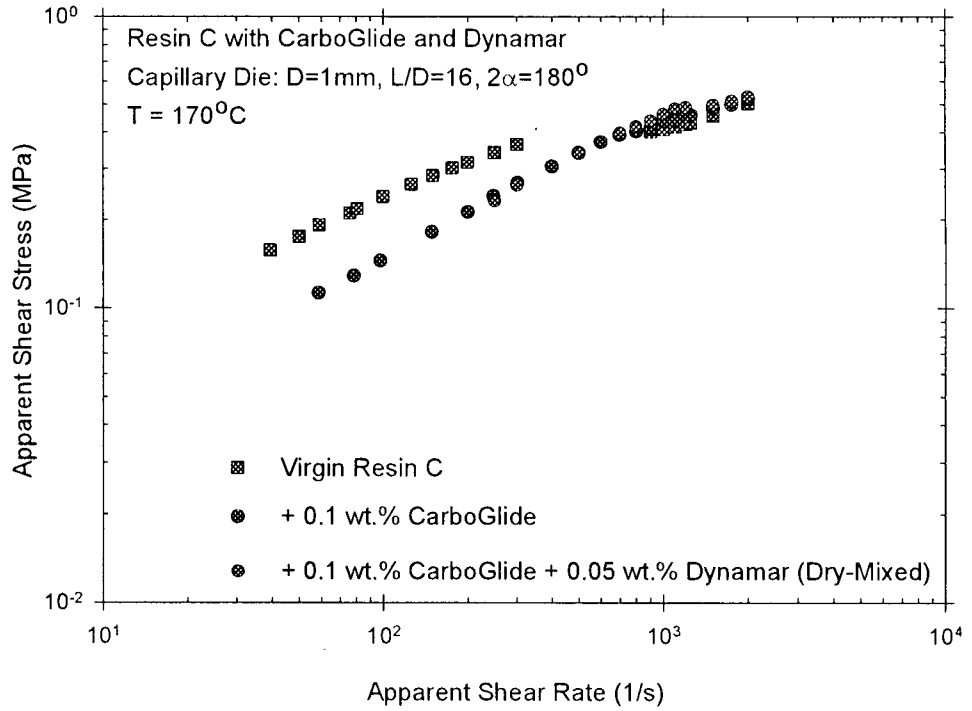

Figure 5.23 Flow curves of Resin C (LLDPE FP-120-F) with and without dry-mixing of fluoropolymer at 170°C.

5.4.2 Crosshead Die Results

In crosshead die extrusion, the design and geometry of the crosshead is such that the flow of the extruding polymer is more streamlined and guided towards the die. This causes the fracture on the surface of the extrudates to be much finer compared to those obtained from capillary die extrusion. Thus it was very difficult to differentiate between sharkskin and gross melt fracture. Therefore, in this case, only critical shear rate associated with sharkskin melt fracture will be discussed.

Table 5.5 summarizes the critical shear rates for pure resins (A to F) and those that contain processing aids. For clarification purposes, the sample that performs the best among the set of resin is highlighted in bold red font. A glance of this Table shows that the effect of dry-mixing fluoropolymer is more evident in crosshead die extrusion than in capillary extrusion. This is consistent with the fact that the effect of BN on melt fracture is usually more evident in crosshead die extrusion rather than in capillary die extrusion *(Rosenbaum et al, 1998b)*.

BN has been shown to be much more effective in the gross melt fracture region *(Kazatchkov et al, 2000)*. However, in the present crosshead die extrusion experiments, the onset of gross melt fracture cannot be easily determined. Therefore, it is difficult to assess the true effect of BN. However, from Table 5.5, it can be seen that the addition of BN shows some degree of improvement in the critical shear rate for some of the resins. The addition of fluoropolymer, on the other hand, results in significant improvement in the processability of all resins.

Table 5.5 Critical shear rates for resins A, B, C, D, E and F and their combinations with PPAs in crosshead die extrusion at 170°C.

Sample ID	Critical shear rate for the onset of sharkskin (S^{-1})
A	65
A-BN	327
A-FP	1800
A-BN-FP	1473
A-BN-FP DM	**1964**
A-BN-FP-FP DM	**1964**
B	229
B-BN	327
B-FP	1145
B-CG	982
B-BN-FP DM	**1309**
B-CG-FP DM	**1309**
C	262
C-BN	262
C-FP	1634
C-CG	1634
C-CG-FP DM	**2127**
D	229
D-BN	262
D-FP	**1636**
D-CG	**1636**
E	98
E-BN	131
E-F	1145
E-CG	982
E-BN-FP DM	**1309**
E-CG-FP DM	1145
F	491
F-BN	1636
F-FP	2455
F-BN-FP	2782
F-BN-FP DM	**3273**
F-BN-FP-FP DM	**3273**

Interestingly, in resin A, the addition of both BN and fluoropolymer at the same time (blend A-BN-FP) shows less improvement compared to the blend that contain only fluoropolymer (A-FP). Again, this phenomenon can be explained by the fact that there is an interaction between BN and fluopolymer and polyethylene. The adsorption of fluoropolymer onto BN hinders the processing aids to perform their main function, as explained in previous section. As can be seen from Table 5.5, the dry-mixing cases for resin A (A-BN-FP DM and A-BN-FP-FP DM) perform the best in most cases in postponing the critical shear rate.

This observation is also supported from the results obtained for resin F. Although, the blend that contains both BN and fluoropolymer (compounded at the same time, F-BN-FP) shows better performance than when either BN (F-BN) or fluoropolymer (F-FP) is used independently, the dry-mixing cases for this resin still show the best performance.

An interesting observation from the crosshead die extrusion is that, unlike in capillary, the dry-mixing addition of fluoropolymer into the blend that contains CarboGlide is able to improve the performance of the processing aids for resins B, C and E. It is noted that, in capillary die extrusion, dry-mixing of fluoropolymer to the blends that contain CarboGlide has shown no effect. One possible explanation for this is that in crosshead die, the contact area between the die wall (including the crosshead tip) and the polymer is larger compared to that in capillary die. This means that more fluoropolymer is actually needed to coat it. Coating of the die wall by these fluoropolymer particles is highly dependent on their surface energy *(Rathod, 2003)*. However, as fluoropolymer migrates

towards the wall, the wall undergoes transient change in surface energy due to presence of fluoropolymer. Ultimately, an equilibrium state will be achieved when the concentration of fluoropolymer on the wall balances the concentration of fluoropolymer in the polymer melt. The speed at which this equilibrium state is achieved and the amount of fluoropolymer coated on the die at this equilibrium state determine the effectiveness of the fluoropolymer coating. If there is sufficient fluoropolymer coating at equilibrium state, there will be an improvement in the critical shear rate. Now, if extra fluoropolymer is added in dry-form to the bulk polymer, the equilibrium state that was achieved by the migration of the compounded fluoropolymer is now disrupted. A new equilibrium state has to be reached due to the presence of extra fluoropolymer. Since the addition of extra fluoropolymer allows more fluoropolymer to migrate towards the wall, the new equilibrium state will usually allow improved fluoropolymer coating on the wall. However, if compounded fluoropolymer is able to coat the walls thoroughly, the addition of extra fluoropolymer, although it may add the amount of fluoropolymer on the walls, it may not result in an improvement in the critical shear rate.

From these results, it can then be concluded that the synergistic effect of BN and fluoropolymer is more evident if the polymer is extruded through a crosshead die. However, an essential requirement to reveal this synergistic effect is to add fluoropolymer in a dry-form separately from BN so as to prevent the interaction effect between BN and fluoropolymer and to render the coating of the die wall by fluoropolymer more efficient.

The flow curves obtained from crosshead die extrusion appear to exhibits two different trends. In one of the trends, it appears that the processing aids have no effect (resins B, E and F), whereas on the other trend, the processing aid seems to reduce the extrusion pressure (resins A, C and D). Plots that show these trends are shown in Figures 5.24 to 5.29. In crosshead die extrusions, the accuracy of the flow curves is typically within $\pm$ 10%.

Figures 5.24 to 5.26 show the flow curves obtained for resins A, C and D and their blends with processing aids. From this Figures, it can be seen that there is a slight decrease in the extrusion pressure at medium shear rate values for the blends that contain fluoropolymer or CarboGlide.

Figures 5.27 to 5.29 show a typical plot for resins B, E and F and their blends with processing aids. It can be seen from these Figures that in this case, there is practically no effect of fluoropolymer or CarboGlide in the extrusion pressure.

All of the plots (Figures 5.24 to 5.29), however, show that the addition of BN does not show any effect. This is again consistent with the trend observed by *Rosenbaum et al (1998b)*. In any case, for all of the resins, it can be seen that at relatively low and high shear rate values, the addition of fluoropolymer or CarboGlide does not affect the flow curves.

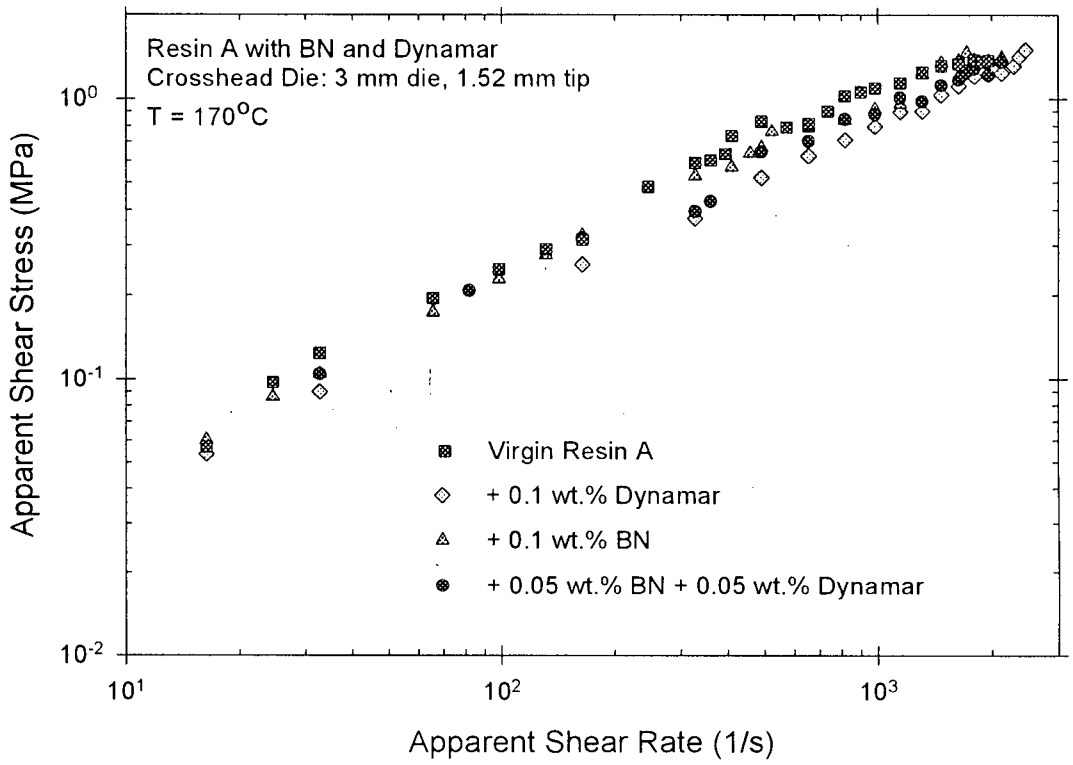

Figure 5.24 Flow curves of Resin A (LLDPE PF-Y821-BP) with and without PPAs in crosshead die extrusion at 170°C.

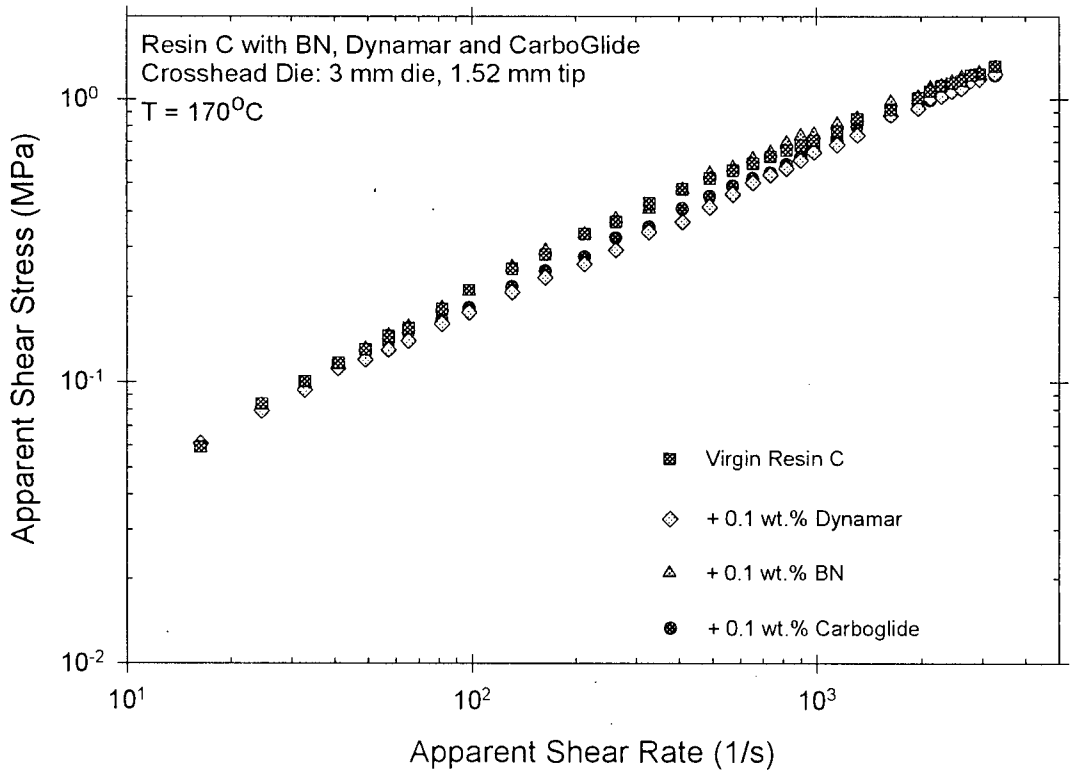

Figure 5.25 Flow curves of Resin C (LLDPE FP-120-F) with and without PPAs in crosshead die extrusion at 170°C.

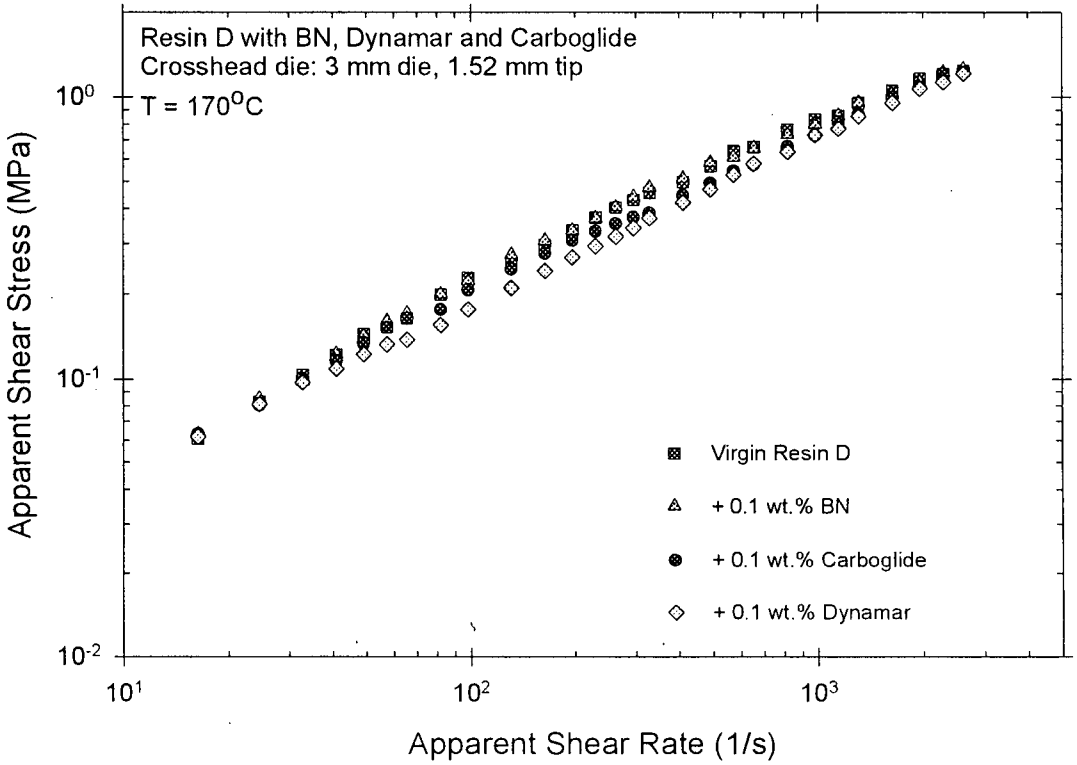

Figure 5.26 Flow curves of Resin D (LLDPE FPs-117-F) with and without PPAs in crosshead die extrusion at 170°C.

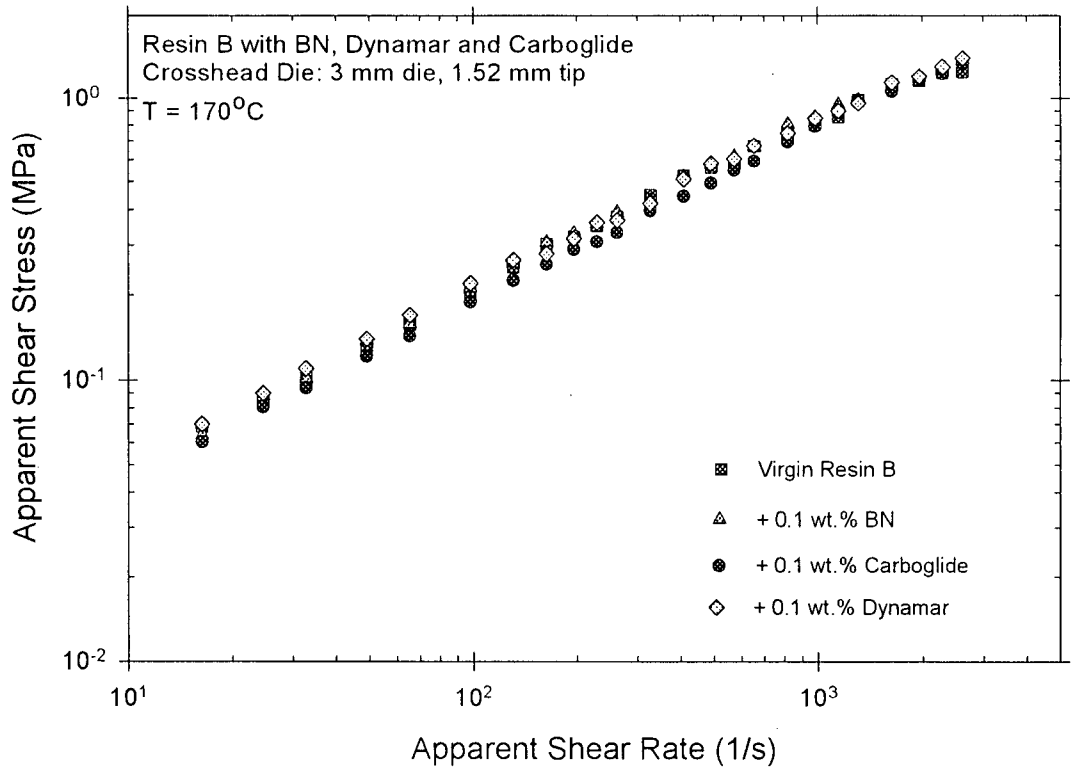

Figure 5.27 Flow curves of Resin B (LLDPE TD-9022-D) with and without PPAs in crosshead die extrusion at 170°C.

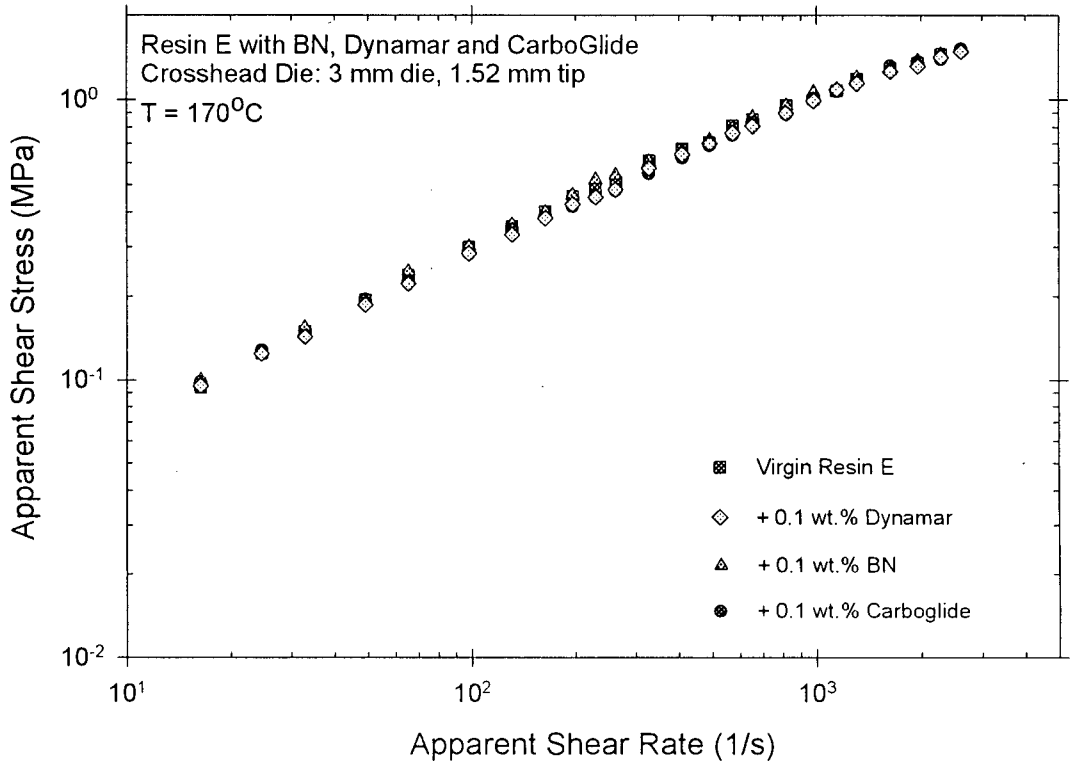

Figure 5.28 Flow curves of Resin E (LLDPE FP-015-A) with and without PPAs in crosshead die extrusion at 170°C.

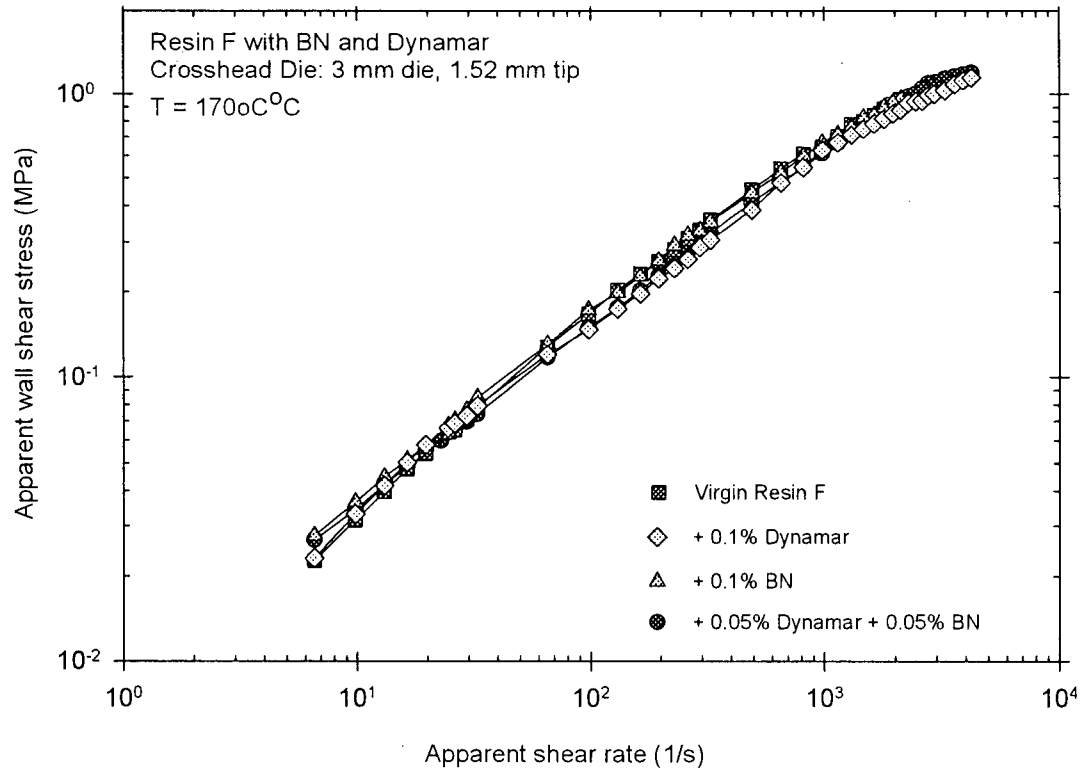

Figure 5.29 Flow curves of Resin F (HDPE 58G) with and without PPAs in crosshead die extrusion at 170°C.

Although the non-effect of BN on the flow curve of polyethylene is expected, the fact that the addition of fluoropolymer does not show any reduction in shear stress is rather surprising. The cause of this trend is not clear. One possible explanation is that depending on the polymer, particular interaction of fluoropolymer with other additives may take place and possibly the fluoropolymer is not possible to adhere to the wall, as suggested by *Priester and Stewart (1992)*. It is also possible that the coating process might need significantly longer time to take place that it is not reached within the duration of the current experiment.

This is a possible and logical explanation as additional dry-mixing of fluoropolymer into resin E (see Figure 5.30) actually reduces the extrusion pressure. This shows that extra fluoropolymer is necessary to coat the crosshead tip and die surfaces efficiently in order to sufficiently promote significant wall slip. This effect is consistently shown by resins B, E and F, where compounding fluoropolymer does not decrease the extrusion pressure. This explanation is further justified from Figures 5.31 and 5.32 which depict the effect of dry-mixing fluoropolymer into resin C. It is noted that, in resin C, the presence of compounded fluoropolymer reduces the extrusion pressure.

From Figure 5.31, it can be seen that the addition of fluoropolymer into CarboGlide^{TM}-compounded resin (sample C-CG) by dry mixing does not cause any significant pressure reduction. This is also the case for the addition of fluoropolymer into BN-compounded resin (sample C-BN) as can be seen from Figure 5.32. This phenomenon is also observed in the dry-mixing cases of resins A and D in which the addition of fluoropolymer does not reduce the extrusion pressure. This can be explained by the fact that in these cases

(resins A, C and D), the compounded fluoropolymer is able to sufficiently over-saturate the crosshead tip and die surfaces with fluoropolymer coating. This promotes maximum wall slip such that extra fluoropolymer in the dry form does not seem to improve the slippage any further.

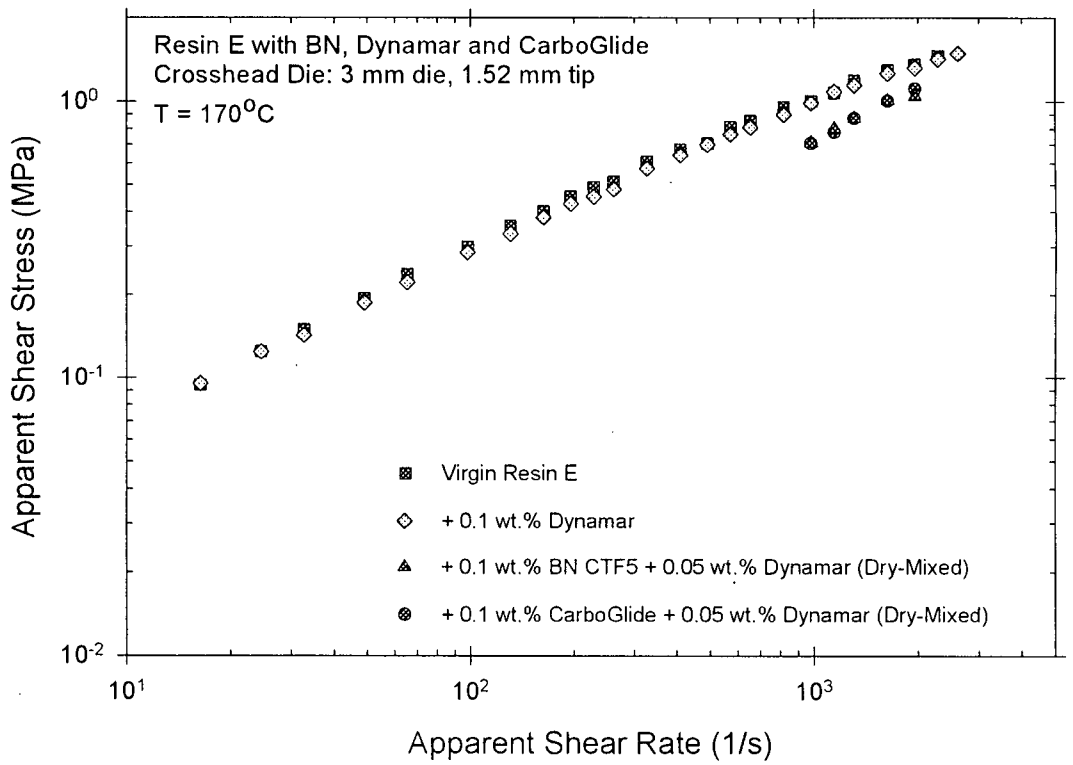

Figure 5.30 Flow curves of Resin E (LLDPE FP-015-A) with (compounded and dry-mixed) and without PPAs in crosshead die extrusion at 170°C.

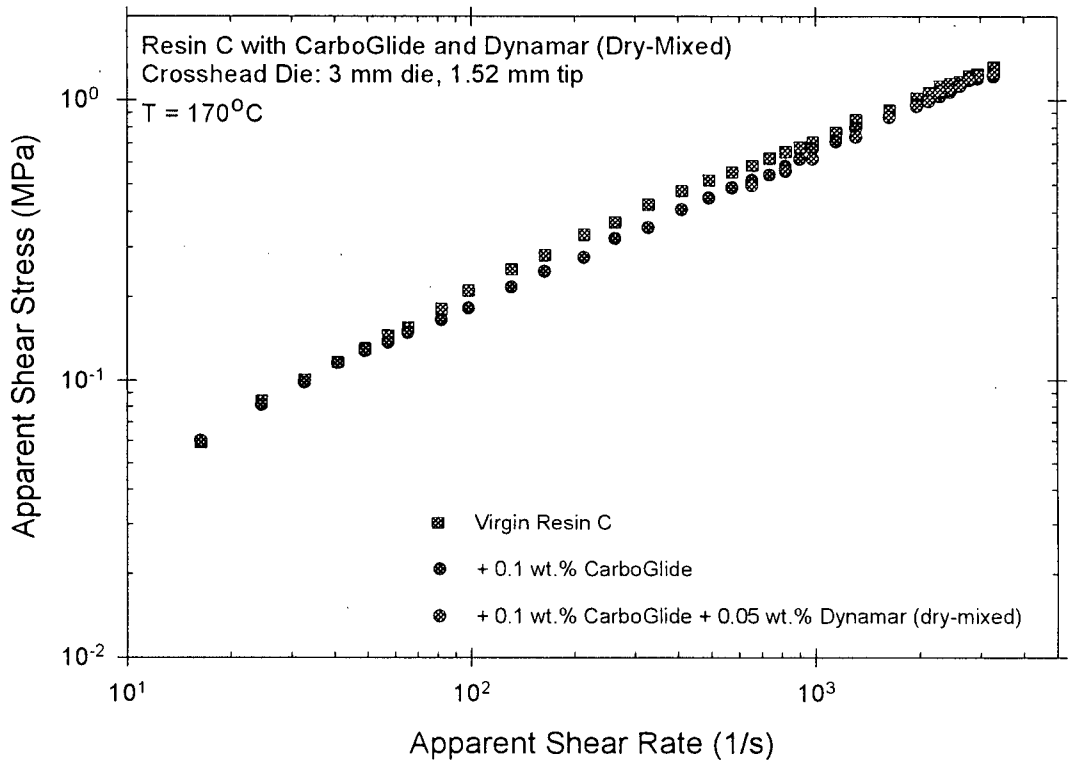

Figure 5.31 Flow curves of virgin Resin C (LLDPE FP-120-F) and with CarboGlide and fluoropolymer (dry-mixed) in crosshead die extrusion at 170°C.

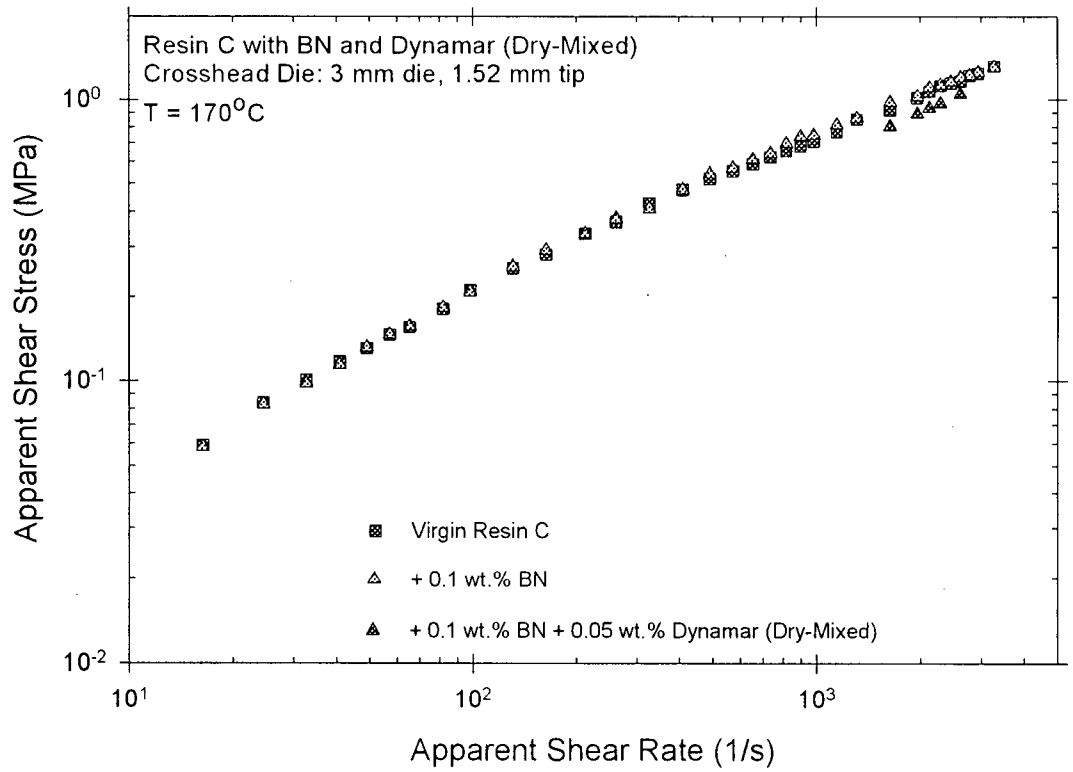

Figure 5.32 Flow curves of virgin Resin C (LLDPE FP-120-F) and with BN and fluoropolymer (dry-mixed) in crosshead die extrusion at 170°C.

5.5 Effect of Masterbatch

As discussed in Chapter 4, blends containing BN and CarboGlide™, prepared by means of diluting 5% concentrates were also prepared for testing. These blends were prepared with resin A as the base polymer. To assess these blends, only crosshead die extrusion experiments were performed. The critical shear rates for these blends are summarized in Table 5.6. It should be noted that for comparison purposes, virgin sample of resin A (coded A2) used to prepare these blends were also supplied and tested.

Table 5.6 Critical shear rates for blends prepared by masterbatch process and the virgin host polymer in crosshead die extrusion.

Sample ID	Critical shear rate for the onset of sharkskin (S^{-1})
A2	130
A2-BN M	327
A2-CG M	1636

From Table 5.6, it can be seen that the critical shear rate of virgin resin A2 (130 s^{-1}) is not comparable to the critical shear rate of virgin resin A (65 s^{-1}). This maybe caused by some differences in the two different batchs of resin A. Thus, we cannot compare the effectiveness of masterbatch directly between these two sets of samples. However, since polymer A2 fractures at higher shear rate compared to resin A, we can expect that the presence of BN should postpone the onset of melt fracture for resin A2 to an even higher shear rate compared to the one shown by resin A. Now, from Tables 5.5 and 5.6, it can be seen that the critical shear rates for the blends that contain BN (blend A-BN (direct dilution) and blend A2-BN M (masterbatch)) both show surface melt fracture at 327 s-1.

From this critical value, it can then be deduced that compounding BN by means of masterbatch does not improve the performance of the BN.

The flow curves of the virgin resins A and A2 and the BN-compounded blends (A-BN and A2-BN M) are shown in Figure 5.33. It can be seen from the Figure that the addition of BN, even by means of masterbatch, does not alter the flow curve; a result observed even with other resins as discussed earlier.

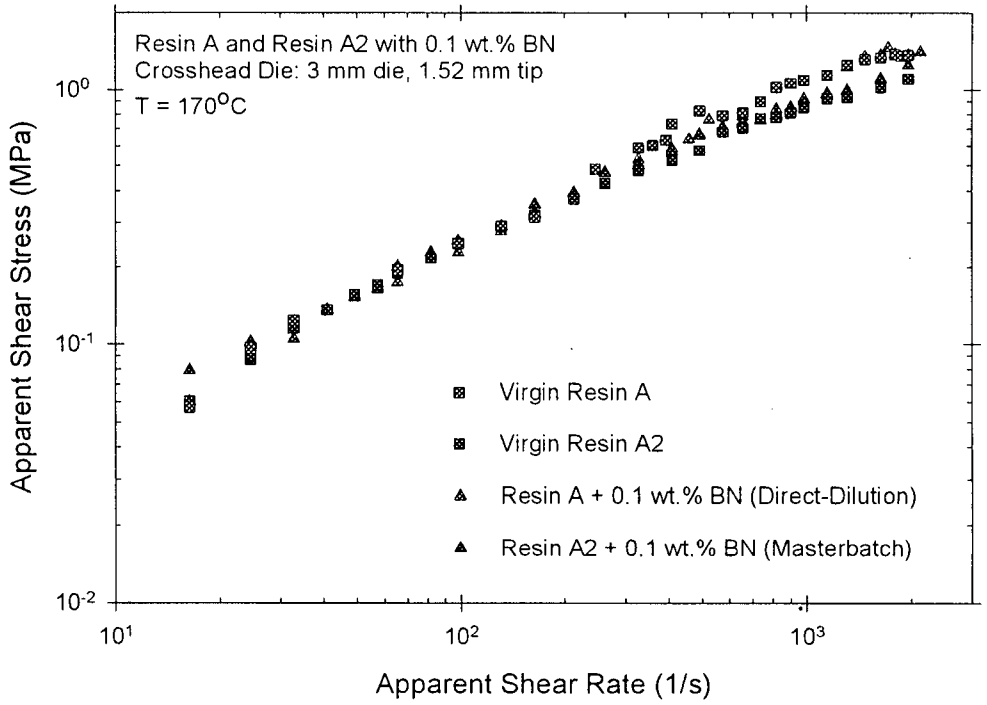

Figure 5.33 Flow curves of virgin Resins A and A2 (LLDPE PF-Y821-BP) and with BN (direct dilution and masterbatch) in crosshead die extrusion.

The last blend that was prepared by means of masterbatch step is blend A-CG M, a blend that contains 0.1 wt.% CarboGlide. It can be seen from Table 5.6 that this blend fractures at about 1636 s^{-1}, a value that is comparable to the one shown by the blend that contains

only fluoropolymer (A-FP). In addition, this critical rate is lower than the one corresponding to the dry-mixing cases (blends A-BN-FP DM and A-BN-FP-FP DM). These observations are consistent with the result shown by the other resins. This again shows that the masterbatch process does not seem to have any additional significant effect on the performance of the processing aid from what can be obtained by direct compounding to final dilution when a twin screw extruder is used.

6 SUMMARY

Six different polyethylenes (five of which are Ziegler-Natta) were used as the host polymers to assess the performance of boron nitride, fluoropolymer, combination of both boron nitride and fluoropolymer and CarboGlide in the processing of the LLDPE. Extrusion experiments to determine the critical shear rates for the onsets of sharkskin, stick-slip and gross melt fracture were performed to assess the performance of the processing aids.

Based on the experiments, the following conclusions can be drawn:

1. Synergistic effect of boron nitride and fluoropolymer allows the combination of these processing aids to show the best performance in eliminating surface melt fracture or postponing the onset of gross melt fracture, provided that fluoropolymer and boron nitride are introduced into the host polymer separately.
2. Relatively new processing aid, CarboGlide^{TM}, is able to perform as well as the combination of boron nitride and fluoropolymer in capillary die extrusion.
3. Boron nitride has no effect on the extrusion pressure.
4. Compounded fluoropolymer may not necessarily reduce the extrusion pressure especially in crosshead die extrusion; rather it depends on the degree of fluoropolymer coating of the die walls which can be achieved by the compounded fluoropolymer. If pressure reduction is achieved by the compounded fluoropolymer, adding extra fluoropolymer in a dry form has no further effect.
5. Dry-mixing of fluoropolymer into the resins seems to be a more effective method than melt compounding.

6. Preparing polymer blends by direct dilution seems to be able to achieve sufficient dispersion of the processing aids to allow effective performance.

REFERENCES

Achilleos, E, Georgiou, G, Hatzikiriakos, S.G., *Role of processing aids in the extrusion of molten polymers*. J. Vinyl Addit. Technol., 8 (1), 7-24 (2002).

Anastasiadis, S.H., Hatzikiriakos S G., *The work of adhesion of polymer/wall interfaces and its association with the onset of wall slip*. J. Rheol. 42, 795-812 (1998).

Benbow, J.J., Lamb, P., *New aspects of melt fracture*. S.P.E. Trans., 3, 7 (1963).

Bergem, N., *Visualization studies of polymer melt flow anomalies in extrusion*. Proc. 8th Int. Congr. Rheol., Gothenberg, p. 50 (1976).

Bird, R.B., Armstrong, R.C., Hassager, O., *Dynamics of polymeric liquids, vol. 1: Fluid mechanics*. Wiley, NY, 1987

Buckmaster, M.D., Henry, D.L., Randa, S.K., *High speed extrusion*. U.S. Pat. No. 5,688,457 (1997).

Cogswell, F.N., *Stretching flow instabilities at the exits of extrusion dies*. J. Non-Newtonian Fluid Mech., 2, 37-47 (1977).

Dealy, J. M., and K. F. Wissbrun, *Melt Rheology and Its Role in Plastics Processing: Theory and Applications*. Reinhold, NY, 1995.

Denn, M.M., *Issues in viscoelastic fluid mechanics*. Annu. Rev. Fluid Mech., 22, 13-34 (1990).

Dyneon, *Dynamar™ Polymer Processing Additives FX-9613: Technical information*, 2001.

Ferry J. D., *Viscoelastic properties of polymers*. 3rd ed., John Wiley, NY 1980.

Hatzikiriakos, S. G., and J. M. Dealy, *Wall Slip of Moleten High Density Polyethylene. II. Capillary Rheometer Studies*, J. Rheol., 36 (4), 703-741 (1992).

Hatzikiriakos, S.G., Dealy, J.M., *The effect of interface conditions on wall slip and melt fracture of high density polyethylene*. SPE ANTEC '91 Tech. Papers, 2311-2314 (1991).

Hatzikiriakos, S.G., *The onset of wall slip and sharkskin melt fracture in capillary flow*. Polym. Eng. Sci., 34 (19), 1441-1449 (1994).

Hatzikiriakos, S.G., Hong, P., Ho, W., Stewart, C.W., *The effect of Teflon coatings inpolyethylene capillary extrusion*. J. Appl. Polym. Sci., 55, 595-603 (1995).

Hatzikiriakos, S.G., *Conventional polymer processing additives in Polymer Processing Instabilities: Understanding and Control*, Hatzikiriakos, S.G. and Migler, K. (Eds.), Marcel Dekker, NY (2004a).

Hatzikiriakos, S. G., *Boron nitride based polymer processing aids in Polymer Processing Instabilities: Understanding and Control*, Hatzikiriakos, S.G. and Migler, K. (Eds.), Marcel Dekker, NY (2004b).

Howells, E.R., Benbow, J.J., *Flow defects in polymer melts*. Trans. Plast. Inst., 30, 240-253 (1962).

Kalika, D.S., Denn, M.M., *Wall slip and extrudate distortion in linear low-density polyethylene*. J. Rheol., 31 (8), 815-834 (1987).

Kazatchkov, I.B., Hatzikiriakos, S.G., Stewart, C.W., *Extrudate distortion in capillary/slit extrusion of a molten polypropylene*. Polym. Eng. Sci., 35, 1864-1871 (1995).

Kazatchkov, I.B, Yip, F., and Hatzikiriakos, S.G., *The effect of boron nitride on the rheology and processing of polyolefins*. Rheol. Acta, 39, 583 (2000).

Kharchenko, S.B., McGuiggan, P.M., Migler, K.B., *Flow induced coating of fluoropolymer additives: Development of frustrated total internal reflection imaging*. J. Rheol. 47, 1523-1545 (2003).

Kurtz, S.J., *Die geometry solutions to sharkskin melt fracture*. Advances in Rheology, ed. B. Mena, A. Garcia-Rejon and C. Rangel Nafaile, UNAM, Mexico City, Vol. 3, 399 (1984).

Kurtz, S.J., *The Dynamics of sharkskin melt fracture: effect of die geometry*. Proc. XIth Int.Congr.on Rheology, Brussels, Belgium. In: Moldenaers P., Keunings R. (eds.) Theretical and applied rheology. Elsevier Science Publishers, 377-379, 1992.

Lee, S; Kim, J; Lee, J. *The effect of boron nitride on the processability of metallocene based LLDPE*. SPE ANTEC '00 Tech. Papers, 2862-2866 (2000).

Leonov, A.I., *A linear model of the stick-slip phenomena in polymer flow rheometers*. Rheol. Acta, 23, 591 (1984).

Lin, Y.-H., *Explanation for slip-stick melt fracture in terms of molecular dynamics in polymer melts*. J. Rheol., 29 (6), 605-637 (1985)

Lupton, J.M., Regester, R.W., *Melt flow of polyethylene at high rates*. Polym. Eng. Sci., 5, 235 (1965).

Migler, K; Lavallee, C; Dillon, M; Woods, S; Gettinger, C. *Visualizing the elimination of sharkskin through fluoropolymer additives: Coating and polymer-polymer slippage.* J. Rheol., 45 (2), 565-581 (2001a).

Migler, K; Lavallee, C; Dillon, M; Woods, S; Gettinger, C. *Flow visualization of polymer processing additives effects.* SPE ANTEC '01 Tech. Papers, 1132-1136 (2001b).

Moynihan, R.H., Baird, D.G.; Ramanathan, R., *Additional observations on the surface melt fracture behavior of LLDPE.* J. Non-Newtonian Fluid Mech., 36, 255 (1990).

Myerholtz R.W., Oscillating flow behaviour of high-density polyethylene melts. J. Appl. Polym. Sci., 11, 687-698 (1967).

Münstedt, H., *Dependence of the elongational behaviour of polystyrene melts on molecular weight and molecular weight distribution.* J. Rheol., 24 (6), 847-867 (1980).

Oriani, S.R., Chapman, G.R., *Fundamentals of melt fracture elimination using fluoropolymer process aids.* SPE ANTEC '03 Tech. Papers, 22-26 (2003).

Petrie, C.J.S., Denn, M.M., *Instabilities in polymer processing.* AIChE J., 22 (2), 209-236 (1976).

Piau, J.M., El Kissi, N., *The influence of interface and volume properties of polymer melts on their die flow stability.* Proc. XIth Int.Congr.on Rheology, Brussels, Belgium. In: Moldenaers P., Keunings R. (eds.) Theretical and applied rheology. Elsevier Science Publishers, 70-74, 1992.

Piau, J.M., El Kissi, N., Trenblay, B., *Influence of upstream instabilities and wall slip on melt fracture and sharkskin phenomena during silicone extrusion through orifice dies.* J. Non-Newtonian Fluid Mech., 34, 145-180 (1990).

Piau, J.M., El Kissi, N., Trenblay, B., *Low Reynolds number flow visualization of linear and branched silicones upstream of orifice dies.* J. Non-Newtonian Fluid Mech., 30, 197 - 232 (1988).

Pudjijanto, S., Denn, M.M., *A stable "island" in the slip-stick region of linear low-density polyethylene.* J. Rheol., 38 (6), 1735-1744 (1994).

Ramamurthy, A.V., *Wall Slip in Viscous Fluids and Influence of Materials of Construction,* J. Rheol., 30 (2), 337–57 (1986).

Rathod, N., *The effect of surface properties of boron nitride on polymer processability.* Master's thesis (2003).

Rohse, N; Bailey, P; Ohlsson, S., *Stretched film from metallocene polyethylene. Metallocene technology makes cost reduction possible.* Kunststoffe, 87 (10), 1374-1378 (1997).

Rosenbaum, E.E., Randa, S.K., Hatzikiriakos, S.G., Stewart, C.W., Henry, D.L., Buckmaster, M.D., *A new processing additive eliminating surface and gross melt fracture in the extrusion of polyolefins and fluoropolymers.* SPE ANTEC '98 Tech. Papers, 952-956 (1998a).

Rosenbaum, E.E. *Rheology and processability of FEP resins for wire coating.* Ph.D. dissertation, The University of British Columbia: Vancouver, BC, 1998b.

Rosenbaum, E.E., Randa, S.K., Hatzikiriakos, S.G., Stewart, C.W., *Boron Nitride as a processing aid for the extrusion of polyolefins and fluoropolymers.* Polym. Eng. Sci., 40, 179 (2000).

Rudin, A., Worm, A.T.; Blacklock, J.E., *Fluocarbon elastomer processing aid for LLDPE, HDPE and PP resins.* Processing and Property Enhancement Utilizing Modifiers and Additives in Polymers: First Intl. Conf., p.71-81 (1985)

Sentmanat M.L., *SER-HV-A01 Universal testing platform instrument manual.* Xpansion Instruments, 1-7-1-8, *(2003a).*

Sentmanat, M.L., *A novel device for characterizing polymer flows in uniaxial extension.* SPE ANTEC '03 Tech. Papers, 992-996 (2003b).

Seth, M., Hatzikiriakos, S.G., Clere, T., *Gross melt fracture elimination: the role of surface energy of boron nitride powders.* Polym. Eng. Sci., 42, 743-752, (2002).

Son, Y; Migler, K. *Observation of the cavitation phenomena upon the gross melt fracture regime in LLDPE extrusion.* SPE ANTEC '02 Tech. Papers, 3742-3746 (2002).

Tordella, J.P., *An unusual mechanism of extrusion of polytetrafluoroethylene at high temperature and pressure.* J. Appl. Polym. Sci., 7, 215-229 (1963).

Tordella, J.P., *Unstable flow of molten polymers.* In Rheology, Vol. 5, F. R. Eirich, ed., Academic Press, NY, p. 57, 1969.

Tordella, J.P., *Fracture in the extrusion of amorphous polymers through capillaries.* J. Appl. Phys., 27, 454 (1956).

Tremblay, B., *Sharkskin defects of polymer melts: the role of cohesion and adhesion.* J. Rheol., 35 (6), 985-998 (1991).

Vinogradov, G.V., Insarova, N.I., Boiko, B.B., Borisenkova, E.K., *Critical regimes of shear in linear polymers*. Polym. Eng. Sci., 12 (5), 323-334 (1972).

Vinogradov, G.V., Malkin, A.Ya., *Rheology of polymers*. Mir, Moscow, Springer, Berlin, 1980.

Vinogradov, G.V., Malkin, A.Ya., Yanovskii, Y.G., Borisenkova, E.K., Yarlykov, B.V., Berezhnaya, G.V, *Viscoelastic properties and flow of narrow polybutadienes and polyisoprenes*. J. Polym. Sci., A2 (10), 1061-1084 (1972).

Waddon, A.J., Keller, A., *A temperature window of extrudability and reduced flow resistance in high-molecular weight polyethylene: Interpretation in terms of flow-induced mobile hexagonal phase*. J. Polym. Sci., B 28, 1063-1073 (1990).

Waddon, A.J., Keller, A., *The temperature window of minimum flow resistance in melt flow of polyethylene. Further studies on the effect of strain rate and branching*. J. Polym. Sci., B 30, 923-929 (1992).

Wang, S.Q., Drda, P.A., Inn, Y.W., *Exploring molecular origins of sharkskin, partial slip, and slope change in flow curves of linear low density polyethylene*. J. Rheol., 40 (5), 875-898 (1996).

World Polyethylene, Market Report – Freedonia Group, 1999.

Yip, F., Hatzikiriakos, S.G., Clere, T., *New boron nitride processing aids for the extrusion of molten polymer*. SPE ANTEC '00 Tech. Papers, 2852-2857 (2000).

Yip, F; Rosenbaum, E; Randa, S; Hatzikiriakos, S; Stewart, C. *The effect of the boron nitride type and concentration on the rheology and processability of molten polymers*. SPE ANTEC '99 Tech. Papers, 1223-1227 (1999).

NOMENCLATURE

A	cross sectional area
b	Rabinowitsch correction
D	capillary diameter, m
d	tip diameter, m
e	Bagley end correction or energy
F	tangential force
F_F	frictional force
F_d	piston force, lb
g	gravitational acceleration, m/s^2
G	shear modulus, Pa
G'	storage modulus, Pa
G''	loss modulus, Pa
G^*	complex modulus, Pa
h	gap between plates, m
K_F	Freundlich constant
K_L	Langmuir constant, l of adsorbent / mg of adsorbate
L, L_o	capillary length or length of sample, m
n	power-law exponent
n	Freundlich index
P	absolute pressure, Pa
P_a	ambient pressure, Pa
P_d	driving pressure, Pa
ΔP_{end}	Bagley correction, Pa
ΔP_{ex}	exit pressure drop, Pa
ΔP_{ent}	entrance pressure drop, Pa
Q	volumetric flow rate, m^3/s
r	capillary radius, m
R	radius of SER windup drum
R_b	radius of barrel, in

T	torque; absolute temperature, K
t	time, s
u	melt velocity, m/s
u_s	slip velocity, m/s
Δx	plate displacement, m

Greek Letters

β	geometrical parameter for shear stress distribution
δ	mechanical loss angle
$\dot{\varepsilon}_H$	Hencky strain rate, s^{-1}
γ	shear strain
$\dot{\gamma}$	shear rate, s^{-1}
$\dot{\gamma}_A$	apparent shear rate, s^{-1}
$\dot{\gamma}_{A,s}$	apparent shear rate, corrected for slip, s^{-1}
$\dot{\gamma}_w$	wall shear rate, s^{-1}
γ_0	strain amplitude in oscillatory shear
μ	viscosity of liquid, mPa .s
ρ	density of liquid, kg/m^3
η	viscosity, Pa · s
η_0	zero-shear viscosity, Pa · s
η^*	complex viscosity, Pa · s
$\eta_E^+(t)$	tensile stress growth coefficient, Pa · s
σ_c	critical shear stress for the onset of melt fracture, Pa
σ_w	wall shear stress, Pa
σ_0	stress amplitude in oscillatory shear, Pa
ω	frequency, rad/s or specific volume, cm^3/g
Ω	angular speed